Molecular analysis of TTL deficiency in pre- and postmitotic cells

Von der Fakultät für Lebenswissenschaften

der Technischen Universität Carolo-Wilhelmina

zu Braunschweig

zur Erlangung des Grades eines

Doktors der Naturwissenschaften

(Dr. rer. nat.)

genehmigte

D i s s e r t a t i o n

von Andreas Fischer

aus Gifhorn

1. Referent: Professor Dr. Jürgen Wehland
2. Referent: Professor Dr. Michael Steinert
eingereicht am: 29.03.2010
mündliche Prüfung (Disputation) am: 01.07.2010

Druckjahr 2010

Vorveröffentlichungen der Dissertation

Teilergebnisse aus dieser Arbeit wurden mit Genehmigung der Fakultät für Lebenswissenschaften, vertreten durch den Mentor der Arbeit, in folgenden Beiträgen vorab veröffentlicht:

Tagungsbeiträge

Marco van Ham, **Andreas Fischer**, Marcin Ura, Christian Erck and Jürgen Wehland (2008). Analysis of the tubulin tyrosination cycle in TTL-deficient cells. *23rd FEBS/ECF Workshop "Mechanics and dynamics of the cytoskeleton", June 22nd – 26th, 2008, Potsdam.*

Marco van Ham, **Andreas Fischer**, Marcin Ura and Jürgen Wehland (2008). Tubulin modifications and cytoskeleton dynamics. *Grant evaluation of the DFG-Research Group FOR629: Molecular mechanism of cellular motility, October 15th, 2008, Hannover.*

Marco van Ham, **Andreas Fischer**, Marcin Ura, Christian Erck and Jürgen Wehland (2009). Analysis of the tubulin tyrosination cycle in TTL-deficient cells. *32nd Annual Meeting of the German Society for Cell Biology, March 24th – 27th, 2009, Konstanz.*

Marco van Ham, **Andreas Fischer**, Marcin Ura, Marcus Gereke, Ramona Baier, Christian Erck and Jürgen Wehland (2009). Analysis of the tubulin tyrosination cycle in TTL-deficient cells. *49th Annual Meeting of the American Society for Cell Biology, December 5th – 9th, 2009, San Diego (USA).*

Marco van Ham, **Andreas Fischer**, Marcin Ura, Marcus Gereke, Ramona Baier, Christian Erck and Jürgen Wehland (2010). Analysis of the tubulin tyrosination cycle in TTL-deficient cells. *33rd Annual Meeting of the German Society for Cell Biology, March 10th – 13th, 2010, Regensburg.*

Table of contents

1. Introduction

The cytoskeleton is a highly dynamic system of filaments that enables the cell to organize its intracellular processes as well as its interaction with the environment. In eukaryotic cells, the cytoskeleton consists of three components: the microfilament system, the microtubule network and the intermediate filaments. These filament systems consist of small subunits, which assemble to polymers. In case of the microfilaments and the microtubules, the incorporation of actin and tubulin subunits, respectively, results in polar filaments. In contrast, intermediate filaments are apolar polymers, which are assembled from antiparallel dimers. Although being rigid structures, all three filament systems have a dynamic behaviour in common. In conjunction, these intertwined cytoskeletal networks are responsible for maintaining cell shape as well as physical stability and organize the general intracellular structure. Intermediate filaments provide mechanical strength, whereas actin filaments mainly provide cell shape, cell polarity and cell motility (Alberts et al., 2008; Galjart, 2005).

The microtubule network fulfils a broad range of cellular functions. Besides the actin cytoskeleton, it plays a substantial role in arranging and adapting the cell shape as well as establishing cell polarity. As stable components of cilia and flagella, microtubules provide cell motility. Furthermore, microtubules are configured in a bipolar mitotic spindle and segregate the replicated chromosomes into the daughter cells during mitosis. By serving as tracks for motor proteins, microtubules are involved in intracellular cargo transport and additionally determine the position of organelles. The great diversity of cellular functions, in which microtubules participate, is not only based on their biochemical characteristics but also on several posttranslational modifications and a large variety of interaction partners (Alberts et al., 2008; Galjart, 2005; Wade, 2009).

This study focusses on the influence on cellular processes and microtubule binding partners by the tyrosination cycle, a posttranslational α-tubulin modification.

1.1. Microtubule structure and organization

Microtubules are formed by the assembly of heterodimers comprised of the globular α-tubulin and β-tubulin subunits, both of which consist of about 450 amino acids and possess a molecular weight of approximately 55 kDa. In vertebrates, α- and β-tubulin are both encoded by at least six differentially expressed genes in a species-specific manner resulting in a set of isotypes, which differ slightly in their amino acid sequences, particularly in the respective C-terminal regions (Wade, 2009). Although both α- and β-tubulin have a binding site for guanosine triphosphate (GTP), only the nucleotide bound to β-tubulin can be hydrolysed or substituted, whereas the GTP molecule of the α-tubulin subunit is spatially fixed within the heterodimer (Fig. 1a). For microtubule formation, the heterodimers assemble in linear protofilaments in a head-to-tail manner and, by that, create polar filaments (Fig. 1b). The addition of αβ-tubulin subunits can take place at both filament ends but preferentially occurs at the end that is exposing β-tubulin. This end is termed plus-end and usually grows faster, whereas the slower growing, α-tubulin-exposing end is referred to as the minus-end. Notably, minus-end growth could only be observed *in vitro* (Dammermann et al., 2003).

In general, 13 protofilaments are arranged in parallel to form a cylindrical tube with a diameter of 25 nm (Fig. 1c). Still, the number of protofilaments in microtubules differs in some organisms and cell types. Neighbouring protofilaments align with a shift of approximately 0.9 nm resulting in a helical succession of tubulin subunits around the microtubule as illustrated in Figure 1c. Since the heterodimers have a length of 8 nm, the mentioned protofilament shift leads to a discontinuity in the microtubule surface that is called the lattice seam (illustrated in Fig. 4b).

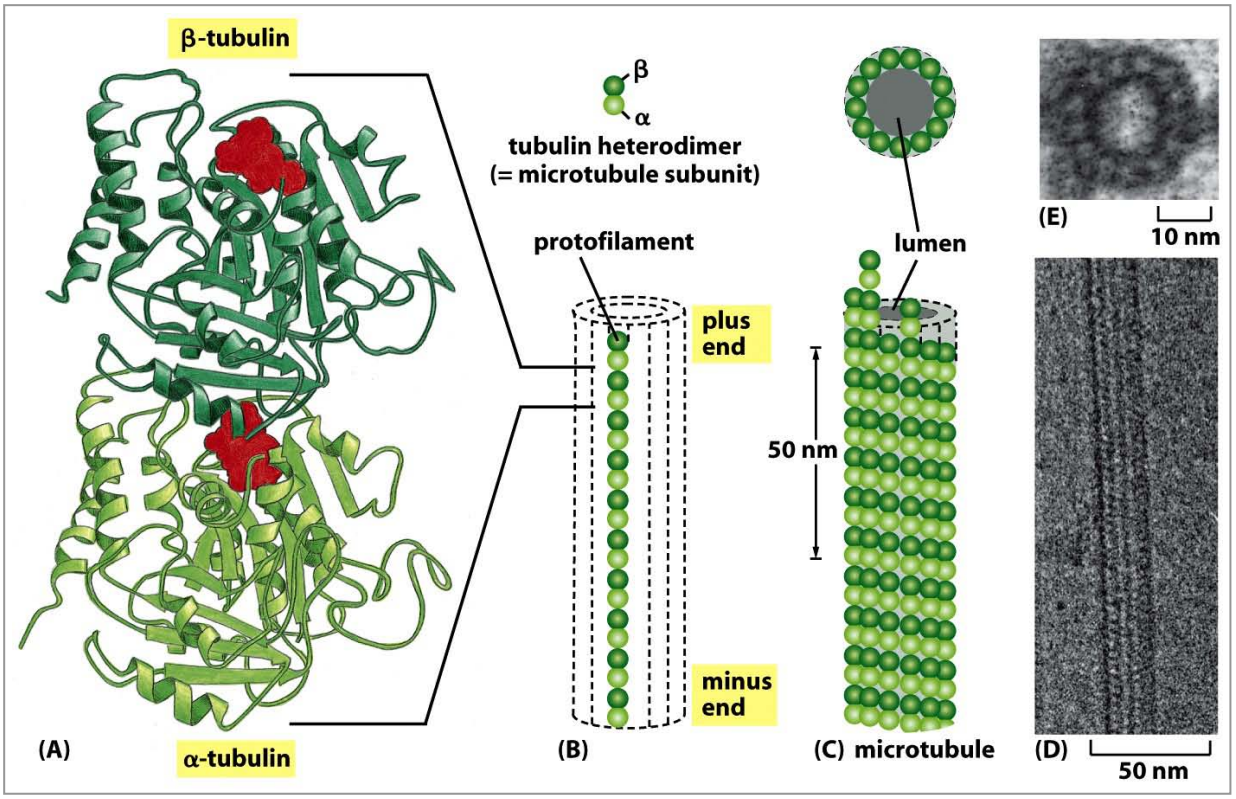

Fig. 1: Structure of tubulin subunits and microtubules. a) Structure of an αβ-tubulin heterodimer with bound GTP molecules (red). **b)** Scheme of an αβ-tubulin heterodimer and a protofilament consisting of head-to-tail assembled heterodimers. **c)** Scheme of a microtubule consisting of 13 linearly arranged protofilaments. Note the shift in protofilaments. **d)** Electron microscope image of a microtubule segment. **e)** Electron microscope image of a cross section of a microtubule consisting of 13 protofilaments (from Alberts et al., 2008).

In most cell types, the microtubule minus-ends are embedded in a so-called microtubule-organizing centre (MTOC), which is located close to the nucleus and prevents depolymerization of microtubules from their minus-ends. Typically, animal cells possess only a single MTOC, which is also referred to as the centrosome. The microtubule minus-ends are generally nucleated in the MTOC by γ-tubulin that shares 30 % identity with α- and β-tubulin (Oakely & Oakely, 1989). Two γ-tubulin molecules and two associated proteins form the γ-tubulin small complex (γ-TuSC) that, together with accessory proteins, assemble to the microtubule-nucleating γ-tubulin ring complex (γ-TuRC). This complex is present in all eukaryotic cells with the exception for yeast (Moritz & Agard, 2001). Models for the nucleation of microtubules in the MTOC are shown in Figures 2a and b.

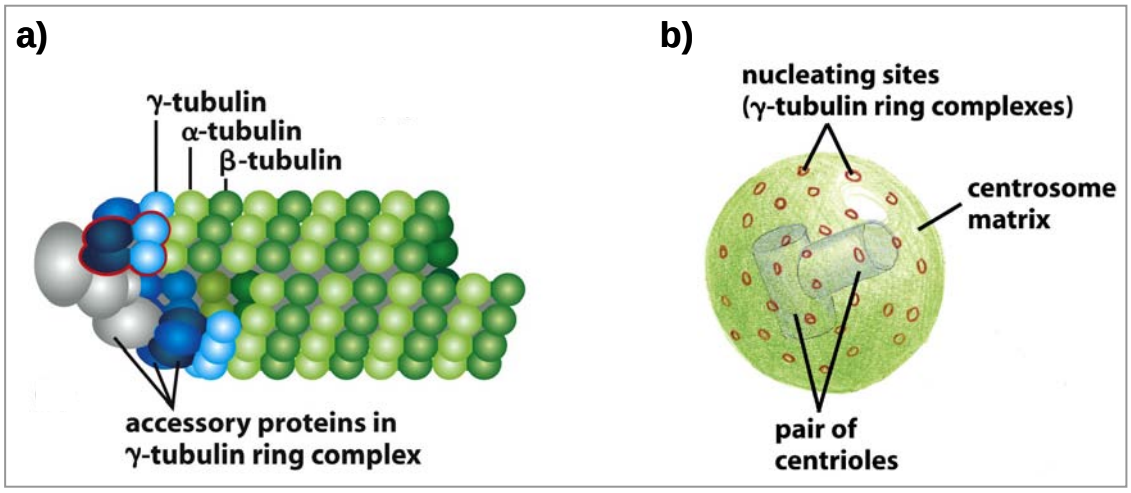

Fig. 2: Microtubule nucleation in the microtubule-organizing centre of animal cells. a) Model of microtubule nucleation by the γ-tubulin ring complex. A subunit of the ring complex, the γ-tubulin small complex, is outlined in red. **b)** Model of a centrosome with γ-tubulin ring complexes. Note the embedded pair of centrioles, another microtubule-based protein complex (from Alberts et al., 2008).

Microtubules can be organized differently depending on the cell cycle phase or the cell type. First, in interphase cells, microtubules radiate from the MTOC into the cell periphery. Except for a stable subpopulation, most of the microtubules are highly dynamic and undergo phases of growth and shrinkage. This mechanism enables the microtubule network to probe and interact with the entire cytoplasmic space (Fig. 3a). Second, during mitosis, the centrosome duplicates and the daughter centrosomes migrate to opposite poles, from which microtubules form the mitotic spindle. Originating in the daughter centrosomes, three types of microtubules can be found: Astral microtubules emanate in the cell cortex, kinetochore microtubules bind to the chromosomes' kinetochores and interpolar microtubules provide stability of the spindle (Fig. 3b). Usually, microtubules occur as single filaments, but they can also appear as doublets or triplets. Finally, in the core of cilia and flagella nine doublet microtubules are arranged in a tube with two single microtubules in the centre. In contrast, basal bodies, which anchor cilia and flagella in the surface of eukaryotic cells, consist of nine triplet microtubules. This typical microtubule arrangement can additionally be found in centrioles (see Fig. 2b; Verhey & Gaertig, 2007).

Besides α-, β- and γ-tubulin, other tubulins have been discovered in eukaryotes. In *Chlamydomonas* δ-tubulin was found, ε-tubulin is expressed in *Paramecium*,

Chlamydomonas as well as in mammals, η-tubulin is present in *Paramecium* and, finally, ζ-tubulin is found in trypanosomes and some animal cells. Although not ubiquitously expressed, these tubulins are all involved in protein complexes of the aforementioned centrioles and/or basal bodies (Dutcher, 2003).

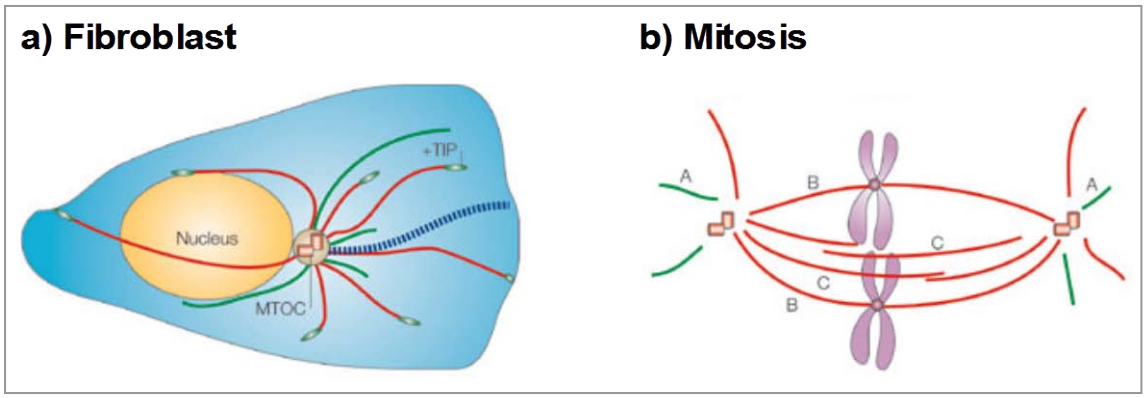

Fig. 3: Microtubule organization in an interphase fibroblast and a dividing cell. a) Scheme of the microtubule network in a migrating fibroblast. Growing microtubules are shown in red, shrinking microtubules in green and stable microtubules in blue. Plus-end tracking proteins (+TIP) are bound to growing microtubule plus-ends. **b)** Scheme of the microtubule network during mitosis. Growing microtubules are shown in red and shrinking microtubules in green. Capitals mark different types of microtubules: A) astral microtubules, B) kinetochore microtubules, and C) interpolar microtubules (from Galjart, 2005).

1.2. Dynamic instability

As already mentioned above, microtubules alternate between phases of growth and shrinkage. This process of dynamic instability was discovered in 1986 by direct microscopical observation (Horio & Hotani, 1986), but had already been predicted two years earlier (Mitchison & Kirschner, 1984). The switch from growth or pausing to shrinkage is referred to as catastrophe. The change from microtubule shrinkage to growth is referred to as rescue. As the microtubule minus-ends are embedded in the MTOC in most of the cells, dynamic instability usually occurs at plus-ends. The polymerization at growing microtubule ends requires αβ-tubulin heterodimers containing a GTP-loaded β-tubulin subunit. At its very end, a growing microtubule exists as an open sheet-like structure, to which additional heterodimers assemble in a non-helical fashion (Fig. 4c, step 1). After incorporation, the GTP molecule on the β-tubulin subunit is hydrolysed due to binding to the penultimate heterodimer. As a

consequence, microtubules primarily contain GDP-loaded β-tubulin subunits except for the newly assembled heterodimers and some randomly distributed GTP-loaded subunits in the lattice, which are proposed to be involved in a rescue mechanism (Dimitrov et al., 2008). With proceeding of microtubule growth the protofilament sheet closes to a cylindrical tube, but the exact mechanism is still unknown. Terminal sheet closure results in a metastable intermediate microtubule that could either pause or start to grow or shrink again (Fig. 4c, step 2). GTP hydrolysis may trigger the conformational change at the very plus-end. Also the opposite mechanism with GTP hydrolysis as result of conformational changes within microtubules is discussed as a possibility. Although GTP is not necessarily needed for the polymerization reaction itself, it is necessary for longitudinal contacts in the growing microtubule (Rice et al., 2008). Additionally, by creating a so-called GTP-cap, it protects the microtubule plus-ends from immediate depolymerization. When a microtubule is capped by GDP-loaded tubulin due to a higher rate of hydrolysis than heterodimer assembly, the subunits can dissociate and cause a phase of shrinkage. Depolymerization appears in a fountain-like release of GDP-loaded heterodimers and small protofilament fragments (Fig. 4c, step 3). After disassembly, the GDP molecule in the β-tubulin subunits of the free heterodimers is being exchanged with GTP (Fig. 4c, step 4). The resulting heterodimers are then able to enter a new round of microtubule polymerization and depolymerization. If these processes occur in a single non-nucleated microtubule with polymerization at the plus-end and depolymerization at the minus-end, tubulin subunits can treadmill through the microtubule (Waterman-Storer & Salmon, 1997).

Regulation of dynamic instability depends on a large variety of interacting proteins influencing the rate and speed of either catastrophe or rescue events. As many interaction partners fulfil additional tasks, the regulation of microtubule dynamics is described in separate chapters.

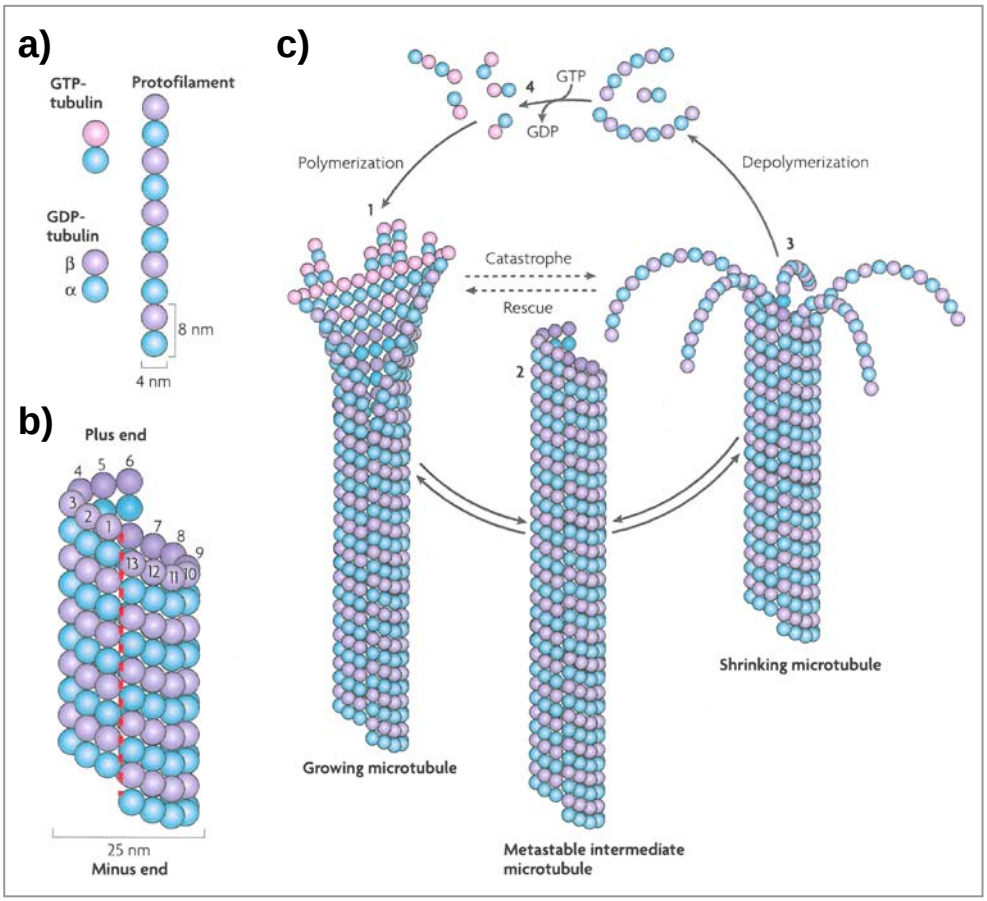

Fig. 4: Microtubule dynamic instability. a) Scheme of the αβ-tubulin heterodimer with either GTP (pink) or GDP (purple) bound to β-tubulin. Additionally, a linear protofilament is shown. **b)** Scheme of a microtubule consisting of 13 protofilaments. The red dashed line marks the lattice seam. **c)** Model of dynamic instability. Numbers mark the different steps of microtubule dynamics: 1) Growing microtubule with polymerization of GTP-loaded tubulin heterodimers at the sheet-shaped plus-end. 2) Metastable intermediate microtubule after closure of the terminal sheet. 3) Shrinking microtubule with depolymerization of GDP-bound subunits. 4) Exchange of GDP with GTP on the depolymerized β-tubulin subunits (from Akhmanova & Steinmetz, 2008).

1.3. Microtubule interaction partners

Microtubule function and dynamics rely on the interaction with other proteins that are known as microtubule-associated proteins (MAPs). In general, MAPs can be differentiated into microtubule lattice-binding and plus-end tracking proteins (+TIPs). Many of those proteins are involved in the regulation of microtubule dynamics by modulating microtubule stability or promoting either rescue or catastrophe events. Others influence either the speed of microtubule growth or shrinkage. Yet another group of MAPs fulfil more specific functions as cargo transport along microtubules or

building up a blockage on the microtubule lattice to hinder motor protein movement. The most important MAP types are subsequently described in more detail.

1.3.1. Lattice-binding MAPs

The class of traditional MAPs, which bind to the microtubule lattice contains many proteins that influence the stability of microtubules. Structural MAPs increase the stability of the microtubule by decorating the microtubule lattice. In contrast, destabilizing MAPs often possess enzymatic activity and promote depolymerization by introducing breaks in the microtubule. Finally, motor proteins are responsible for intracellular transport, but additionally could be involved in decreasing microtubule stability (Van der Vaart et al., 2009). A model illustrating the interplay of lattice-binding MAPs is shown in Figure 5.

1.3.1.1. Structural MAPs

The group of structural MAPs covers proteins without any enzymatic activity that bind to the microtubule lattice. The members of the MAP1 family, MAP2, tau, MAP4 and doublecortin (DCX) are the most prominent structural MAPs in vertebrates.

In most vertebrates, the MAP1 family consists of MAP1A, MAP1B and MAP1S, which all are complexes of multiple heavy chains and light chains. However, the exact stoichiometric compositions are still unknown (Halpain & Dehmelt, 2006). In contrast, MAP2, tau, MAP4 and doublecortin appear as single chain proteins (Drewes et al., 1997). Structural MAPs are predominantly expressed in neurons and play an important role in neuronal development, degeneration and cortical migration (Halpain & Dehmelt, 2006; Gleeson et al., 1999). Still, those MAPs differ in their respective spatial and temporal expression pattern. MAP1A is located in dendrites of adult neurons, whereas MAP1B is expressed in developing neurons and is enriched in axons. The localisation of MAP2 is limited to the neuronal cell body and dendrites, whereas tau is enriched in axons. However, both MAP2 as well as tau show functional redundancy with MAP1B (DiTella et al., 1996; Teng et al., 2001).

In contrast to the expression of the aforementioned MAPs, doublecortin is only expressed in migrating and differentiating neurons (Francis et al., 1999).

All structural MAPs stabilize microtubules by decorating the microtubule lattice and, thereby, decreasing catastrophe frequency and shrinkage speed. Furthermore, they

protect the microtubules from being severed by destabilizing enzymes (Halpain & Dehmelt, 2006) and, additionally, hinder motor proteins to move along the microtubule lattice by diminishing the frequency of possible motor-microtubule interactions (see Fig. 5; Baas & Qiang, 2005). Microtubule-binding domains on both the heavy and the light chains mediate microtubule binding of MAP1A and B, whereas MAP1S only has a microtubule-binding domain in its light chain. In addition to their microtubule binding character, the light chains of the MAP1 family members are also able to bind filamentous actin (F-actin). However, it is unknown whether a single MAP1 molecule can bind tubulin and actin simultaneously. MAP2, tau and MAP4 all have conserved C-terminal microtubule-binding domains characterized by three to four basic pseudorepeats framed by two proline-rich regions (Drewes et al., 1997). The microtubule binding affinity of structural MAPs is regulated by their phosphorylation state. MAP1B is reported to be phosphorylated by the glycogen synthase kinase-3β (GSK3β) at serine residue 1260 and threonine residue 1265 (Trivedi et al., 2005), whereas tau is phosphorylated by the microtubule-affinity regulating kinase (MARK; Drewes et al., 1997). In both cases, this phosphorylation strongly reduces the microtubule binding affinity and results in dissociation from the microtubule lattice. The hyperphosphorylation of tau leads to its aggregation in paired helical filaments and is found in neurodegenerative diseases like Alzheimer`s disease (Baas & Qiang, 2005).

1.3.1.2. Destabilizing MAPs

Beside structural MAPs that promote microtubule stability there are other lattice-binding MAPs, which destabilize microtubules by breaking them or by promoting depolymerization.

In general, microtubule-severing proteins possess an ATPase activity and use the energy from ATP hydrolysis to fragment microtubules. Most prominent microtubule-severing proteins are katanin and spastin, both belonging to the family of ATPases associated with various cellular activities (AAA proteins). A close relative is fidgetin, a third microtubule-severing AAA protein that is much less investigated. Katanin is the best-studied AAA protein and appears as a heterodimer consisting of a 60 kDa (p60) and an 80 kDa (p80) subunit. The p60 subunit is composed of an N-terminal microtubule-binding domain and a C-terminal catalytic domain homologous to

ATPases of the AAA-protein family. In contrast, the p80 subunit mediates katanin targeting and regulates ATPase activity (McNally et al., 2000). Both katanin and spastin play an important role in mitotic spindle dynamics, neuron differentiation and flagellar physiology in animal cells (Wade, 2009; Zhang et al., 2007). According to the model for microtubule severing, the AAA proteins form a hexameric ring around the microtubule lattice followed by the introduction of a break (Fig. 5).

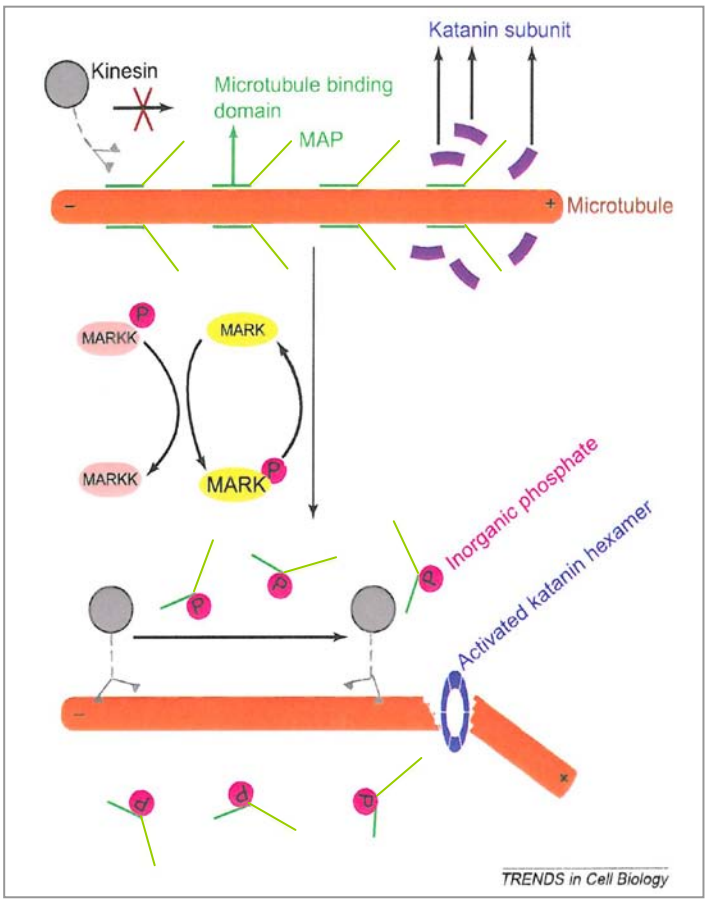

Fig. 5: Model illustrating the interplay of lattice-binding microtubule-associated proteins. The upper scheme shows a microtubule that is decorated with unphosphorylated MAPs (e.g. tau). By that, kinesin motor proteins (see chapter 1.3.1.3.) are hindered in their plus-end-directed movement. Furthermore, bound MAPs suppress the formation of an active hexamer ring of katanin subunits around the microtubule (upper part). If the microtubule-affinity regulating kinase (MARK) is phosphorylated by the MARK kinase (MARKK), it can phosphorylate MAPs and thereby induce their dissociation from the microtubule. As a consequence, motor proteins can interact more frequently with the microtubule and move in direction of the plus-end, whereas katanin subunits can hexamerize and sever the microtubule (lower part; from Baas & Qiang, 2005).

In mitosis, katanin is reported to sever microtubules close to the kinetochore-attached plus-ends, whereas spastin and fidgetin release nucleated microtubule minus-ends. These effects result in microtubule depolymerization from both ends leading to the poleward flow of kinetochore-microtubules, thereby segregating the chromosomes (Zhang et al., 2007).

In addition to microtubule-severing proteins, also three kinesin families contain members with microtubule-depolymerizing activity. In general, kinesins are motor proteins that conventionally move along the microtubule lattice towards the plus-end (see chapter 1.3.1.3. and Fig. 5 and 6). Yet, the kinesin-13 family includes non-motile members that promote microtubule depolymerization. Additionally, members of the kinesin-8 and kinesin-14 families with slow motor activities also promote the depolymerization of microtubules (Van der Vaart et al., 2009; Wade, 2009). The kinesin-13 family is represented in mammals by the proteins Kif2A, Kif2B and Kif2C/MCAK (Mitotic centromere-associated kinesin), which predominantly bind microtubule plus-ends and promote catastrophe events in an ATP-dependent manner (Newton et al., 2004). For example, MCAK is reported to be a processive depolymerase that forms an ATP-hydrolyzing complex at the microtubule plus-end and removes up to twenty $\alpha\beta$-tubulin heterodimers from a protofilament. As a consequence, the dissociation rate of tubulin dimers can be increased up to 100-fold by the presence of MCAK proteins (Hunter et al., 2003). Finally, kinesin-13 family members play an important role in microtubule depolymerization during mitosis, though at different places. Kif2A and B are primarily located at the centrosomes, whereas Kif2C/MCAK is concentrated at kinetochores.

Another microtubule-destabilizing kinesin is Kif18A, a member of the kinesin-8 family. Both Kif18A and Kip3, the *Saccharomyces cerevisiae* orthologue, possess a slow plus-end-directed motor activity and accumulate at the microtubule plus-ends, where they promote disassembly of $\alpha\beta$-tubulin heterodimers (Gupta et al., 2006).

Finally, the stimulation of microtubule depolymerization by the kinesin-14 family members Ncd (from *Drosophila melanogaster*), Kar3 (from *Saccharomyces cerevisiae*) and Klp2 (from *Schizosaccharomyces pombe*) has been reported. In contrast to the previously mentioned and conventional kinesins, kinesin-14 members are characterized by a slow minus-end-directed movement along microtubules while depolymerizing them from the plus-end (Van der Vaart et al., 2009).

1.3.1.3. Motor proteins

Intracellular trafficking is mediated by the so-called motor proteins, which use the energy of ATP hydrolysis to move along cytoskeletal filaments. In eukaryotes, two families of microtubule-based molecular motors exist, the already mentioned kinesins and the dyneins. In general, both protein families possess a head or motor domain that binds to the microtubule and determines the direction of movement. The tail, however, determines the intracellular function due to its cargo-specificity.

Kinesins form a superfamily of ATPases with fourteen subfamilies in mammals. The majority of kinesins have an N-terminal motor domain and move along microtubules towards the plus-end. Interestingly, kinesin-13 members contain a central motor domain and are non-motile, whereas kinesin-14 members use a C-terminal motor domain to move towards the minus-end. Conventional kinesins as kinesin-1 consist of two heavy and two light chains, but also monomeric, homodimeric, trimeric and homotetrameric kinesins exist. Motor domains usually are located in the heavy chains followed by a coiled-coil region involved in dimer formation (Wade, 2009). The motor activity of motile kinesins is regulated by their conformation. Folding of the protein inactivates the motor domain, while cargo-binding is still possible and unfolds the molecule (Dunn et al., 2008). Moreover, phosphorylation of kinesin light chains results in inactivation. Movement along microtubules occurs by ATP hydrolysis-driven conformational changes that alternate between the two motor domains of the kinesin dimer and lead to cycling between microtubule binding, release and rebinding of the single head domains (Alberts et al., 2008; Dunn et al., 2008). By that, the protein moves along the microtubule in steps of 8 nm, the exact length of a $\alpha\beta$-tubulin heterodimer (Nan et al., 2005). In contrast, monomeric kinesins move diffusively from binding-site to binding-site while complete detachment is prevented by electrostatic interaction between a kinesin region called K-loop and the tubulin C-termini (Okada & Hirokawa, 2000).

In their function as intracellular transporters, kinesins transport a large variety of cargo, as for instance vesicles, membrane-enclosed organelles, protein complexes, mRNA, membrane proteins and signalling-molecules. In addition to that, they are associated with several kinases like the c-Jun N-terminal kinase (JNK) and the mitogen-activated protein kinase-kinases 4 and 7 (MKK4 and MKK7; Daire et al., 2009). The transport of kinases is mediated by scaffold proteins like the JNK-

interacting protein 1 (JIP1), which directly bind to motor proteins (Verhey et al., 2001). Furthermore, kinesins play an important role in mitosis and, as described in chapter 1.3.1.2., kinesin-8, -13 and -14 members promote microtubule depolymerization. However, the spatial and temporal regulation of kinesin activity is not completely understood. The affinity to microtubules and, therefore, the velocity of kinesin movement is influenced by posttranslational modifications at microtubules (see chapter 1.4.), which can act as regulatory mechanisms (Dunn et al., 2008).

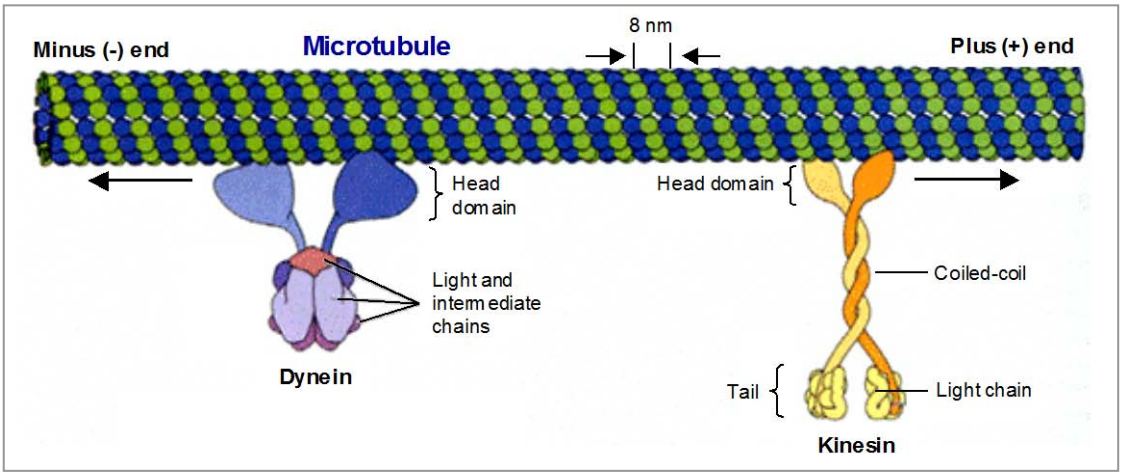

Fig. 6: Schematic molecular structures of kinesin and dynein. Models for the microtubule-based motor proteins kinesin and dynein. The majority of kinesins mediate the intracellular cargo transport on microtubules in plus-end direction, whereas dyneins move towards the minus-end. The illustrated kinesin structure corresponds to the conventional kinesins formed by two heavy and two light chains. The head domain possesses the motor activity, whereas the tail determines the cargo. The coiled-coil region mediates dimerization. Dyneins usually are composed of at least two heavy chains, which form the head domains including the motor and microtubule-binding domains. Additionally, many dyneins are complexed with a number of intermediate, light intermediate and light chains, which mediate cargo interaction (figure from http://bernstein.harvard.edu/research/motor_protein.htm).

Dyneins are the largest and fastest molecular motors and can be divided into two types, the cytoplasmic and the axonemal dyneins. Cytoplasmic dyneins fulfil a broad range of functions in eukaryotic cells, as for example vesicle and organelle transport, Golgi and nucleus localisation, chromosome segregation and orientation of the mitotic spindle. In contrast, axonemal dyneins mainly mediate the beating of cilia and flagella (Vallee et al., 2003). They are composed of up to three heavy chains with a molecular weight of more than 500 kDa each and a variety of intermediate, light

intermediate and light chains. The heavy chains include an N-terminal cargo-binding site as well as the motor domain and the microtubule-binding domain (Wade, 2009). Motor activity is driven by energy from ATP hydrolysis and enables minus-end-directed movement along the microtubule (Fig. 6). Dyneins belong to the AAA protein family and possess a ring of six ATPase domains (AAA1 – AAA6) within the motor domain (Samso et al., 1998). Between AAA4 and AAA5 of the heavy chain the so-called stalk is positioned, which is a 325 amino acid projection with a microtubule-binding site at its tip (Gee et al., 1997). When ATP is bound, the microtubule-binding domain is detached from the microtubule, but gets reattached by a conformational change resulting from the release of ADP and an inorganic phosphate. As a result, the dynein complex moves with a step of 8 nm towards the microtubule minus-end (Alberts et al., 2008). The N-terminal part of dynein heavy chains interacts not only with the respective cargo, but is also responsible for binding of accessory chains.
Particularly intermediate chains interact with the cargo and, additionally, with $p150^{Glued}$, a subunit of the dynactin complex. Since $p150^{Glued}$ interacts with the microtubule plus-end tracking proteins EB1 and CLIP-170, it links the dynein/dynactin complex to microtubule plus-ends (see chapter 1.3.2.). The dynactin complex supports dynein targeting and, therefore, is important for cargo loading and transport initiation. Interestingly, $p150^{Glued}$ is also reported to act as an anchor for the plus-end-directed motors kinesin-2 and kinesin-5 (Blangy et al., 1997; Deacon et al., 2003; Kardon & Vale, 2009; Vaughan & Vallee, 1995; Watson & Stephens, 2006).

1.3.2. Microtubule plus-end tracking proteins

The plus-end tracking proteins (+TIP) form a group of MAPs consisting of unrelated multidomain proteins that, in most cases, associate with growing microtubule plus-ends. In general, these proteins influence microtubule dynamics and mainly act as rescue factors by preventing catastrophes or promoting polymerization resulting in increased microtubule growth and stability. Additionally, +TIPs are involved in the attachment of microtubule ends to cellular structures for targeted microtubule function. In eukaryotes, the most prominent +TIPs are the end binding proteins (EB), the cytoplasmic linker proteins (CLIP), the CLIP-associated proteins (CLASP), Xenopus laevis microtubule-associated protein of 215 kDa (XMAP215) and the dynactin subunit $p150^{Glued}$. The vertebrate +TIPs as well as their homologues in

Saccharomyces cerevisiae (budding yeast) and *Schizo-saccharomyces pompe* (fission yeast) are summarized in Table 1.

Table 1: Vertebrate plus-end tracking proteins with their homologues in budding yeast and fission yeast.

Vertebrates	Budding yeast	Fission yeast	Microtubule-binding domain(s)
EB1, EB2, EB3	Bim1p	Mal3p	Calponin homology domain
CLIP-170, CLIP-115	Bik1p	Tip1p	two CAP-Gly domains
p150^{Glued}	Nip100p	Ssm4p	CAP-Gly domain
Dynein heavy chain	Dyn1	Dhc1	Dynein motor domain
LIS1 (Lissencephaly 1)	Pac1p	-	WD40 repeats
CLASP1, CLASP2	Stu1p	-	TOG domain (HEAT repeats)
XMAP215	Stu2p	Dis1p, Alp14p	TOG domains (HEAT repeats)

Adapted from Lansbergen & Akhmanova, 2006

Besides the microtubule binding itself, the localisation at microtubule plus-ends and the functionality also depend on interactions with other plus-end tracking proteins. Furthermore, dimerization of some +TIPs is rather common. Although all +TIPs bind to microtubule plus-ends, the microtubule-binding domains differ between the +TIP families. Binding of +TIPs is spatially restricted to a 0.5 – 2 µm distal region at the very plus-end, in which the accumulation of +TIP resemble a comet-like structure. As this region appears to be larger than the length of the GTP-cap, binding of +TIPs seems to depend on other differences between the near plus-end region and the microtubule lattice (Akhmanova & Steinmetz, 2008; Van der Vaart, 2009; Wade, 2009). The exact structural property at microtubule plus-ends that is recognized by +TIPs and used as their binding site is still unknown. Since for instance CLIP-170 can bind cytoplasmic tubulin heterodimers, a co-polymerization of +TIPs and tubulin subunits at microtubule plus-ends was proposed (Arnal et al., 2004). Alternatively, it was hypothesized that +TIPs are immobilized at the very plus-end and undergo treadmilling, that is they dissociate when the microtubule end is converted into a lattice structure (Perez et al., 1999). In contrast to that, the current model of +TIP binding to microtubule plus-ends describes a fast turnover instead of a constant binding. Fluorescence recovery after photobleaching (FRAP) experiments showed

reappearance of fluorescence in plus-end comets after bleaching GFP-fused EB3 or CLIP-170. This reappearance implies that bleached GFP-labelled proteins were rapidly exchanged by non-bleached proteins indicating that multiple binding events occur at a single binding site (Bieling et al., 2008; Dragestein et al., 2008). Similar results were also obtained for CLASP2 (Wittmann & Waterman-Storer, 2005). According to the fast exchange model, specific binding sites for +TIPs disappear with further distance to the microtubule plus-end resulting from conformational changes as for instance closure of the terminal protofilament sheet (Fig. 7).

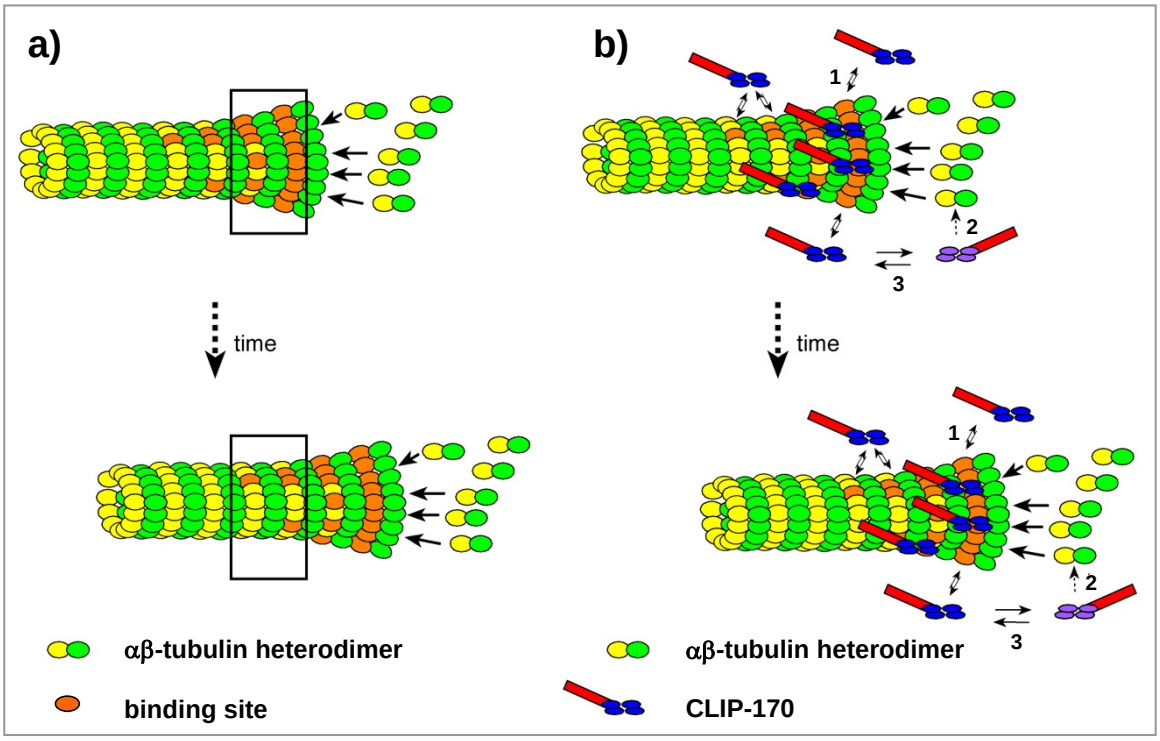

Fig. 7: Fast exchange model for microtubule binding of plus-end tracking proteins.

a) Polymerization of αβ-tubulin heterodimers at the microtubule plus-end generates a large number of potential binding sites for +TIPs (depicted in orange). During microtubule growth, binding sites disappear in further distance from the plus-end most probably due to conformational changes in the microtubule structure as shown in the region marked by the rectangle. **b)** The +TIP CLIP-170 exchanges on binding sites in a rapid manner (reaction 1). By that, a binding site can interact several times with CLIP-170 molecules until it disappears. On the other hand, co-polymerization of CLIP-170 (reaction 2) cannot completely be excluded although it does not explain the comet-like appearance at microtubule plus-ends. Moreover, posttranslational modifications of CLIP-170 could influence its affinity towards tubulin (reaction 3; from Dragestein et al., 2008).

Although +TIPs usually bind to growing microtubule plus-ends, there are a few exceptions. The most prominent +TIP that has the ability to bind depolymerizing microtubule plus-ends is XMAP215, while its *Saccharomyces cerevisiae* homologue Stu2 is able to bind plus-ends of both stable and shrinking microtubules (Lansbergen & Akhmanova, 2006). XMAP215 forms a complex with free tubulin in a 1:1 ratio and is capable of adding up to 25 αβ-tubulin heterodimers to the plus-end before it detaches. By that, XMAP215 functions as a processive microtubule polymerase and inverts depolymerization to polymerization. Especially during mitosis XMAP215 and homologous proteins play a key role in promoting microtubule polymerization for spindle elongation (Brouhard et al., 2008; Severin et al., 2001).

Different mechanisms are engaged to regulate microtubule binding as well as the activity of plus-end tracking proteins. First, several multidomain +TIPs possess the ability to undergo intramolecular interactions and, by that, to inhibit themselves. In that state, the +TIP is not able to localise at microtubule plus-ends and has to be unfolded by the interaction with another ligand. Second, the phosphorylation of amino acid residues within the microtubule-binding domain of +TIPs represents an additional mechanism to reduce the affinity for microtubules, as microtubules carry a negative charge. Finally, posttranslational modifications of the tubulin subunits incorporated in microtubules can influence +TIP localisation as described later.

In the following chapters, the +TIP members of end binding proteins, cytoplasmic linker proteins and cytoplasmic linker protein-associated proteins are described in more detail.

1.3.2.1. End binding proteins

In vertebrates, the family of end binding proteins (EBs) is represented by EB1, EB2 and EB3. The family members are highly conserved, small dimeric proteins consisting of 268, 326 and 281 amino acids, respectively. Microtubule binding is primarily mediated by a globular calponin homology (CH) domain located at the N-terminus and requires the presence of GTP-loaded β-tubulin subunits (Dragestein et al., 2008). The C-terminus contains a coiled-coil domain for parallel dimerization that is essential for EB activity and is connected to the N-terminal CH domain by a flexible linker. Furthermore, the C-terminal amino acid motif EEY/F resembles that of α-tubulin C-terminus and can fold back on the CH domain resulting in an autoinhibitory

conformation. Both the flexible linker and the acidic tail of EB proteins are also involved in microtubule binding, which is based on electrostatic interactions (Zhu et al., 2009). Moreover, the C-terminal tail serves as interaction site for other +TIPs as for instance CLIP-170, p150^{Glued} or the APC (adenomatous polyposis coli) tumor suppressor protein (Bieling et al., 2008; Honnappa et al., 2005; Howard & Hyman, 2003). The CH domain consists of eight α-helices that are packed around the central helix α3 forming a globular structure (Fig. 8). In addition to the acidic tail, the coiled-coil domain is able to bind interaction partners mediated by a hydrophobic cavity and a polar rim (Fig. 8; Honnappa et al., 2005; Slep & Vale, 2007). This specific coiled-coil region comprises approximately 50 conserved amino acids and is typical for EB proteins. Therefore, it is also referred to as end binding homology (EBH) domain (Akhmanova & Steinmetz, 2008).

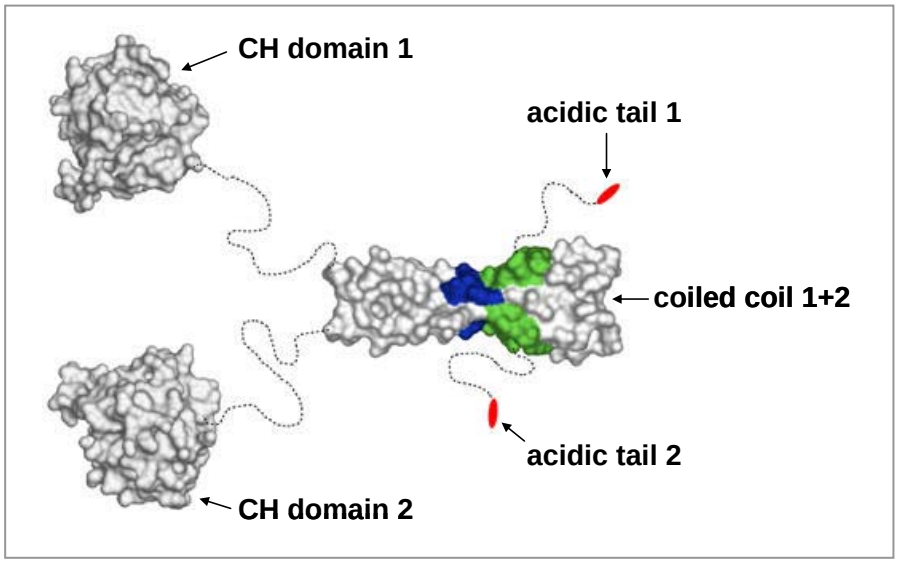

Fig. 8: Structural organization of an EB1 dimer. Surface view of dimerized active EB1. The globular CH domains of monomer 1 and 2 are responsible for microtubule binding. The C-terminal coiled-coil domains of the monomeric proteins dimerize and contain the hydrophobic cavity (green), the polar rim (blue) and the acidic tail (red), which all are important for the interaction with other +TIPs (from Honnappa et al., 2005).

In contrast to the majority of +TIPs, EB proteins are capable of autonomous binding to microtubule plus-ends. As they interact with numerous +TIPs through their acidic C-terminal tail and target them to the microtubule plus-ends, they occupy a central role in the plus-end protein complex.

EB proteins are involved in a large number of cellular functions, particularly by facilitating plus-end binding of other +TIPs. By controlling the plus-end-associated protein complex, EB proteins highly influence microtubule dynamics. Primarily, EB proteins increase the dynamic behaviour of microtubules by inhibiting catastrophes and thereby promoting polymerization and rescue events. As a key-regulator of microtubule dynamics, EB proteins have a major influence on the formation of the mitotic spindle and are involved in the attachment of kinetochores to microtubules. Furthermore, plus-end binding of EB stimulates closure of the terminal sheet-like structure of plus-ends and favours the formation of microtubules consisting of 13 protofilaments. EB proteins additionally stabilize contacts between protofilaments and the lattice seam as demonstrated for the fission yeast EB1 homolog Mal3p. By influencing the structural properties of the microtubule plus-end, EB simultaneously affects the presence of binding sites for other +TIPs (Akhmanova & Steinmetz, 2008; Komarova et al., 2009; Sandblad et al., 2006; Vitre et al., 2008). However, the stimulation of sheet closure by EB can also promote catastrophe, as shown in *Drosophila melanogaster* and for the budding yeast homologue Bim1p (Slep, 2009).
Moreover, EB proteins are essential for the attachment of microtubule ends to the cell cortex by recruiting APC to growing plus-ends, which then mediates the interaction between microtubules and the actin cytoskeleton (Honnappa et al., 2005; Lansbergen & Akhmanova, 2006). Finally, anchoring of microtubules at centrosomes and the formation of cilia in *Clamydomonas* fibroblasts also depend on the involvement of EB proteins (Rehberg and Gräf, 2002; Schröder et al., 2007).
Regulation of EB localisation at microtubule plus-ends and, thereby, of EB activity occurs by phosphorylation. A cluster of six serine residues within the positively charged flexible linker region of the budding yeast EB1 homologue Bim1p was identified as target of the mitotic Aurora B kinase Ipl1p (Zimniak et al., 2009). Here, multiple phosphorylations decreased the affinity of Bim1p for microtubules and resulted in its detachment from plus-ends. Particularly during the mitotic anaphase, Bim1p disassembly from interpolar microtubules plays an important role for a correct spindle elongation. Mutant non-phosphorylatable Bim1p remained at the plus-ends and inhibited depolymerization resulting in an overelongated spindle. Furthermore, Zimniak and colleagues (2009) showed that the flexible linker of Bim1p is essential for its targeting to plus-ends. The flexible linker enhances synergistically with the CH

domain microtubule binding of Bim1p, but alone is not sufficient to facilitate the binding of Bim1p to microtubules.

Another phosphorylation-mediated mechanism for EB regulation is its protection from degradation. Serine residue 176 of human EB3 was identified to be a phosphorylation target of the mitotic kinases Aurora-A and -B. The phosphorylation inhibits the interaction of EB3 with the ubiquitin ligase SIAH-1 and, therefore, protects EB3 from proteasome-mediated degradation. This mechanism ensures the correct cell-cycle progression (Ban et al., 2009).

1.3.2.2. Cytoplasmic linker proteins

The familiy of cytoplasmic linker proteins (CLIP) consists, in vertebrates, of two members, which are termed CLIP-170 and CLIP-115 according to their molecular weights. Notably, CLIP-170 has been discovered as first protein that tracks growing microtubule plus-ends (Pierre et al., 1992). Both CLIP-170 and CLIP-115 are expressed in two splice variants with isoforms A representing the full length proteins consisting of 1428 and 1047 amino acids, respectively. Isoforms B are based on alternatively spliced mRNA that is lacking one exon. Consequently, isoform B proteins lack 35 amino acid residues within the coiled-coil region (www.ncbi.nlm.nih.gov). The CLIP-170 isoform A is also referred to as restin (Galjart, 2005; Griparic & Keller, 1998).

N-terminal cytoskeleton-associated protein glycine-rich (CAP-Gly) domains represent a characteristic of CLIPs. These domains are responsible for interactions with microtubules, EB and the CLIP-170 C-terminus. Whereas the yeast homologues only have one CAP-Gly domain, CLIPs of higher eukaryotes combine two tandem domains at their N-terminus. Both CAP-Gly domains are flanked by serine-rich regions, which also possess low microtubule-binding activities and facilitate the functionality of the CAP-Gly domains (Gupta et al., 2008; Hoogenraad et al., 2000). Next to both CLIPs, also the dynactin subunit $p150^{Glued}$ contains an N-terminal CAP-Gly domain responsible for its interaction with microtubules and CLIP-170. The domain composition of CLIP-115 and CLIP-170 as well as an alignment of human CAP-Gly domain sequences and surface views of CAP-Gly domains are illustrated in Figure 9. CAP-Gly domains possess a highly conserved GKNDG (glycine-lysine-asparagine-aspartic acid-glycine) sequence motif as part of a hydrophobic cavity and

glycine residues for correct folding of the globular domain structure (Fig. 9b and c). In CLIP-170, the GKNDG motif of the first CAP-Gly domain (amino acids 97 – 101) is structurally stabilized by two conserved neighbouring salt bridges within the amino acid pairs arginine 63 – aspartic acid 93 and aspartic acid 100 – arginine 107 (Slep & Vale, 2007). Analogous structural features are conserved in all CAP-Gly domains (Fig. 9b). The C-terminal acidic tails of α-tubulin, EB1-3 and CLIP-170 are characterized by an EEY/F motif, which could serve as a specific interaction target for the GKNDG motif of CAP-Gly domains (Fig. 9d; Honnappa et al., 2006). Nevertheless, CLIP-170 has been shown to bind regions of α-tubulin and β-tubulin different from the acidic tail (Gupta et al., 2010).

The by far largest part of both CLIPs comprises a coiled-coil domain that mediates parallel homodimerization. In contrast to CLIP-115, CLIP-170 contains two metal-binding zinc knuckles at its C-terminus. Since the zinc knuckles are able to interact with CAP-Gly domains, they can fold back on the intramolecular CAP-Gly domains. Consequently, the coiled-coil region is folded and the CLIP-170 molecule transferred to an inactive, closed conformation. Interestingly, the first CLIP-170 zinc knuckle is preferentially involved in autoinhibition by binding to its second CAP-Gly domain, whereas the second zinc knuckle primarily interacts with the CAP-Gly domains of CLIP-115 and $p150^{Glued}$ (Lansbergen et al., 2004; Mishima et al., 2007).

Although the first and second CAP-Gly domains of CLIP-170 share 97 % similarity, structure analyses revealed a more positively charged groove in the second CAP-Gly domain compared with the first CAP-Gly domain due to additional basic amino acids. Therefore, the second CAP-Gly domain binds the negatively charged acidic tails of α-tubulin and EB1/EB3 more tightly. In contrast, the first CAP-Gly domain of CLIP-170 and the $p150^{Glued}$ CAP-Gly domain show weaker affinities for the acidic α-tubulin and EB tails (Mishima et al., 2007). As the CAP-Gly domains of CLIP-115 are highly similar to their respective counterparts in CLIP-170, they most likely possess similar binding properties (see Fig. 9b and Hoogenraad et al., 2000).

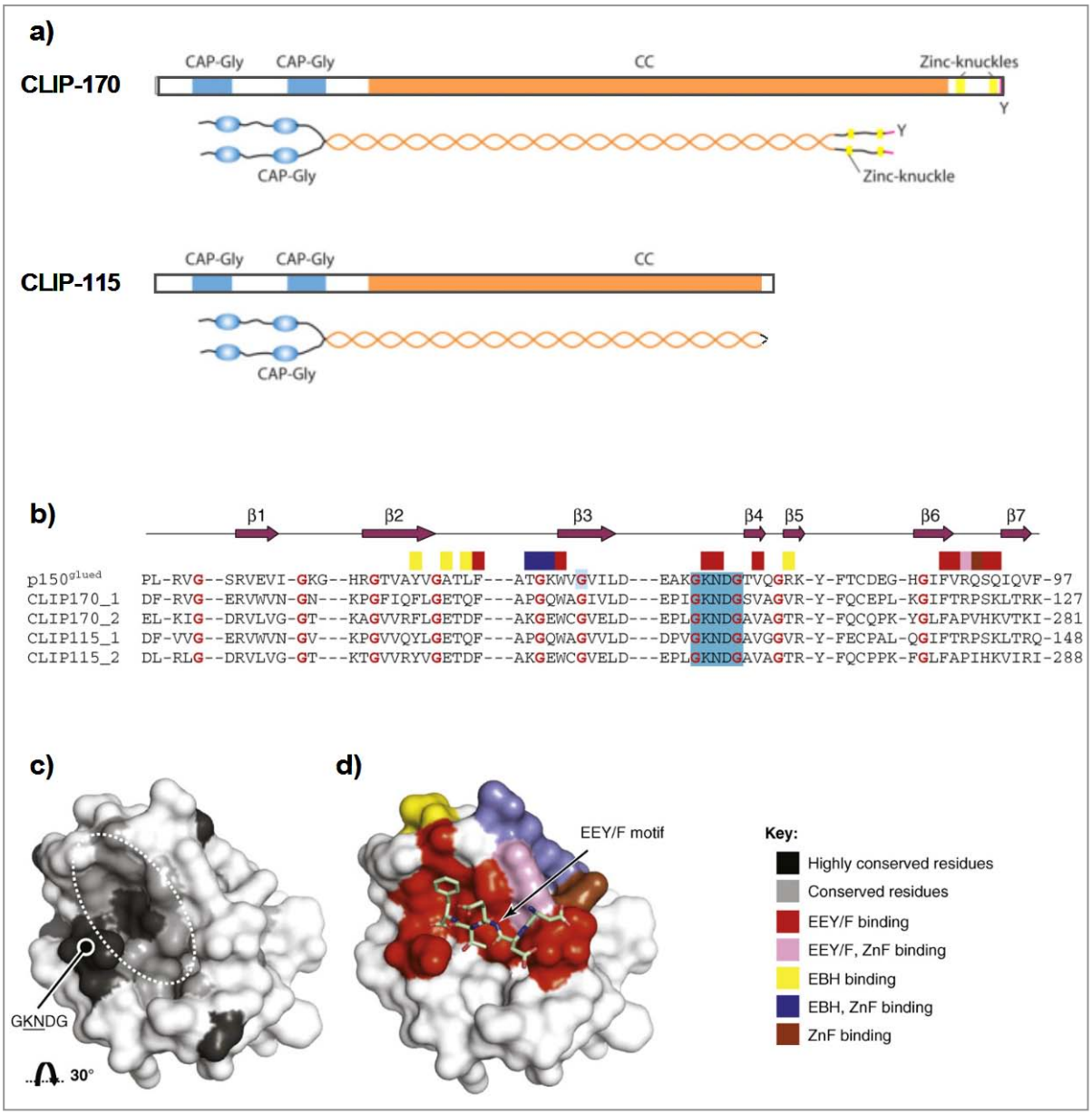

Fig. 9: Domain organization of CLIPs, conserved human CAP-Gly domain sequences, overall structure and interaction mode of a CAP-Gly domain. a) Scheme of CLIP-170 and CLIP-115 domain compositions with the respective dimers (from Bieling et al., 2008). **b)** Sequence alignment of the CAP-Gly domains from human p150^{Glued}, CLIP-170 and CLIP-115. The characteristic GKNDG motif is highlighted in light blue, whereas glycine residues are highlighted in red. Coloured boxes above the alignment mark residues involved in protein interactions as illustrated by the colour key in d. **c)** Surface view of a CAP-Gly domain with highly conserved and conserved residues in black and grey, respectively. The hydrophobic cavity is marked by the dashed oval. **d)** Surface view of the p150^{Glued} CAP-Gly domain in complex with the EEY/F motif of the C-terminal acidic tail of CLIP-170. The colours correspond to the colours given in the alignment (from Steinmetz & Akhmanova, 2008).

By binding tubulin, CLIPs neutralize the negative charge of the acidic tubulin tails and stimulate microtubule polymerization as well as nucleation. Thus, the most prominent function of CLIPs is their contribution to microtubule dynamics as rescue factors. Both CLIP-170 and CLIP-115 redundantly promote the shift from microtubule shrinkage into growth. However, the exact mechanism how CLIPs trigger rescue events still remains unclear according to their restricted localisation to growing microtubule plus-ends instead of depolymerizing ends (Galjart, 2005). As CLIP-170 recruits $p150^{Glued}$ via its second zinc knuckle, it links the dynein/dynactin motor complex to the growing microtubule plus-ends and, therefore, supports intracellular trafficking towards the minus-ends as well as correct positioning of the mitotic spindle (Weisbrich et al., 2007). Besides linking the dynein/dynactin motor complex to microtubule plus-ends, CLIP-170 additionally interacts with membrane organelles facilitating minus-end-directed organelle transport by loading them onto dynein motors (Lomakin et al., 2009). In prometaphase of mitosis, CLIP-170 binds unattached kinetochore protein complexes through its C-terminus and subsequently links them to microtubules (Coquelle et al., 2002). CLIP-170 forms a complex with IQGAP1, an effector of the small GTPases Cdc42 and Rac1. This CLIP-170/IQGAP1 complex links microtubules to the cortical actin network and contributes to cell polarization (Fukata et al., 2002; Gundersen, 2002). Moreover, through its metal-binding domains CLIP-170 recruits the actin-nucleating formin mDia1 to places of phagocytosis. The enrichment of mDia1 results in local actin polymerization underneath the plasma membrane and, by that, triggers phagocytosis (Lewkowicz et al., 2008).

Interestingly, a hemizygous CLIP-115 deletion is involved in a genetical disorder reffered to as Williams syndrome. The CLIP-115 gene (CYLN2, cytoplasmic linker protein gene 2) is located in a chromosomal region of approximately 1.6 Mb called the Williams syndrome critical region (WSCR). This region contains, besides *CLIP-115*, at least 16 genes and is assumed to be deleted by incorrect recombination resulting in the Williams syndrome. Symptoms of this haploinsufficiency are growth defects, brain abnormalities, hippocampal dysfunction and defective motor coordination resembling the phenotype of *CLIP-115* knockout mice (Hoogenraad et al., 2002). Furthermore, depletion of CLIP-115 leads to increased accumulation of dynactin and CLIP-170 at microtubule plus-ends (Hoogenraad et al., 2002). Hence,

an additional role of CLIP-115 as regulator of CLIP-170 function by competitive inhibition via the metal-binding domains can be taken into account.

Several factors are known to regulate CLIP-115 and CLIP-170 localisation at microtubule plus-ends. In contrast to EB proteins, full length CLIP-170 is not able to bind microtubules autonomously and requires the presence of EB1 or EB3 at the growing plus-end to become activated from its autoinhibited state *in vivo* (Komarova et al., 2005; Bieling et al., 2008). Autoinhibition acts as a negative regulatory mechanism for CLIP-170 binding to microtubule plus-ends, whereas CLIP-115 is not capable of autoinhibition since it lacks metal-binding domains. However, CLIP-115 localisation at microtubule plus-ends has also been reported to be strongly facilitated by EB1 and EB3 (Komarova et al., 2005). The fission yeast homologue of CLIP-170 even is transported to the microtubule plus-ends by a kinesin, which is recruited to the plus-ends by the EB1 homologue (Bieling et al., 2007). As for EB proteins, phosphorylation plays an important role in CLIP regulation. CLIP-170 is known to be phosphorylated at multiple sites by different kinases. For instance, cdc2 phosphorylates threonine residue 287 resulting in correct plus-end localization of CLIP-170 during the later phases of the cell cycle (Yang et al., 2009). Another kinase that stimulates microtubule binding of CLIP-170 is the FKBP12-rapamycin-associated protein (FRAP). However, it was also demonstrated that phosphorylation of CLIP-170 leads to its dissociation from microtubules (Choi et al., 2002; Hoogenraad et al., 2000; Rickard & Kreis, 1991). CLIP-115 phosphorylation also reduces the capacity to bind microtubules, as demonstrated by *in vitro* experiments (Hoogenraad et al., 2000). Furthermore, posttranslational modifications of microtubules influence CLIP-115 and CLIP-170 binding. Microtubule association of CLIPs and other CAP-Gly domain-containing proteins was reported to depend on the C-terminal tyrosine of the α-tubulin subunit, as the affinity for detyrosinated α-tubulin is much lower (Bieling et al., 2008; Peris et al., 2006; see also chapter 1.4.1.).

1.3.2.3. Cytoplasmic linker protein-associated proteins

In mammals, two cytoplasmic linker protein-associated proteins (CLASP1 and CLASP2) were identified by yeast two-hybrid experiments (Akhmanova et al., 2001). Both proteins directly interact with CLIPs, EB proteins, microtubule plus-ends and the Golgi apparatus. The CLASPs appear in several isoforms (CLASP1/2α, -2β and -2γ)

with differences in their respective N-termini resulting from alternative splicing. CLASP1 isoforms are expressed ubiquitously, whereas CLASP2 isoforms are predominantly present in the brain.

In general, all CLASP isoforms contain a basic serine- and arginine-rich domain that can bind to growing microtubule plus-ends and EB1/3. Moreover, CLASP localisation to the microtubule lattice in the lamella of migrating PtK1 cells has been reported through this region (Wittmann & Waterman-Storer, 2005). The conserved C-terminus mediates interactions with CLIPs, the Golgi apparatus and the cell cortex (Mimori-Kiyosue et al., 2005). It includes huntingtin elongation factor-3, protein phosphatase-2A and target of rapamycin (HEAT) repeats, which are also present in the N-terminal regions and function as protein interaction sites (see Fig. 10a). CLASP1α and CLASP2α are the longest isoforms, which possess an additional N-terminal Tumour-overexpressed gene (TOG)-like domain (Fig. 10a). By that, they resemble the TOG domain-containing *Drosophila melanogaster* homologue Orbit/multiple asters (MAST). TOG domains usually contain six HEAT repeats, each comprised of a pair of parallel helices (Fig. 10b). The loops connecting the helices contain conserved lysine residues as well as a conserved arginine and tryptophan residue creating a positive charge that mediates CLASP binding to tubulin monomers as well as polymerized microtubules. Generally, TOG domains serve as microtubule interaction sites in XMAP215 family proteins that stabilize microtubules and promote polymerization at microtubule plus-ends. (Brouhard et al., 2008; Severin et al., 2001; Slep & Vale, 2007). Besides direct microtubule binding through their central serine-rich region, CLASP1/2 recruitment to plus-ends is enhanced by interactions with CLIPs and EB proteins (Mimori-Kiyosue et al., 2005). Interestingly, the brain-specific CLASP2β isoform contains an N-terminal palmitoylation motif that includes two cysteines as attachment sites for palmitate, a saturated fatty acid that targets the protein to membranes (Akhmanova et al., 2001).

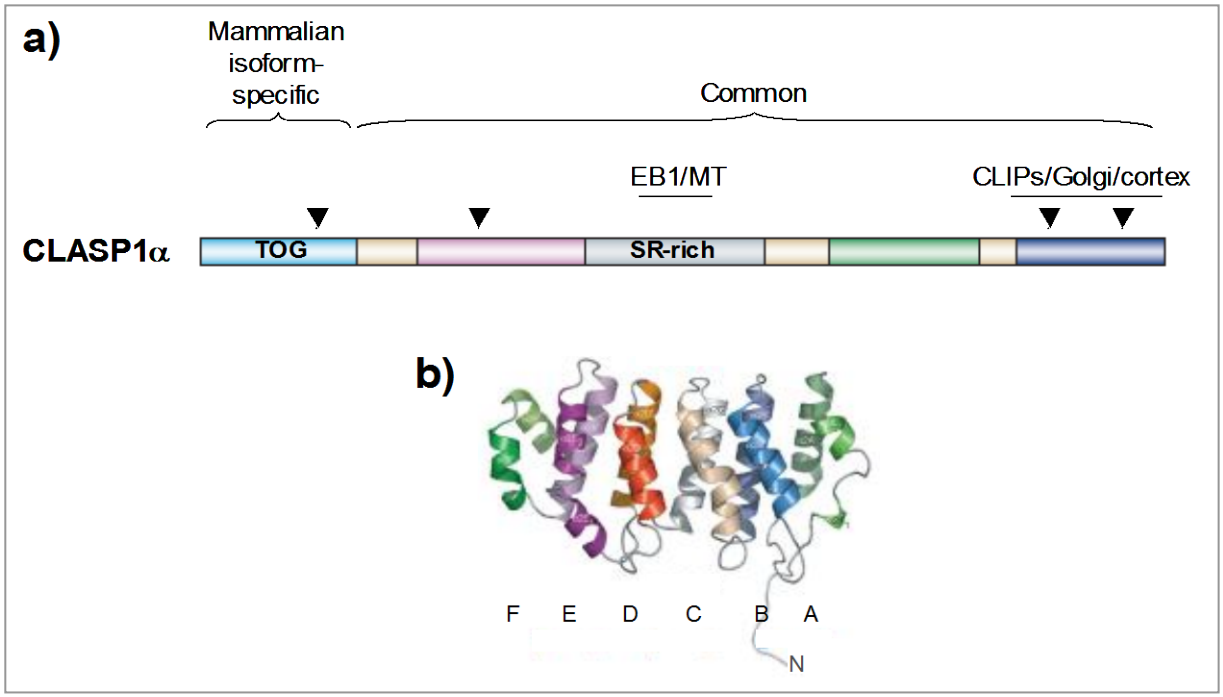

Fig. 10: Domain organization of CLASP1α and TOG domain structure. a) CLASP1α is the longest CLASP isoform and possesses the same domain structure as its *Drosophila melanogaster* homologue, Orbit/MAST. The N-terminal domain, which is isoform-specific in mammals, contains a TOG-like domain similar to those in microtubule-stabilizing proteins of the XMAP215 family. The central serine-rich domain contributes to the interaction with EB1 and microtubules (MT), whereas the C-terminus interacts with CLIPs, the Golgi apparatus and cell cortex components. Arrowheads indicate positions of potential HEAT repeats, which mediate protein interactions. Conserved domains are labelled in different colours (adapted from Galjart, 2005). **b)** Ribbon diagram of the second TOG domain from Stu2p, the XMAP215 homologue of *Saccharomyces cerevisiae*, showing the six parallel helix pairs of the HEAT repeats (A – F) and the connecting loops (from Slep & Vale, 2007).

In contrast to CLIPs, which promote microtubule rescue events throughout the entire cell, the functions of CLASPs are spatially restricted to the mitotic spindle and the cell cortex. Respective homologues in *Saccharomyces cerevisiae* (Stu1p), *Drosophila melanogaster* (Orbit/MAST) and *Caenorhabditis elegans* (cls-2) all are associated with the mitotic spindle and play essential roles during mitosis. Orbit/MAST is the best investigated family member and, besides maintaining the bipolarity of the mitotic spindle, is involved in kinetochore attachment, chromosome alignment and cytokinesis by stabilizing interior spindle microtubules (marked by a “C” in Fig. 3; Inoue et al., 2004; Maiato et al., 2002). Also mammalian CLASPs are present at kinetochores and fulfil comparable functions as illustrated by the formation of

monopolar spindles in cells microinjected with CLASP1-specific antibodies (Maiato et al., 2003). In migrating fibroblasts, CLASPs mainly localise to microtubule plus-ends at the leading edge of the cell. By capturing microtubules at the cell cortex through an interaction with the cortex-associated proteins LL5β and ELKS (Lansbergen et al., 2006), CLASPs contribute to cell polarization. Moreover, CLASP2α has been shown to bind filamentous actin via both its N-terminal TOG-like domain and the central serine-rich region (Tsvetkov et al., 2007). Therefore, it links the microtubule plus-ends to the actin cytoskeleton in the cell cortex and supports cell polarization.

The main function of CLASPs at dynamic microtubule plus-ends is to promote pausing, or rather shorten the phases of growth and shrinkage. During catastrophe, CLASPs partially remain at the shrinking end and recruit EB1 resulting in stimulation of rescue events (Lansbergen & Akhmanova, 2006). As demonstrated by RNA interference experiments, CLASPs stabilize microtubules and, as a consequence, levels of acetylated and detyrosinated tubulin are increased. Since CLASP knockdown additionally leads to a reduction of microtubule density and CLASPs also localise to centrosomes, an additional function in microtubule nucleation can be assumed. Knockdown of either CLASP1 or CLASP2 alone did not result in the described effects, and the double knockdown phenotype could be rescued by the expression of only one of both CLASPs demonstrating functional redundancy for both proteins (Mimori-Kiyosue et al., 2005).

The binding of CLASPs to microtubules is regulated by phosphorylation through the glycogen synthase kinase-3β (GSK3β). Analogous to structural MAPs (see chapter 1.3.1.1.), phosphorylation decreases the affinity for microtubules and leads to dissociation of CLASPs. Thus, the spatial activity of GSK3β regulates the subcellular microtubule-binding pattern of CLASPs. In migrating epithelial cells, a high GSK3β activity in the cell body restricts CLASPs to microtubule plus-ends, whereas local GSK3β inactivation results in microtubule lattice binding in the very distal region of the leading edge (Wittmann & Waterman-Storer, 2005). Furthermore, the presence of distinct motifs for microtubule plus-end binding and lattice association within the microtubule-binding domain of CLASP2 could be shown. Only the motif responsible for plus-end binding is phosphorylated by GSK3β at multiple sites. Partial phosphorylation of this motif reduces the affinity for the microtubule lattice, whereas

the phosphorylation of all included sites results in the complete inhibition of microtubule plus-end binding as well as EB1 interaction (Kumar et al., 2009).

1.4. Posttranslational modifications of tubulin

As described in the previous chapter, microtubule functions are widely regulated by microtubule-associated proteins. Additionally, posttranslational modifications of the incorporated α- and/or β-tubulin subunits contribute to the regulation of interactions with MAPs and therefore directly influence microtubule functions. Posttranslational modifications also affect microtubule dynamics, for example by altering interactions with +TIPs. In general, stable microtubules accumulate more posttranslational modifications than dynamic microtubules. The physiological impact of the tubulin modifications and the involved enzymes are still poorly understood (Hammond et al., 2008). A schematic overview of posttranslational modifications concerning α- and β-tubulin subunits is shown in Figure 11.

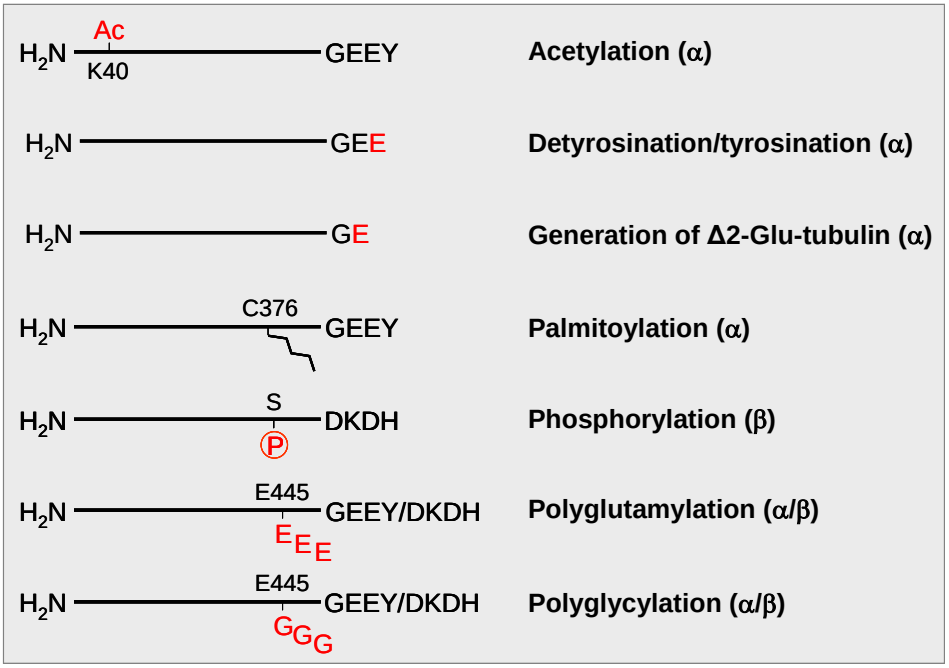

Fig. 11: Overview of posttranslational modifications of tubulin. Several posttranslational modifications affect microtubule dynamics and functions. Tubulin molecules are illustrated schematically from their N-termini to the acidic C-termini according to the amino acid sequence of mouse tubulin 1. The respective modifications are highlighted in red, whereas the modified tubulin subunit (α and/or β) is added in brackets. Numbers give the position of the affected amino acid in the

tubulin molecule. Abbreviations: Ac = acetate; C = cysteine; D = aspartic acid; E = glutamic acid; G = glycine; H = histidine; K = lysine; P = phosphate; S = serine; Y = tyrosine (adapted from Westermann & Weber, 2003).

Apart from the generation of Δ2-Glu-tubulin all posttranslational modifications are reversible. Moreover, modifications usually occur at the microtubule surface and directly influence interactions with binding partners, except for acetylation, which affects the lumen-exposed lysine residue 40 of α-tubulin but still influences interactions. The following chapters describe the respective modifications in more detail.

1.4.1. Acetylation

Besides being the only posttranslational modification that takes place in the microtubule lumen, acetylation also represents the only modification that appears in the N-terminal region. Acetylation occurs at a conserved lysine residue (K40) of α-tubulin after being incorporated into microtubules. Hence, it mainly accumulates on stable microtubules and can be used as a marker for their stability. Although the enzyme that acetylates microtubules is still unknown, two deacetylases were identified. Both the histone deacetylase 6 (HDAC6) and sirtuin type 2 (SIRT2, human orthologue of the silent information regulator 2 protein from *Saccharomyces cerevisiae*) were shown to deacetylate α-tubulin (Matsuyama et al., 2002; North et al., 2003). As mutation of the acetylated lysine residue as well as suppression of general acetylation activity did not lead to an obvious phenotype, the function of microtubule acetylation appears to be non-essential. However, kinesin-1 association to microtubules and, thereby, kinesin-mediated transport is promoted by microtubule acetylation (Reed et al., 2006).

1.4.2. Palmitoylation and phosphorylation

Palmitoylation has been mapped to occur predominantly at cysteine residue 376 of α-tubulin. The involved enzymes and the exact cellular function of this posttranslational modification still remain unclear. A reduction of the palmitoylation level by mutating the involved cysteine in *Saccharomyces cerevisiae* evoked a high number of astral microtubules with an abnormal length or wrong orientation.

Furthermore, the spindle translocation through the bud neck appeared defective, while mitosis itself was not affected. Thus, microtubule palmitoylation could be involved in astral microtubule organization during mitosis (Caron et al., 2001; Hammond et al., 2008).

Phosphorylation occurs either at serine residue 441 or 444 of β-tubulin. Although the phosphorylated serine is located in the acidic C-terminal tail that is important for microtubule interactions, a clear physiological relevance is not known yet. As the acidic tubulin tail already is negatively charged, the introduction of a phosphate and thereby an additional negative charge may not have a major effect on microtubule function (Westermann & Weber, 2003). Interestingly, also unpolymerized tubulin heterodimers can be phosphorylated. During early mitosis, the cyclin-dependent kinase 1 (Cdk1) phosphorylates serine residue 172 of β-tubulin subunits and, by that, inhibits their incorporation into microtubules (Fourest-Lieuvin et al., 2006).

1.4.3. Polyglutamylation and polyglycylation

Polyglutamylation as well as polyglycylation appear in the acidic C-terminal tail of both α- and β-tubulin predominantly at the conserved glutamate residue 445. As both modifications could be identified at the same tubulin subunit, the existence of multiple modification sites in the neighbourhood of glutamate 445 is very likely (Hammond et al., 2008).

Polyglutamylation involves the attachment of up to 20 acidic glutamate residues as a tubulin side-chain and mainly occurs in neurons and stable microtubule structures like axonemes, centrioles and the mitotic spindle. In mammals, eight tubulin glutamylases are identified. They belong to the family of tubulin-tyrosine-ligase-like (TTLL) domain-containing proteins and possess different specificities for α- and β-tubulin isotypes. Glutamylase activity has been shown for TTLL1, 4 – 7, 9, 11 and 13, which either catalyse the initiation or the elongation of the polyglutamate chain (Etienne-Manneville, 2009; Hammond et al., 2008). Polyglutamylation influences interactions between microtubules and their associated proteins, most probably by increasing the negative charge of the microtubule lattice. For example, α-tubulin polyglutamylation promotes the loading of kinesin-3, whereas kinesin-1 association is promoted by polyglutamylated β-tubulin. Moreover, polyglutamylation marks

microtubules for severing proteins. The mutation of polyglutamylation sites in β-tubulin decreased katanin-mediated microtubule cleavage and inhibited the completion of cytokinesis in the ciliate protozoa *Tetrahymena thermophila* (Sharma et al., 2007). Besides affecting microtubule-protein interactions, polyglutamylation plays an important role in axonemal structures, and its inhibition results in defective cilia and flagella motility (Hammond et al., 2008; Westermann & Weber, 2003).

The addition of up to 34 neutral glycine residues in polyglycylation of both α- and β-tubulin occurs at the same glutamate residues as the aforementioned polyglutamylation. It is predominantly found at axonemal microtubules and is the most common tubulin modification in mammalian sperm cells. Analogous to polyglutamylation, the glycylation reactions are most probably catalysed by the TTLL domain containing proteins TTLL3, 8, 10 and 12 (Etienne-Manneville, 2009). Interestingly, the indicated functions of polyglycylation resemble those of polyglutamylation, although the respective polypeptide chains are differently charged. Accordingly, site-directed mutagenesis experiments in *Tetrahymena thermophila* demonstrated a major role of polyglycylation in the assembly and maintenance of axonemes, the motility of cilia and flagella and in cytokinesis (Thazhath et al., 2002; Xia et al., 2000).

1.4.4. Detyrosination/tyrosination and generation of Δ2-Glu-tubulin

When α-tubulin is incorporated in microtubules, the C-terminal acidic tail is placed in an exposed position at the microtubule surface. A still unidentified carboxypeptidase then is able to remove the extreme C-terminal tyrosine residue from the α-tubulin subunits. This reaction generates detyrosinated α-tubulin subunits with a C-terminal glutamic acid residue, which are also called Glu-tubulin. Accordingly, stable microtubules are rich of Glu-tubulin, whereas dynamic microtubules contain predominantly tyrosinated tubulin (Tyr-tubulin). After disassembly of the Glu-tubulin subunits from the depolymerizing microtubule, the tubulin-tyrosine ligase (TTL) adds a new tyrosine residue to the C-terminal glutamic acid. Consequently, Tyr-tubulin is restored and can again be incorporated in microtubules. The tubulin-tyrosine ligase belongs to the glutathione-synthetase ADP-forming enzymes, which are characterized by an ATP-dependent ligase activity (Galperin & Koonin, 1997).

Surprisingly, the TTL binds to the β-tubulin subunit of the soluble heterodimers and catalyzes the tyrosination of the α-tubulin subunit (Wehland & Weber, 1987a). Since the TTL-binding site on β-tubulin most probably is masked in microtubules, only non-assembled heterodimers can be a substrate of the TTL. As the α-tubulin subunits cycle through alternating detyrosination and tyrosination events, this process is also referred to as tyrosination cycle of α-tubulin (Fig. 12). Newly synthesized α-tubulin always possesses the C-terminal tyrosine, since this residue is genetically encoded. Additionally, the C-terminal glutamic acid residue of Glu-tubulin can be removed by the activity of an unknown peptidase. This reaction generates Δ2-Glu-tubulin, which is not a substrate of TTL (Paturle-Lafanechère et al., 1991; Rüdiger et al., 1994; Westermann & Weber, 2003).

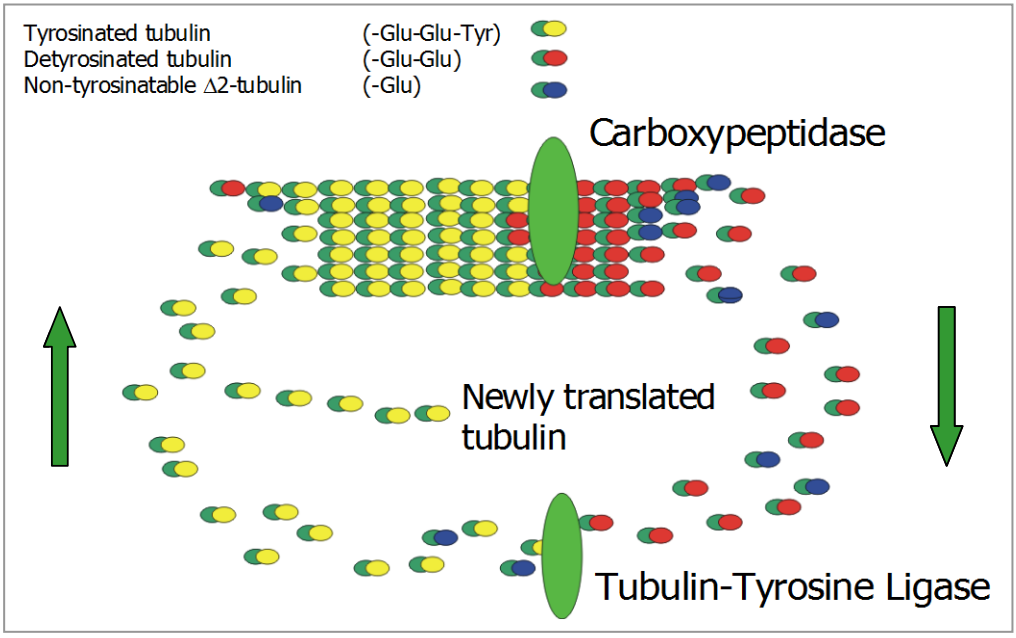

Fig. 12: Tyrosination cycle of α-tubulin. Newly translated tubulin subunits assemble to microtubules. A yet unknown carboxypeptidase removes the C-terminal tyrosine residue of α-tubulin from the incorporated tubulin subunits resulting in detyrosinated tubulin (Glu-tubulin). After depolymerization, the tubulin-tyrosine ligase can re-add a tyrosine residue to the soluble Glu-tubulin subunits, thus, generating tyrosinated tubulin (Tyr-tubulin) that can be incorporated in the microtubule again. Glu-tubulin can also lose the C-terminal glutamic acid resulting in Δ2-Glu-tubulin that cannot be tyrosinated. The pool of Tyr-tubulin is steadily filled by ongoing protein biosynthesis.

As detyrosinated tubulin predominantly occurs in stable microtubules, detyrosination was at first assumed to be a modification for microtubule stabilization. But, notably, detyrosination is only a concomitant effect of stable microtubules and does not stabilize microtubules by itself (Webster et al., 1990). The formation of detyrosinated microtubules has also been connected with interactions with the actin cytoskeleton and the intermediate filament system. Detyrosination can be triggered by a signal transduction cascade via Rho GTPases, which can also influence actin-based cellular functions. Furthermore, vimentin intermediate filaments co-localise preferentially with detyrosinated microtubules (Cook et al., 1998; Gurland & Gundersen, 1995). In vertebrate cancers, tumour progression is accompanied by decreased TTL activity resulting in high levels of Glu-tubulin and reduced Tyr-tubulin levels (Lafanechère et al., 1998; Mialhe et al., 2001).

In order to gain more insight into the physiological importance of the tyrosination cycle, *TTL* knockout mice were generated (Erck et al., 2005). As a consequence of ongoing protein biosynthesis, proliferating cells that lack TTL contain a residual pool of Tyr-tubulin. In contrast, postmitotic cells like neurons, in which reduced protein synthesis occurs, lack Tyr-tubulin. Interestingly, TTL-deficient cells show a correctly organized microtubule network. Although homozygous *TTL* knockout mice pass a normal embryonic development, newborns die within 24 hours after birth. Histological analyses of embryonic organs revealed a disorganized structure of the cortical layers in brains derived from 19.5 days old *TTL* knockout embryos (Fig. 13). During embryogenesis developing neurons migrate in radial direction through the cortex and establish the characteristic layered pattern (see scheme and wild type brain section in Fig. 13). Obviously, this layer formation in *TTL* knockout mice is defective and, moreover, is accompanied by a higher apoptosis rate resulting in the generation of enlarged ventricles. In addition, neuronal differentiation is affected by TTL deficiency. Neurons lacking TTL show erratic neurite growth and shrinkage as well as a premature and abnormal axonal development. Furthermore, the microtubule plus-end tracking protein CLIP-170 is mislocalised in *TTL* knockout neurons, whereas the distribution of EB1 remains unaffected. Compared to wild type neurons, CLIP-170 is strongly reduced in neurite extensions and growth cones.

In fibroblasts lacking TTL, a general mislocalisation of +TIPs containing CAP-Gly domains is reported. CLIP-170, CLIP-115 and $p150^{Glued}$ are unable to bind to

microtubule plus-ends in *TTL* knockout mouse embryonic fibroblasts (MEF), which completely lack tyrosinated tubulin. On the other hand, the localisation of EB proteins and CLASPs is unaffected (Peris et al., 2006). Moreover, defective cell polarization and spindle positioning is prominent in TTL-deficient MEFs. These results indicate a major role of CAP-Gly domain-containing +TIPs in cell migration and spindle orientation by linking microtubule plus-ends to the cell cortex. Finally, detyrosination also influences microtubule interactions with motor proteins, as shown by preferential binding of kinesin-1 to detyrosinated microtubules (Liao & Gundersen, 1998).

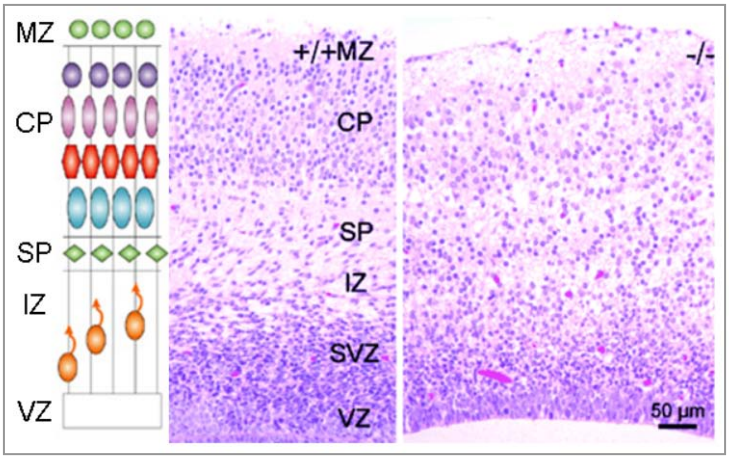

Fig. 13: *TTL* knockout leads to disorganization of cortical layers in the murine brain.
Coronal brain sections show the cortical layer organization in brains from 19.5 days old wild type and *TTL* knockout mice. Note the disordered layering in brains derived from *TTL* knockout mice. Abbreviations: MZ = mantle zone; CP = cortical plate zone; SP = subplate zone; IZ = intermediate zone; SVZ = subventricular zone; VZ = ventricular zone (from Erck et al., 2005, and Gupta et al., 2002).

1.5. Aim of this study

The aim of this thesis was the characterization of fibroblasts lacking the tubulin-tyrosine ligase in order to reveal the physiological impact of the tyrosination cycle. So far, irregular cell polarization and migration were assumed to be regulated by tubulin tyrosination. The recent generation of *TTL* knockout mice has opened a wide field of possibilities to unravel the cellular functions that are influenced by the tyrosination status of α-tubulin. A strong neuronal phenotype accompanied with severe malformations of the brain could be observed in *TTL* knockout mice (Erck et

al., 2005), whereas other cell types seemed not to be affected. To study the influence of the tubulin tyrosination cycle in a more simple cell system, both immortalized and primary mouse embryonic fibroblasts (MEFs) were analysed. Since ongoing protein biosynthesis serves for a residual pool of tyrosinated tubulin in *TTL* knockout cells, one aspect of this study was to obtain a comprehensive depletion of Tyr-tubulin in TTL-deficient fibroblasts. For that, chemical treatments and microinjection of antibodies that specifically bind to the tyrosinated α-tubulin C-terminus and block remaining functional Tyr-tubulin subunits were performed. To ascertain the putative influence of TTL deficiency on cell polarization and migration, cells with reduced Tyr-tubulin levels were investigated in wound-healing assays.

Peris and collegues (2006) published that CAP-Gly domain-containing +TIPs only bind to tyrosinated microtubules, since these +TIPs are unable to bind microtubule plus-ends in *TTL* knockout MEFs lacking tyrosinated tubulin. As described in chapter 1.3.2., +TIPs play a major role in regulating microtubule dynamics and functions. This indicates that impaired microtubule binding of CAP-Gly domain-containing +TIPs in the absence of TTL would massively affect microtubule-dependent cellular processes. Moreover, the exact mechanism of +TIP/microtubule binding and the regulation of these interactions are still poorly understood. Therefore, in the presented study major focus was appointed to the characterization of wild type and TTL-deficient cells regarding the microtubule plus-end tracking proteins CLIP-170, CLIP-115 and EB1 by using biochemical and immunological methods. The absence of TTL and the subsequent lack of Tyr-tubulin resulted in differences in the phosphorylation status and the subcellular localisation of CLIP-115. Site-directed mutagenesis experiments on CLIP-115 were performed to unravel potential mechanisms of plus-end tracking and to functionally analyse the involvement of single amino acid residues in CLIP-115/microtubule association. Finally, mass spectrometry analyses of CLIP-115 were used to corroborate the results obtained by site-directed mutagenesis and to identify additional putative phosphorylation sites.

2. Material and Methods

2.1. Chemicals and reagents

All used chemicals and reagents were, if not specified separately, obtained from Becton, Dickinson and Company (BD), Bio mol, Biontex, Bio-Rad, Clontech, Fluka, GE Healthcare, Gibco, Interchim, Invitrogen, Lonza, Macherey-Nagel, Mallinckroth Baker B.V., MBI Fermentas, Merck, Pierce, Promega, Qiagen, Riedel-de Haën, Roche, Roth, Serva, Sigma-Aldrich and Stratagene.

2.2. Media and plastic ware for cell culture

Media and additives from Gibco and Sigma-Aldrich were used for cell culturing. Plastic ware was purchased from Corning, Falcon and Nunc. Tubes, reaction cups, sterile pipettes and pipette tips were obtained from Eppendorf, Greiner, Sarstedt, Sterilin and Thermo Scientific.

2.3. Bacterial culture

2.3.1. Bacterial strains

Escherichia coli (*E. coli*) TG2 cells (Stratagene) were used for amplification of plasmids and constructs. Highly competent *E. coli* XL1-Blue supercompetent cells and *E. coli* Top10 competent cells were from Stratagene and Invitrogen, respectively.

2.3.2. Media for bacterial culture

All ingredients were solved in deionised water (H_2O_{deion}) followed by sterilization by autoclaving. When necessary, 100 µg/ml ampicillin or 50 µg/ml kanamycin was added.

LB medium (Luria Bertani broth):

10 g/l Bacto-tryptone

5 g/l Bacto-yeast extract

10 g/l NaCl

LB-Agar plates:

16 g Agar

in 1 l of LB medium

SOB medium:

20 g/l Bacto-tryptone

5 g/l Bacto-yeast extract

0.6 g/l NaCl

0.19 g/l KCl

SOC medium:

SOB medium with

10 mM $MgCl_2$

10 mM $MgSO_4$

2 mM glucose

2.3.3. Growth conditions

E. coli cultures were incubated at 37 °C overnight. Liquid cultures were additionally shaken at 180 rpm.

2.4. Molecular biological methods

2.4.1. Plasmids and constructs

Plasmids and constructs used in this study are listed in Table 2. Full length *CLIP-115* was ordered from ImaGenes GmbH (AccNo. BC053048, isoform b).

Table 2: Plasmids and constructs used in this study.

Name	Resistance	Use	Source
pEGFP-C1	Kanamycin	cloning of *CLIP-115* C-terminus	Clontech
pEGFP-C3	Kanamycin	cloning of *CLIP-115* full length	Clontech
pEGFP-N1	Kanamycin	cloning of *CLIP-115* full length	Clontech
pEGFP-N3	Kanamycin	cloning of *CLIP-115* C-terminus	Clontech
pEGFP-Actin	Kanamycin	testing transfection reagents	P. Hagendorff

pmRFP-Actin	Kanamycin	testing transfection reagents; EGFP in original plasmid (pEGFP) was substituted by mRFP	P. Hagendorff
pEGFP-C1-CLIP-115 C-terminus	Kanamycin	testing polyclonal anti-CLIP-115 antibodies (C. Erck)	this study
pEGFP-C3-CLIP-115	Kanamycin	site-directed mutagenesis	this study
pEGFP-N1-CLIP-115	Kanamycin	site-directed mutagenesis	this study
pEGFP-N3-CLIP-115 C-terminus	Kanamycin	testing polyclonal anti-CLIP-115 antibodies (C. Erck)	this study
pEGFP-C1-CLIP-170	Kanamycin	site-directed mutagenesis	C. Erck
pGEX-6p2-CLIP-115 C-terminus	Ampicillin	*CLIP-115* C-terminus for cloning in pEGFP-C1 and -N3	C. Erck
pIRES2-EGFP-TTL sense	Kanamycin	rescue of WT phenotype in *TTL*-/- MEFs	C. Erck, M. van Ham
pIRES2-EGFP-TTL antisense	Kanamycin	control for rescue experiments	C. Erck, M. van Ham
pYX-Asc-Clip2	Ampicillin	full length *CLIP-115* cDNA clone	ImaGenes

2.4.2. Preparation of plasmid DNA

To isolate plasmid DNA from bacteria, 2 ml for mini-preparations and 100 ml of LB medium for midi-preparations containing the appropriate antibiotic were inoculated with material of a single bacterial clone and incubated overnight at 37 °C while shaking. The DNA preparations were performed using the NucleoSpin® Plasmid kit for mini-, and the NucleoBond® AX100 kit for midi-preparations pursuant to the manual (Macherey-Nagel). Harvested bacteria were re-suspended in pre-cooled buffer containing RNase (A1 or S1, respectively) and lysed by an alkaline SDS-containing buffer (A2 or S2, respectively). A potassium acetate-containing buffer (A3 or S3, respectively) neutralized the lysates and precipitated chromosomal DNA as well as proteins. The plasmid DNA was then bound to an anion-exchange column, washed (buffers AW and A4 or N3, respectively), and eluted (buffers AE or N5, respectively). To increase the concentration after midi-preparation plasmid DNA was precipitated by the addition of 2-propanol, washed with 70 % ethanol, and re-dissolved in 50 – 200 µl of sterile H_2O_{deion}.

2.4.3. Isolation of genomic DNA from mouse tails

Genomic DNA was isolated from mouse tails for genotyping. Therefore, tail tips were overnight incubated in 720 µl tail buffer complimented with 30 µl 10 mg/ml Proteinase K at 54 °C while shaking. After 10 min centrifugation at 13000 rpm at room temperature, supernatants were transferred to reaction cups containing 600 µl 2-propanol and mixed by inverting. Samples were spun down at 12000 rpm for 5 min and supernatants were removed completely. Pellets were washed with 500 µl 70 % ethanol, air-dried and dissolved in 200 µl sterile H_2O_{deion} by shaking at 54 °C for 3 – 12 h. Samples were ready to be used for genotyping as described in 2.4.5.

Tail buffer:

100 mM Tris base-HCl, pH 8.5
5 mM EDTA, pH 8.0
200 mM NaCl
0.2 % SDS

2.4.4. Quantification of DNA

Solutions containing nucleic acids show a maximal absorption at a wavelength of λ = 260 nm. According to the extinction coefficient (ε) the optical density at 260 nm (OD_{260}) of 1.0 corresponds to a DNA concentration (c_{DNA}) of 50 ng/µl. The OD_{260} of in water diluted DNA solutions was measured using a photometer (GeneQuant II, Pharmacia Biotech) and DNA concentrations were calculated according to the following equation:

$$c_{DNA} = OD_{260} \text{ x dilution factor x } 50 \text{ ng/µl}$$

2.4.5. Polymerase Chain Reaction

The polymerase chain reaction (PCR) is used to amplify specific DNA fragments and in this study was employed for genotyping mouse embryos, cloning *EGFP-CLIP-115* constructs and site-directed mutagenesis of both CLIP-115 and CLIP-170. Site-directed mutagenesis is described in chapter 2.4.7.

In general, DNA amplification by PCR is performed by repeated cycles of denaturation, annealing and elongation. First, the double-stranded template DNA is heated at 95 – 98 °C to obtain single stranded DNA. Next, temperature is decreased

to allow the primers to anneal thereby generating short parts of double-stranded DNA. The annealing- or melting temperature (T_m) is primer-specific and is calculated as follows:

$$T_m = 69.3 + 0.41 \times (GC\ \%) - 650 / (\text{primer length in bp})$$

Finally, during the elongation step a thermo-resistant DNA polymerase uses the sites where primers have bound as starting point for DNA synthesis at 68 – 72 °C. Duration of this step depends on the fragment size and is usually calculated with 1min/kb. The respective PCR-mixes and programmes for genotyping and cloning are shown below. The corresponding oligonucleotides used as primers are listed in Table 3 (chapter 2.4.6.). To perform the PCR reactions the T3 Thermocycler from Biometra was used.

Genotyping:

PCR-mix:	2.5 µl	5x Green GoTaq® Flexi Buffer (Promega)
	1.0 µl	25 mM $MgCl_2$ (Promega)
	1.0 µl	dNTP-mix (each 2.5 mM)
	0.1 µl	100 µM forward-primer
	0.1 µl	100 µM reverse-primer
	0.0625 µl	5 U/µl Taq polymerase (Promega)
	0.5 µl	DNA (final amount 10 – 50 ng)
	ad 12.5 µl	sterile H_2O_{deion}

Oligonucleotides Del and Neo2 were used as forward primers for genotyping of wild type and *TTL* knockout, respectively. In both reactions DelNeoRev was used as reverse primer.

Temperature programme:

95 °C	-	3 min	
95 °C	-	1 min	} 35 cycles
62 °C	-	1 min	
72 °C	-	1 min	
72 °C	-	5 min	
4 °C	-	hold	

CLIP-115 amplification for cloning:

PCR-mix:	4.0 µl	5x Phusion HF Reaction Buffer (Finnzymes)
	0.8 µl	dNTP-mix (each 2.5 mM)
	0.6 µg	forward-primer
	0.6 µg	reverse-primer
	0.2 µl	2 U/µl Phusion DNA polymerase (Finnzymes)
	2.0 ng	DNA
	ad 20 µl	sterile H_2O_{deion}

Temperature programme:

98 °C	-	30 s	
98 °C	-	10 s	35 cycles
65 °C	-	30 s	
72 °C	-	2 – 4 min	
72 °C	-	5 min	
4 °C	-	hold	

2.4.6. Oligonucleotides

Oligonucleotide primers for sequencing *CLIP-115* and *CLIP-170* constructs were designed using the online software “Primer3” (freeware from Geneious). Primers for cloning of *EGFP-CLIP-115* as well as for site-directed mutagenesis were designed using the respective sequences. For cloning the *EGFP-CLIP-115* constructs restriction sites, kozak sequences or stop codons had to be introduced. All oligonucleotide primers were purchased from MWG.

Table 3: Oligonucleotide primers used in this study. Introduced restriction sequences are underlined, kozak sequences are underlined in italic, and stop codons are in bold.

Name	Sequence (5’ – 3’)	Use
34MGE	CCA AAA TCA ACG GGA CTT TCC	pEGFP-N sequencing
35MGE	GGT CCT GCT GGA GTT CGT	pEGFP-C sequencing
93MGE	GGT GTG GGA GGT TTT TTA AAG C	pEGFP-C sequencing
97MGE	GGA CAC GCT GAA CTT GTG G	pEGFP-N sequencing
Del	GTC ACA GAC TAG AAA ATG TGC TTA GA	genotyping wt forward

DelNeoRev	CCC AAC ATC ACA TTC TCC AAA TCT CA	genotyping wt and *TTL*-/- reverse
Neo2	GAT TCC CAC TTT GTG GTT CTA AGT AC	genotyping *TTL*-/- forward
M57	CCG AAT TCT CAG TGT TTG TCC TCC TG	*CLIP-115* amplification
M64	GGC CTC GAG ATG CAG AAG CCC AGT G	*CLIP-115* amplification
M65	GGC AGG AAC CAG GTT CTT CCA GTG CCC ACC	CLIP-115 Y270F forward
M66	GGT GGG CAC TGG AAG AAC CTG GTT CCT GCC	CLIP-115 Y270F reverse
M67	GGC AGG AAC CAG GGA GTT CCA GTG CCC ACC	CLIP-115 Y270E forward
M68	GGT GGG CAC TGG AAC TCC CTG GTT CCT GCC	CLIP-115 Y270E reverse
M69	GAC CTC TTC GCG CTT TGC CCG GAA GAT CTC	CLIP-115 Y348F forward
M70	GAG ATC TTC CGG GCA AAG CGC GAA GAG GTC	CLIP-115 Y348F reverse
M71	GAC CTC TTC GCG CGA AGC CCG GAA GAT CTC	CLIP-115 Y348E forward
M72	GAG ATC TTC CGG GCT TCG CGC GAA GAG GTC	CLIP-115 Y348E reverse
M73	CAC AGC ATG AGC AGT TTG TTG CAG AAG CCG	CLIP-115 Y407F forward
M74	CGG CTT CTG CAA CAA ACT GCT CAT GCT GTG	CLIP-115 Y407F reverse
M75	CAC AGC ATG AGC AGG AGG TTG CAG AAG CCG	CLIP-115 Y407E forward
M76	CGG CTT CTG CAA CCT CCT GCT CAT GCT GTG	CLIP-115 Y407E reverse
M77	GCT CCA GGA CAA ATT TGA GCA CAT GCT AAA G	CLIP-115 Y533F forward
M78	CTT TAG CAT GTG CTC AAA TTT GTC CTG GAG C	CLIP-115 Y533F reverse
M79	GCT CCA GGA CAA AGA GGA GCA CAT GCT AAA G	CLIP-115 Y533E forward
M80	CTT TAG CAT GTG CTC CTC TTT GTC CTG GAG C	CLIP-115 Y533E reverse
M81	GGC CAA TGA GAA GTT CGC TCA GGA GGT GG	CLIP-115 Y554F forward
M82	CCA CCT CCT GAG CGA ACT TCT CAT TGG CC	CLIP-115 Y554F reverse
M83	GGC CAA TGA GAA GGA GGC TCA GGA GGT GG	CLIP-115 Y554E forward
M84	CCA CCT CCT GAG CCT CCT TCT CAT TGG CC	CLIP-115 Y554E reverse
M85	GAA AAG AAG ATG CTA GAT TTC GAG ATG CTG CAG AGG G	CLIP-115 Y732F forward
M86	CCC TCT GCA GCA TCT CGA AAT CTA GCA TCT TCT TTT C	CLIP-115 Y732F reverse
M87	GAA AAG AAG ATG CTA GAT GAG GAG ATG CTG CAG AGG G	CLIP-115 Y732E forward
M88	CCC TCT GCA GCA TCT CCT CAT CTA GCA TCT TCT TTT C	CLIP-115 Y732E reverse
M93	GTG GAA TCC CTC ACG	*CLIP-115* sequencing
M94	TCA GGC ACC ACA GC	*CLIP-115* sequencing
M96	AAG CCA TCG AGT TCC	*CLIP-115* sequencing
M97	TAC TCG AG*C CGC C*AT GCA GAA GC	*CLIP-115* kozak, *Xho* I

M98	CCG AAT TC**T CG**G TGT TTG TCC TCC TG	*CLIP-115* **stop**, *Eco* RI
M99	GAG GAT CC*C ACC* ATG ACA TCC CAG ATG GAC	*CLIP-115*C *kozak*, *Bam* HI
M100	TGG CAG ACC TCA AGG	*CLIP-115* sequencing
M105	GGG TGG CGT GCG CTT CTT CGA GTG CCC GG	CLIP-115 Y130F forward
M106	CCG GGC ACT CGA AGA AGC GCA CGC CAC CC	CLIP-115 Y130F reverse
M107	GGG TGG CGT GCG CGA GTT CGA GTG CCC GG	CLIP-115 Y130E forward
M108	CCG GGC ACT CGA ACT CGC GCA CGC CAC CC	CLIP-115 Y130E reverse
M122	CTC CGA TCA GCA ACC	*CLIP-170* sequencing
M123	GGA ACG GGA TCT GG	*CLIP-170* sequencing
M124	TGA AGG AGC ATT TTG G	*CLIP-170* sequencing
M125	TTC CGA AGG TAA ATC G	*CLIP-170* sequencing
M126	GAA ACA AGC CAC AAC C	*CLIP-170* sequencing
M127	GCA GAT GAA GAG AAA GC	*CLIP-170* sequencing
M128	GGC AGG AGT TCG GTT TTT CCA GTG TGA AC	CLIP-170 Y108F forward
M129	GTT CAC ACT GGA AAA ACC GAA CTC CTG CC	CLIP-170 Y108F reverse
M130	GGC AGG AGT TCG GGA GTT CCA GTG TGA AC	CLIP-170 Y108E forward
M131	GTT CAC ACT GGA ACT CCC GAA CTC CTG CC	CLIP-170 Y108E reverse
M132	GCT GGA ACA AGG TTT TTT CAG TGT CAA CC	CLIP-170 Y261F forward
M133	GGT TGA CAC TGA AAA AAC CTT GTT CCA GC	CLIP-170 Y261F reverse
M134	GTT GCT GGA ACA AGG GAA TTT CAG TGT CAA CC	CLIP-170 Y261E forward
M135	GGT TGA CAC TGA AAT TCC CTT GTT CCA GCA AC	CLIP-170 Y261E reverse
M159	GGC AGG AAC CAG GGC CTT CCA GTG CCC ACC	CLIP-115 Y270A forward
M160	GGT GGG CAC TGG AAG GCC CTG GTT CCT GCC	CLIP-115 Y270A reverse
T7	TAA TAC GAC TCA CTA TAG GG	Sequencing of purchased *CLIP-115* clone

2.4.7. Site-directed mutagenesis

Point mutations were introduced in *CLIP-115* and *CLIP-170* sequences by using the QuikChange® Site-directed mutagenesis kit (Stratagene) according to the manufacture's protocol. An online-based phospho-scan of the CLIP-115 sequence using the NetPhosK 1.0 as well as the NetPhos 2.0 Server (Technical University of Denmark, www.cbs.dtu.dk/services/NetPhosK) revealed six tyrosines as putative phosphorylation sites. To mimic phosphorylation or dephosphorylation, the tyrosines 270, 348, 407, 533, 554 and 732 of CLIP-115 were either substituted by glutamic acid or phenylalanine, respectively. After initial experiments also tyrosine 130 of

CLIP-115 and the tyrosines 108 and 261 of CLIP-170 were substituted as described. Tyrosine 270 of CLIP-115 was additionally mutated into alanine as an independent control of mimicking dephosphorylation. In site-directed mutagenesis, point mutations are introduced into the target gene by PCR-mediated amplification of the complete plasmid using primers carrying the changed nucleotides. Thus, the resulting PCR products are complete plasmids. The reaction mixture was either prepared according to the manual or as described below:

5 µl	10x reaction buffer
125 ng	forward-primer
125 ng	reverse-primer
8 µl	dNTP-mix (each 2.5 mM)
10 – 20 ng	DNA
1 µl	3 U/µl Pfu DNA polymerase (Promega)
ad 50 µl	sterile H_2O_{deion}

Temperature programme:

95 °C	-	30 s	
95 °C	-	30 s	16 – 18 cycles
55 °C	-	1 min	
68 °C	-	8 – 10 min	
4 °C	-	hold	

H_2O_{deion} was used as negative control. After the mutagenesis reaction, template DNA was digested by the addition of 10 U *Dpn* I and 1 h of incubation at 37 °C. This restriction enzyme specifically recognizes methylated DNA and therefore digests the template DNA, which was isolated from bacteria and consequently carries methylations. The reaction product was then checked for correct size by agarose gel electrophoresis as described in 2.4.10. and introduced into *E. coli* by heat-shock transformation (see 2.4.13.) for amplification and sequencing.

2.4.8. DNA sequencing

The BigDye® Terminator v3.1 Cycle Sequencing Kit from AB Applied Biosystems was employed to sequence the newly generated *CLIP-115* and *CLIP-170* constructs as well as the DNA products obtained by site-directed mutagenesis.

PCR-mix:	2 µl	Big Dye
	1 µl	5x Sequencing buffer
	3.2 pmol	sequencing primer (see Tab. 3)
	1 µl	DNA (mini-preparation)
	ad 10 µl	sterile H_2O_{deion}

Temperature programme:

96 °C	-	5 min	
96 °C	-	15 s	25 cycles
50 °C	-	15 s	
60°C	-	4 min	
4 °C	-	hold	

PCR products were sent to GATC Biotech GmbH (Konstanz, Germany) for automatic sequencing. The received sequence files (FASTA format) were aligned using Vector NTI® Software (Invitrogen).

2.4.9. DNA restriction digests with endonucleases

Restriction endonucleases are bacterial enzymes used as molecular biological tools to digest foreign DNA at specific cleavage sites of usually 4 – 8 nucleotides. Restriction digests result in double-stranded DNA fragments with blunt, 5`- or 3`-sticky ends, depending on the restriction enzyme.

In this study generally up to 5 µg DNA was digested in 10 – 30 µl 1x restriction buffer containing 0.4 U/µl of each restriction enzyme. Depending on the used enzymes the reaction could also be performed in 2x restriction buffer, e.g. when *Bam* H1 and *Eco* R I were used in combination. After 1 – 2 h incubation at 37 °C reactions were mixed with 5x DNA loading buffer and analysed by agarose gel electrophoresis (see next chapter).

2.4.10. Agarose gel electrophoresis

As DNA fragments are negatively charged, they are motile in an electric field and can be separated according to their size in an agarose matrix. Therefore, 1 % (w/v) agarose in 1x TAE buffer was heated until the agarose was completely dissolved. The solution was cooled to 60 °C and poured in a gel chamber. To visualize the DNA after separation 0.5 µM ethidiumbromide (according to standard protocols) was added to the agarose solution. Ethidiumbromide is a DNA-intercalating agent and fluoresces at UV light. The agarose gel was transferred to an electrophoresis chamber (Bio-Rad, Whatman) and soaked in 1x TAE buffer. DNA samples were mixed with 5x loading buffer and loaded in the gel slots. Additionally, a DNA standard with a fragment size from 200 – 10000 bp (SmartLadder, Eurogentec) was loaded to identify the DNA fragment sizes in the samples. For separating the DNA samples a voltage of 65 V was applied (powersupply from Biometra). Finally, the gel was exposed to UV light and images were recorded.

5x DNA loading buffer:

15 % (v/v) Ficoll
50 mM EDTA pH 8
0.5 % (v/v) SDS
2 % (v/v) 50x TAE buffer
0.05 % (w/v) Bromophenol blue
0.05 % (w/v) Xylencyanol

TAE buffer, pH 7.5:

40 mM Tris base
20 mM Sodium acetate
1 mM EDTA

2.4.11. DNA extraction from agarose gels

For cloning, DNA fragments obtained from restriction digests were separated by agarose gel electrophoresis as described in 2.4.10. The target bands were then cut out of the gel under UV light and extracted by using the NucleoSpin® Extract II kit from Macherey-Nagel according to the manual.

2.4.12. Ligation

To generate new constructs, DNA fragments were ligated into linearised plasmids. For that, a molecular ratio between insert and plasmid of approximately 3:1 supplemented with 1 U T4 DNA ligase in a total volume of 10 µl 1x ligation buffer was incubated overnight at 4 °C. Mixtures were then used to transform *E. coli* as described in 2.4.13.

2.4.13. Bacteria transformation

To obtain single clones containing the target construct competent the respective PCR or ligation products were introduced in *E. coli* by heat-shock transformation. Therefore, 50 µl of competent cells were thawed on ice and mixed with up to 500 ng of DNA. After 15 min incubation on ice bacteria were incubated at 42 °C for 90 s in a thermomixer (Eppendorf) immediately followed by additional 2 min incubation on ice. Then, 900 µl SOC medium was added followed by incubation at 37 °C under agitation at 650 rpm for 60 min in a thermomixer. Finally, bacteria were plated on LB-Agar containing the appropriate antibiotic and incubated overnight at 37 °C.

2.5. Biochemical methods

2.5.1. Standard buffers

All buffers were prepared in H_2O_{deion} and autoclaved if necessary. Adapted protocols as well as not frequently used buffers are mentioned separately in the respective paragraphs.

PBS, pH 7.4:

137 mM NaCl

2.7 mM KCl

10 mM $Na_2HPO_4 \cdot 2H_2O$

2 mM KH_2PO_4

TBS, pH 7.6:

20 mM Tris base

137 mM NaCl

2.5.2. Antibody purification

In this study, monoclonal antibodies were either purified from cell culture supernatants using protein G columns or from rat ascites (Biotem, France) by ammonium sulphate precipitation. Non-adherent hybridoma cells release antibodies into the culture medium, which then can directly be used in immunofluorescence or for purifying the contained antibodies as described in 2.5.2.1.

2.5.2.1. Purification with protein G column

The mouse antibody 20C6 against tyrosinated α-tubulin was purified from cell culture supernatant using the antibody binding capacity of protein G. Columns containing protein G-coupled sepharose beads were equilibrated with 10 ml PBS before applying up to 150 ml supernatant. After flow-through of the supernatant, the column was washed with up to 150 ml PBS corresponding with the loaded volume of supernatant. The bound antibodies were then eluted with 20 ml 0.1 M glycine buffer (pH 3.0). Aliquots of 1 ml were collected in cups containing 100 µl 1.5 M Tris base (pH 8.8) for immediate neutralization. All samples were used to determine antibody presence by measuring the protein concentration at OD_{280} (as described in 2.5.5). Antibody-containing fractions were then pooled and concentrated by centrifugation in Centricon tubes (Vivaspin, cut-off: 10 kDa). To re-use the protein G sepharose it was washed with 0.1 M glycine buffer (pH 3.0) until the flow-through had an OD_{280} of 0.10. The sepharose was then stored in PBS at 4 °C.

2.5.2.2. Ammonium sulphate precipitation

The rat antibody YL1/2 was purified from ascites to obtain sufficient amounts of antibody necessary for further experiments. Therefore, the ascites was cleaned from cell residues by filtration through a sterile filter with a pore size of 3 µm followed by centrifugation at 10000 rpm and 4 °C for 30 min. Antibodies of the type IgG2 precipitate in an ammonium sulphate concentration of 50 %. For that reason, 3 ml ice-cold saturated ammonium sulphate was added drop-wise to 3 ml of ascites supernatant over the time of 30 min while stirred on ice. After an additional hour of stirring, the mixture was centrifuged at 13000 rpm and 4 °C for 30 min. The pellet was re-dissolved in 3 ml of dialysis buffer and transferred to a dialysis skin. To desalt the antibody solution, dialysis was performed in a total volume of 2 l of dialysis buffer

overnight at 4 °C. To dissolve precipitated antibodies, 3 ml of dialysis buffer was added followed by centrifugation for 30 min at 10000 rpm and 4 °C. The supernatant was then purified by anion exchange chromatography using a FPLC from Pharmacia Biotech. Therefore, the antibody solution was loaded onto a MonoQ 5/5 column. Bound antibodies were eluted by increasing NaCl concentration. Therefore, the rate of elution buffer increased from 0 – 100 % during the flow-through of 10 – 42 ml after sample injection (according to standard protocol). Immediately after sample injection, 1 ml fractions were collected. Antibody-containing fractions were determined by measuring the OD_{280}, pooled and concentrated in PBS using Centricon tubes.

Dialysis buffer:
20 mM Tris base-HCl, pH 7.9

Elution buffer:
20 mM Tris base-HCl, pH 7.9
350 mM NaCl

2.5.3. Production of F_{ab} fragments

Antibodies consist of an F_c part and two F_{ab} fragments, which are arranged by two heavy and two light chains. Each F_{ab} fragment carries an epitope-binding site, so that one antibody can bind two antigens. In order to uncouple the two binding sites of an antibody and thereby preventing cross-linking of the antigen, single F_{ab} fragments were produced employing the ImmunoPure® Fab Preparation Kit from Pierce.
Antibody cleavage is achieved using immobilized papain followed by a protein A-mediated purification. For that, 10 mg antibody was concentrated into a volume of 0.5 ml PBS by using Centricon tubes. Next, 0.5 ml of freshly prepared digestion buffer was added. Then, 0.5 ml of washed immobilized papain was added to the sample. Antibody digestion was performed at 37 °C overnight while shaking. After centrifugation at 1000 xg for 5 min the antibody-containing supernatant was transferred to a new tube. The resulting papain-containing pellet was washed twice with 1 ml binding buffer. The supernatant from each wash step was added to the antibody solution. To isolate the F_{ab} fragments a protein A-coupled sepharose column that binds the F_c parts and undigested antibodies was equilibrated with 13 ml

binding buffer and loaded with the sample. Next, the column was washed with 6 ml binding buffer and the F_{ab} fragment-containing eluate was collected. The eluate was dialysed overnight at 4 °C in 3 l PBS and concentrated using Centricon tubes. For re-usage, the protein A-coupled sepharose was regenerated by washing with 10 ml of 0.1 M citric acid, pH 3.0, and stored in 0.02 % sodium azide in H_2O_{deion} at 4 °C.
Alternatively, the F_{ab} fragments could also be purified after the papain digest by incubation with 150 µl of protein G-coupled sepharose for 2 h at 4 °C under steady rotation.

Phosphate buffer, pH 7.0:
20 mM Sodium phosphate
10 mM EDTA

Digestion buffer:
12 ml provided phosphate buffer (pH 10.0)
42 mg Cysteine·HCl

Provided buffers:
Phosphate buffer, pH 10.0
Binding buffer

2.5.4. Protein precipitation

Proteins from total cell lysates that will be analysed by 2-dimensional SDS-PAGE were concentrated and desalted by methanol-chloroform-extraction (Wessel & Flügge, 1984). Therefore, 200 µl of total cell lysate were thoroughly mixed with 800 µl methanol, 200 µl chloroform and 600 µl H_2O_{deion}. Centrifugation at 9000 rpm for 5 min resulted in three phases: a lower chloroform phase, a protein-containing interphase and an upper aqueous phase. After removing the upper aqueous phase 600 µl methanol was carefully added for washing. The resulting supernatant was completely removed and the remaining protein-containing phase air-dried and dissolved in 500 µl soaking solution by shaking at 500 rpm overnight at 18 °C. Protein concentrations were then determined by a Bradford protein assay (Bio-Rad).

Soaking solution:

5.4 g urea solved in 10 ml H_2O, then addition of:

1.5 g Thiourea

400 mg CHAPS

2 mg Tris

30 mM DTT

0.01 mg Leupeptin

100 µl of 100 mM Pefablock

Before use, 100 µM sodium vanadate and 1 µM sodium fluoride were added to inhibit phosphatase activity.

2.5.5. Protein quantification

The concentration of antibodies in aqueous solutions was measured at a wavelength of λ = 280 nm with a GeneQuant II photometer from Pharmacia Biotech. An optical density at 280 nm (OD_{280}) of 1.0 corresponds with a protein concentration (e.g. antibody concentration, $c_{antibody}$) of 0.714 mg/ml. The concentration of diluted antibody solutions was calculated as follows:

$c_{antibody} = OD_{280}$ x dilution factor x 0.714 mg/ml

Additionally, protein concentrations of total cell lysates were determined using the MicroBC Assay (Uptima) according to the manual. The kit includes three solutions (A, B, C), which were mixed in a ratio of 25:25:1 to produce the reagent for the assay. Then, 100 µl protein solution was mixed with 100 µl of reagent in a 96-well plate. After incubation at 37 °C for 1 h, the OD_{562} was measured with an ELISA-reader from Tecan and concentrations were calculated using a linear regression. The reference solutions had bovine serum albumin (BSA) concentrations of 0, 0.5, 1, 2.5, 5, 10, 15, 25, 50 and 100 µg/ml. In general, cell lysates were diluted 1:20 and 1:100. Each sample was measured in duplicates and the average taken to calculate protein concentrations using Microsoft Excel 2000.

2.5.6. SDS-PAGE

Sodium dodecylsulfate-polyacrylamide gel electrophoresis (SDS-PAGE) was employed to separate proteins according to their molecular weight as described by Laemmli (Laemmli *et al.*, 1970). Recipes of separation gels with acrylamide concentrations ranging from 5 % to 12.5 % and of 5 % stacking gels are listed in Table 4.

Table 4: Recipes for polyacrylamide gels used in this study.

	Stacking gel [ml]	**Separation gel [ml]**				
Acrylamide concentration	**5 %**	**5 %**	**6 %**	**7.5 %**	**10 %**	**12.5 %**
H_2O_{deion}	1.8	3.5	3.3	3.0	2.5	1.75
0.5 M Tris base-HCl, pH 6.8	0.32	-	-	-	-	-
1.5 M Tris base-HCl, pH 8.8	-	1.5	1.5	1.5	1.5	1.5
30 % acrylamide, 0.8 % bisacrylamide	0.33	1.0	1.2	1.5	2.0	2.75
10 % SDS	0.025	0.06	0.06	0.06	0.06	0.06
TEMED	0.0125	0.008	0.008	0.008	0.008	0.008
25 % APS	0.0125	0.008	0.008	0.008	0.008	0.008

After polymerisation, gels were transferred to a minigel chamber from Biometra. Protein samples were mixed with 4x SDS sample buffer, boiled for 10 min at 99 °C and loaded on the gel. As molecular weight standard either a pre-stained or an unstained protein ladder from MBI Fermentas was used. The molecular weights of the pre-stained protein ladder are approximately 11, 17, 25, 34, 43, 55, 72, 95, 130 and 170 kDa, and of the unstained protein ladder 10, 15, 20, 25, 30, 40, 50, 60, 70, 85, 100, 120, 150 and 200 kDa.

Electrophoresis was performed in SDS running buffer at a voltage of 100 V to 180 V (powersupply from Biometra) depending on the acrylamide concentration of the gel. Finally, gels were analysed either by Coomassie staining or Western blotting (see chapterss 2.5.8. and 2.5.9., respectively).

4x SDS sample buffer:

3.4 % (w/v) SDS

25 mM Tris base-HCl, pH 6.8

2.4 % (v/v) Glycerol

0.34 % (v/v) Mercaptoethanol

0.008 % (w/v) Bromophenol blue

SDS running buffer:

25 mM Tris base

192 mM Glycine

0.1 % SDS

2.5.7. Two-dimensional SDS-PAGE

In this study, 2-dimensional SDS-PAGE was performed by the conventional method as well as by NEPHGE (non-equilibrium pH gel electrophoresis). The methods differ in the isoelectric focussing, which is either conventionally performed using gel strips that include a fixed pH gradient or performed in a urea gel that builds up a pH gradient under voltage (NEPHGE). The 2-dimensional SDS-PAGE was performed in the "Cellular Proteomics" group at the HZI (Dr. L. Jänsch, Dr. J. Wissing, E. Dornbusch, R. Munder).

2.5.7.1. Conventional 2-dimensional SDS-PAGE

Following the conventional protocol, 24 cm gel strips with a pH gradient from 5.5 to 6.7 (Immobiline™ DryStrip from GE Healthcare) were equilibrated in 500 µl soaking solution (see 2.5.4.). The samples containing up to 1 mg total protein were mixed with 1 % of IPG buffer (pH 5.0 – 6.0 and 5.5 – 6.7, GE Healthcare) and 1.5 µl of 1 % bromophenol-blue in soaking solution before loading to the strip. In different experiments the samples were either loaded at the acidic or the basic end or evenly distributed over the whole strip at a voltage of 30 V for 5 h. The strips were covered with silicon oil and protein focussing (1^{st} dimension) was performed by a voltage gradient with 150 kVh to maintain a steady ion flow. A typical programme started with a rehydration step at 30 V for 14 h. The following steps were 3 h at 100 V, 3 h at 300 V, 3 h at 3000 V, up to 48 h at 3500 V, 2 h at 8000 V and a final hold at 100 V. After

separation in the 1st dimension, strips were washed with equilibration buffer containing 1 % (w/v) DTT followed by a second wash step in 4.8 % (w/v) iodacetamide in equilibration buffer. Then the strips were transferred onto 8 % SDS-polyacrylamide gels and embedded in 2 % agarose for fixation. The gels were run in SDS running buffer (see 2.5.6.) at 1000 V with an ISO• DALT® Electrophoresis System (Hoefer) in the 2nd dimension followed either by Commassie-staining or Western blotting (wet-blot system, Bio-Rad) as described in 2.5.8. and 2.5.9., respectively.

Equilibration buffer:

50 mM Tris base, pH 8.8
6 M Urea
30 % Glycerol
2 % SDS

2.5.7.2. Non-equilibrium pH gel electrophoresis

For the performance of NEPHGE (according to Klose & Kobalz, 1995) a 9 M urea gel was poured in a glass tube with an inner diameter of 0.9 mm. 100 µg of protein were loaded to the urea gel, the gel ends put in electrode buffers and a current gradient (see below) applied to build up the pH gradient from a pH of 2 – 11, which is necessary for protein focussing.

Current gradient:	60 min	-	100 V
	60 min	-	200 V
	17.5 h	-	400 V
	60 min	-	600 V
	30 min	-	1000 V
	10 min	-	1500 V
	5 min	-	2000 V

The 2nd dimension was performed by transferring the urea gel onto a 15 % SDS-polyacrylamide gel that is of high stability followed by a fixation in 2 % agarose. The gel was run at a current of 35 mA for 15 min followed by 5 h at 65 mA. After finishing

the 2nd dimension, gels were either stained with Coomassie or blotted in a wet-blot chamber from Bio-Rad (see chapters 2.5.8. and 2.5.9.).

2.5.8. Coomassie-blue staining

SDS protein gels as well as PVDF-membranes after Western blotting can be stained with Coomassie-blue staining solution for a minimum of 60 min to visualize protein bands. Gels and membranes were destained in 40 % methanol containing 10 % acetic acid. Since its higher sensitivity to proteins, SDS gels loaded with proteins to be analysed by mass spectrometry were stained with colloidal Coomassie. In this case gels were destained by wash steps in H_2O_{deion}.

Coomassie-blue staining solution

0.1 % (w/v) Coomassie brilliant blue R250
25 % (v/v) 2-Propanol
10 % (v/v) Acetic acid
→ Filtration

Colloidal Coomassie:

2 g Coomassie brilliant blue G250
1 l H_2O
55.5 ml H_2SO_4
→ >3 h stirring, then filtration and addition of
220 ml 10 N NaOH
310 ml 100% tri-chloric acid (TCA)

2.5.9. Western blotting

For protein transfer from SDS gels to PVDF membranes (Immobilon™ from Millipore) either a semi-dry blot system from PHASE or a wet-blot system from Bio-Rad was employed. For semi-dry blots two sheets of Whatman paper were soaked in blot buffer and put on the cathode. After a short equilibration in blot buffer the SDS gel (7 cm x 9 cm) was transferred onto the Whatman paper and covered with a methanol-activated PVDF membrane. Finally, another two pre-wetted sheets of Whatman

paper were put on the membrane and covered by the anode. Protein transfer was performed at a current of 150 mA for 90 – 120 min.

Gels from 2-dimensional SDS-PAGE were blotted in a wet-blot system. Therefore, the above described construction of Whatman paper, SDS gel, PVDF membrane and another layer of Whatman paper was built up in a holder between two stuff mats. The holder was then transferred to the blot chamber and soaked in blot buffer, and a current of 1 A was applied for a minimum of 3 h.

After protein transfer membranes were incubated overnight in block buffer at 4 °C and incubated with primary antibodies diluted in blocking solution for 1 h at room temperature. Next, membranes were washed step-wise with wash buffers A, B and C for 10 min followed by short rinsing with wash buffer A to remove the Triton X-100. Membranes were then incubated for 1 h at room temperature with the peroxidase-coupled secondary antibody in blocking solution. Subsequently, membranes were washed as described above, incubated for 1 – 2 min in ECL-solution (Enhanced Chemiluminescence) and exposed to a film (Amersham Hyperfilm™ ECL, GE Healthcare). Films were developed using the Curex 60 machine (AGFA). Used membranes were stained with Coomassie as described in 2.5.8.

Blot buffer:

50 mM Tris base
39 mM Glycine
0.037 % (w/v) SDS
20 % (v/v) Methanol

Block buffer:

10 % Fetal calf serum (FCS) in wash buffer A

Wash buffers:

A) TBS + 0.1 % Tween 20 (= TBS-T)

B) TBS-T + 0.5 M NaCl

C) TBS-T + 0.5 % Triton X-100

ECL-solutions:

1.) Lumi-Light Western blotting solution (Roche)

2.) Home-made ECL-solution:

Solution 1: 250 mM luminol (0.44 g of 3-aminophtalhydrazide from Sigma in 10 ml DMSO)

Solution 2: 90 mM p-coumaric acid (0.15 g p-coumaric acid from Sigma in 10 ml DMSO)

Recipe:

Solution A: 8.85 ml H_2O_{deion}
1 ml 1 M Tris base-HCl, pH 8.5
100 µl solution 1
44 µl solution 2

Solution B: 9 ml H_2O_{deion}
1 ml 1M Tris base-HCl, pH 8.5
6 µl 30 % H_2O_2

Solutions A and B were mixed and immediately used.

2.5.10. Peptide synthesis

In this study, peptides used as standards in mass spectrometry (MS) analysis (described in 2.5.11.) and for rabbit immunization to produce polyclonal antibodies were synthesized by the peptide synthesis facility at the HZI headed by Dr. W. Tegge.

Table 5: Peptides synthesized for this study.

Name	Sequence (N – C)	Use
CLIP115Y270	KPPCQFY	Reference in MS analysis
CLIP115Y270P	KPPCQFY-phospho	Reference in MS analysis
115 270	QF Y RTGAVAGDNKG	Antibody production
115 phos 270	QF Y(phospho) RTGAVAGDNKG	Antibody production

2.5.11. Mass spectrometry

In mass spectrometry (MS) charged peptides are produced from protein samples by tryptic cleavage and are separated according to their mass/charge ratio (m/z) resulting in a protein-specific fingerprint. The most intense peptides can additionally be fragmented and sequenced using MS/MS to analyse peptides in more detail. Mass spectrometry was performed in the “Cellular Proteomics” group at the HZI (Dr. L. Jänsch, Dr. M. Nimtz, K. Minkhart, R. Munder).

In this study, MS analysis was employed to identify a potential phosphorylation or possible interaction partners of CLIP-115 obtained by immunoprecipitated cell lysates. An additional phosphate residue would cause a characteristic shift of 79.9663 Da (molecular mass of HPO_3) divided by the peptide charge, whereas co-precipitated proteins were identified by the peptide composition. Protein samples were separated by SDS-PAGE, and Coomassie-stained protein bands of interest were cut out the gel. After rinsing the gel pieces in H_2O_{dest}, slices were washed with 0.1 M NH_4HCO_3 (Promega). To reduce disulfide bonds and to protect cysteines against oxidation samples were exposed to carbaminomethylation. Therefore, the gel slices were incubated in 20 mM dithiothreitol (DTT) in 0.1 M NH_4HCO_3 for 30 min at 56 °C. Next, gel slices were incubated in 50 mM iodacetamide in 0.1 M NH_4HCO_3 for 2 h at room temperature followed by an additional washing step with 0.1 M NH_4HCO_3. The supernatant was removed, whereas the gel slices were incubated for 15 min with 40 % acetonitrile in 0.1 M NH_4HCO_3 for shrinking. After that, the supernatant was removed again and the gel slices incubated for 5 min in 100 % acetonitrile. After removing the supernatant the gel slices were dried using a SpeedVac RC 1010 (Thermo Electron Corporation). Samples were then ready to be used for trypic digestion. To digest the proteins gel slices were incubated in 30 – 60 µl 20 ng/ml trypsin in 0.1 M NH_4HCO_3 at 37 °C overnight. Finally, the peptides were extracted from the gel slices in three steps. First, the gel slices were incubated in 300 µl H_2O_{dest} followed by the second incubation in 300 µl 1.0 % trifluoroacetic acid (TFA) and the third incubation in 300 µl 40 % acetonitrile in 0.1 % TFA. All incubation steps were performed at 37 °C for at least 1 h while shaking. The supernatants of all extraction steps were pooled and dried in a SpeedVac. Further purification was achieved by using ZipTip C18 microcolumns (Millipore) according to the manufacture’s manual.

Protein samples were separated by HPLC using a nano Acquity Ultra Performance-LC system (Waters) with a nano Acquity UPLC BEH300 C18 column (1.7 µm, 75 µm x 250 mm, Waters). Subsequently, MS analysis was either performed using a Q-TOF micro (Waters) or a LTQ Orbitrap XL (Thermo Fisher). Data gathered by the Q-TOF system was analysed using a MASCOT server (version 1.9, Matrix Science) and MassLynx 4.1 software (Waters Laboratory Informatics). Data obtained from the Orbitrap system was processed using the Xcalibur software (Thermo Scientific).

2.6. Immunological methods

2.6.1. Antibodies

In Table 6 all commercially available and newly generated primary antibodies used in this study are listed. All secondary antibodies used in this study are listed in Table 7.

Table 6: Primary antibodies used in this study.

Antigen	Name	Type*	Use (dil./conc.)**	Source
Actin	A2066	rabbit (pc)	WB (1:5000)	Sigma-Aldrich
Actin	A5060	rabbit (pc)	WB (1:10000)	Sigma-Aldrich
CLASP2	#2358	rabbit (pc)	IF (1:300), WB (1:2000)	Akhmanova *et.al.*, 2001
CLIP-115	#2238	rabbit (pc)	IF (1:250), WB (1:2000)	Hoogenraad *et.al.*, 2000
CLIP-115	#2163	rabbit (mc)	IF (1.9 – 7.6 µg/ml), IP (7.6 µg/ml), WB (0.38 µg/ml)	HZI
CLIP-115	97E11D11	rat (mc)	IF (supernatant, 1:2)	HZI
CLIP-115 (pY270)		rabbit (pc)	WB (1 µg/ml)	BioGenes GmbH
CLIP-115 (Y270)		rabbit (pc)	WB (1 µg/ml)	BioGenes GmbH
CLIP-170	#2360	rabbit (pc)	IF (1:250), WB (1:2000)	Coquelle *et.al.*, 2002
EB1	11B11	rat (mc)	IF (1:500)	Absea
EB1	clone 5	mouse (mc)	IF (1:500), WB (1:2500)	BD Biosciences
EB_{pan}	15H11	rat (mc)	IF (1:500)	Absea
FAK pY397	44-624G	rabbit (mc)	IF (1:100)	SySy
GFP	101G4B2	mouse (mc)	IF (6 µg/ml), WB (supernatant)	HZI
GFP	270F3	mouse (mc)	IF (1:500)	SySy
GFP	27F5	mouse (mc)	IF (4.44 µg/ml)	HZI

GFP	H5-8	rabbit (pc)	IF (1:100), WB (1:1000)	HZI
GFP	MAB3580	mouse (mc)	IF (1:500)	Millipore
Golgi	golgin 97	mouse (mc)	IF (1:1000)	Santa Cruz Biotech.
IQGAP1	sc-10792	rabbit (pc)	IF (1:100)	BD Biosciences
p150^{Glued}	610474	mouse (mc)	IF (1:200)	BD Biosciences
phospho-Serine	P3430	mouse (mc)	WB (1:500)	Sigma-Aldrich
phospho-Threonine	71-8200	rabbit (pc)	WB (1:1000)	Zymed
phospho-Threonine	P3555	mouse (mc)	WB (1:100)	Sigma-Aldrich
phospho-Tyrosine	pY99	mouse (mc)	IF (1:100), WB (1:1000)	Santa Cruz Biotech.
Tubulin (acetyl.)	6-11B-1	mouse (mc)	IF (1:200)	Sigma-Aldrich
Tubulin (α)	α3A2	mouse (mc)	IF + WB (1:50000)	Biotem, France
Tubulin (β)	T4026	mouse (mc)	IF (1:300), WB (1:2000)	Sigma-Aldrich
Tubulin (β)	2.3B11	mouse (mc)	IF + WB (1:20000)	Biotem, France
Tubulin (γ)	GTU-88	mouse (mc)	IF (1:250)	Sigma-Aldrich
Tubulin (Δ2-Glu)	L4, L7	rabbit (pc)	IF (1:1000), WB (1:5000)	Paturle-Lafanechère *et.al.*, 1994
Tubulin (Glu)	1D5	mouse (mc)	IF + WB (supernatant)	Wehland & Weber, 1987
Tubulin (Tyr)	20C6	mouse (mc)	IF (2 µg/ml, supernatant), MI (0.25 – 0.5 mg/ml), WB (supernatant)	Wehland & Weber, 1987
Tubulin (Tyr)	YL1/2	rat (mc)	IF (2.9 µg/ml, supernatant), MI (0.5 – 4.6 mg/ml), WB (supernatant)	Kilmartin *et al.*, 1982; Wehland *et.al.*, 1983
TTL	1D3	mouse (mc)	IF (2.4 µg/ml)	Wehland & Weber, 1987

*****mc = monoclonal, pc = polyclonal

******IF = immunofluorescence, IP = immunoprecipitation, MI = microinjection, WB = Western blot, dil. = dilution, conc. = concentration

Table 7: Secondary antibodies used in this study.

Name	Antigen*	Tag	Use (dilution)**	Source
A1a	mouse IgG (H + L)	Fluorescein	IF (1:100)	Dianova
A2b	mouse IgG, $F(ab')_2$	Rhodamin	IF (1:100)	Dianova
A2e	mouse IgG, Fc	Rhodamin	IF (1:100)	Dianova
A4a	mouse IgG + IgM (H + L)	Peroxidase	WB (1:2000)	Dianova
A7a	mouse IgG + IgM (H + L)	Cy3	IF (1:2000)	Dianova
A9a	mouse IgG + IgM (H + L)	Cy2	IF (1:100)	Dianova
A12c	mouse IgG (H + L)	Alexa Fluor 488	IF (1:400), MI (1:4)	Invitrogen
A13c	mouse IgG (H + L)	Alexa Fluor 594	IF (1:200)	Invitrogen
A16c	mouse IgG (H + L)	Alexa Fluor 350	IF (1:100)	Invitrogen
B1c	rabbit IgG (H + L)	Fluorescein	IF (1:100)	Dianova
B4c	rabbit IgG (H + L)	Peroxidase	WB (1:2000 – 1:5000)	Dianova
B7c	rabbit IgG (H + L)	Cy3	IF (1:500)	Dianova
B9c	rabbit IgG (H + L)	Cy2	IF (1:100)	Dianova
B12c	rabbit IgG (H + L)	Alexa Fluor 488	IF (1:200 – 1:400), MI (1:4)	Invitrogen
B13c	rabbit IgG (H + L)	Alexa Fluor 594	IF (1:400 – 1:500)	Invitrogen
C4a	rat IgG + IgM (H + L)	Peroxidase	WB (1:2000)	Dianova
C4c	rat IgG + IgM (H + L)	Peroxidase	WB (1:2000)	Dianova
C7c	rat IgG (H + L)	Cy3	IF (1:2000)	Dianova
C12c	rat IgG (H + L)	Alexa Fluor 488	IF (1:400)	Invitrogen
C13c	rat IgG (H + L)	Alexa Fluor 594	IF (1:200)	Invitrogen
C16c	rat IgG (H + L)	Alexa Fluor 350	IF (1:100)	Invitrogen
D12c	human IgG (H + L)	Alexa Fluor 488	MI (1:4)	Invitrogen

*****H = heavy chain, L = light chain

******IF = immunofluorescence, IP = immunoprecipitation, MI = microinjection, WB = Western blot

2.6.2. Immunoprecipitation

In this study, immunoprecipitation was used to isolate CLIP-115, and possible interaction partners, from total cell lysates for subsequent mass spectrometry analyses. Therefore, cells were washed twice with ice-cold PBS and harvested by scratching in PBS. After centrifugation for 5 min at 1000 rpm and 4 °C the supernatant was removed and the cell pellet lysed on ice in 0.5 – 1 ml of IP lysis buffer containing 50 µM sodium vanadate that inhibits tyrosine phosphatases.

Lysates were then centrifuged for 10 min at 10000 rpm and 4 °C and supernatants transferred to new tubes. Pellets were frozen and stored at -70 °C.

Protein G-coupled sepharose (Amersham Bioscience) was prepared by three times washing with IP wash buffer. Then, 100 µl of 50 % protein G sepharose slurry was added to 500 µl cell lysates and incubated at 4 °C under rotation for 30 – 60 min. The mixture was centrifuged at 2000 rpm and 4 °C for 1 min, and the pre-cleared supernatant was transferred to a new tube. Next, the antibody #2163 against CLIP-115 was added in a concentration of 7.6 µg/ml followed by incubating for 1 h at 4 °C under rotation for protein binding. Then, 100 µl protein G-coupled sepharose was added followed by 1 h of rotation at 4 °C. After centrifugation at 2000 rpm and 4 °C for 30 s the supernatant was transferred to a new tube and stored at -70 °C for further analysis. The sepharose beads, containing the bound CLIP-115, were washed four times with 500 µl IP wash buffer. Finally, the beads were transferred to a new tube and washed with 500 µl IP wash buffer containing 50 µM sodium vanadate to inhibit phosphatases. The beads were resuspended in 8x SDS sample buffer followed by boiling at 99 °C for 10 min. After centrifugation, the supernatant was loaded on an SDS gel followed by Western blot analysis or mass spectrometry.

IP lysis buffer, pH 7.5:

20 mM Tris base
100 mM NaCl
0.5 % Triton X100
1 tablet protease inhibitor cocktail, complete, EDTA-free (Roche) in 10 ml

IP wash buffer, pH 7.5:

20 mM Tris base
100 mM NaCl
0.05 % Triton X100
1 tablet protease inhibitor cocktail, complete, EDTA-free (Roche) in 10 ml

2.6.3. ELISA

To investigate the specificity of newly generated antibodies against non-phosphorylated or tyrosine 270-phosphorylated CLIP-115 the Enzyme-linked

Immunosorbent Assay (ELISA) was used. Synthetic CLIP-115 peptides (see Tab. 4) were immobilized on MaxiSorp 96-well plates (Nunc) and antibody-binding capacity quantified using peroxidase-coupled secondary antibodies.

For immobilization 1 ng peptide per 50 µl PBS was loaded in each well of a 96-well plate and incubated overnight at 4 °C. To block unspecific binding sites 200 µl blocking solution was added to each well. After incubating at room temperature for 30 min wells were washed three times with PBS. Next, 200 µl of 1 µg/ml antibody in blocking solution was added to each well and incubated for 1 h at room temperature. Wells were washed three times with PBS and incubated at room temperature for 1 hour with 200 µl secondary antibody (B4c) diluted 1:2000 in blocking solution. After again three washing steps with PBS, 200 µl of ortho-phenyldiamine solution was added to the wells as a substrate for peroxidase. Next, reactions were stopped by adding 50 µl 3.5 M H_2SO_4 to the wells and the OD_{492} was measured with an ELISA-reader (Tecan).

Blocking solution:

10 % FCS in PBS

Ortho-phenyldiamine solution:

5 ml 0.1 M Citric acid

5 ml 0.2 M Na_2HPO_4

10 ml H_2O_{deion}

8 mg ortho-phenyldiamine (Sigma)

8 µl 30 % H_2O_2

2.6.4. Immunofluorescence

For immunoflourescent stainings cells were grown on untreated glass coverslips. Prior to staining cells were fixed using the following protocol. Cells were washed twice with PBS and then fixed in pre-cooled methanol containing 1 mM EGTA for 10 min at -20 °C. After removing the methanol, the following steps were performed at room temperature. For further fixation cells were incubated with 4 % paraformaldehyde (PFA) in PBS for 20 min, washed twice with PBS and permeabilized with 0.15 % Triton X-100 in PBS for 5 min. Then, cells were incubated

with blocking solution for a minimum of 45 min. Depending on the employed primary antibodies or when phalloidin was used for actin staining, the fixation step with methanol was left out. Cells were incubated with the primary antibody diluted in blocking solution for 1 h. Coverslips were twice washed with blocking solution for 5 min and incubated with the secondary antibody in blocking solution for an additional hour. Antibody incubations were performed either in 24-well plates or in a humid chamber on parafilm. After incubation with the secondary antibody, coverslips were twice washed with blocking solution for 5 min followed by washing steps with 70 % ethanol (2 min) and pure ethanol (1 min). Finally, coverslips were air-dried and embedded in a drop of pre-warmed mounting medium on microscope glass slides (SuperFrost). Embedded samples were stored over night at room temperature in the dark and then transferred to 4 °C for long-time storage.
The employed phalloidin was either coupled to Alexa Fluor 488 (green) or Alexa Fluor 594 (red; both from Invitrogen) and diluted 1:200 in blocking solution.

Blocking solution:
1 % BSA
0.05 % Tween 20
in PBS

Mounting medium:
2.4 g Mowiol
6 g Glycerol (87 %)
6 ml H_2O_{deion}
→ Stir over night at room temperature
0.2 ml 200 mM Tris base-HCl, pH 8.5
→ Warm up to 60 °C for 10 min followed by centrifugation at 17000 xg for 30 min

900 µl of mounting medium + 100 µl anti-bleach solution (25 mg/ml n-propylgalate in 87 % glycerol)

2.7. Cell biological methods

2.7.1. Cell lines

All cell lines used in this study are listed in Table 8. To obtain mouse embryonic fibroblasts (MEFs), *TTL*+/- mice (Erck *et.al.*, 2005) were crossed and fibroblasts were isolated as described in 2.7.3.

Table 8: Cell lines used in this study.

Name	Description	Source
CLIP-115 knockout	primary mouse embryonic fibroblast, ***CLIP-115-/-***	Hoogenraad *et.al.*, 2002
CLIP double knockout	primary mouse embryonic fibroblast, ***CLIP-115-/-*, *CLIP-170-/-***	Schober *et.al.*, 2007
MEF01	primary mouse embryonic fibroblast, ***TTL+/-***	this study
MEF02	primary mouse embryonic fibroblast, **WT**	this study
MEF03	primary mouse embryonic fibroblast, ***TTL-/-***	this study
MEF04	primary mouse embryonic fibroblast, ***TTL+/-***	this study
MEF05	primary mouse embryonic fibroblast, ***TTL+/-***	this study
MEF06	primary mouse embryonic fibroblast, **WT**	this study
MEF07	primary mouse embryonic fibroblast, ***TTL+/-***	this study
MEF08	primary mouse embryonic fibroblast, ***TTL-/-***	this study
MEF09	primary mouse embryonic fibroblast, **WT**	this study
MEF21	primary mouse embryonic fibroblast, ***TTL-/-***	this study
MEF22	primary mouse embryonic fibroblast, ***TTL-/-***	this study
MEF33	primary mouse embryonic fibroblast, ***TTL-/-***	this study
MEF34	primary mouse embryonic fibroblast, **WT**	this study
MEF59	primary mouse embryonic fibroblast, ***TTL-/-***	this study
MEF67	primary mouse embryonic fibroblast, **WT**	this study
MEF68	primary mouse embryonic fibroblast, **WT**	this study
MEF69	primary mouse embryonic fibroblast, ***TTL-/-***	this study
MEF91	primary mouse embryonic fibroblast, ***TTL-/-***	this study
MEF92	primary mouse embryonic fibroblast, **WT**	this study
MEF103	primary mouse embryonic fibroblast, ***TTL-/-***	this study
MEF107	primary mouse embryonic fibroblast, **WT**	this study
MEF110	primary mouse embryonic fibroblast, **WT**	this study
MEF111	primary mouse embryonic fibroblast, ***TTL-/-***	this study
MEF132	primary mouse embryonic fibroblast, **WT**	this study

MEF133	primary mouse embryonic fibroblast, ***TTL-/-***	this study
MEF136	primary mouse embryonic fibroblast, ***TTL-/-***	this study
MEF137	primary mouse embryonic fibroblast, ***TTL-/-***	this study
MEF143	primary mouse embryonic fibroblast, **WT**	this study
NIH 3T3	immortalized murine fibroblast cell line	ATCC® CRL-1658™
PtK_2	Potorous tridactylis (kangaroo rat) kidney cells	ATCC® CCL-56™
TTL knockout (I)	***TTL-/-*** MEF immortalized by SV40 large T antigen, temperature-dependent (mitosis at 32 °C)	C. Erck
TTL knockout (II)	***TTL-/-*** MEF immortalized by SV40 largeT antigen, mitosis depends on availability of doxycycline (2 µg/ml)	C. Erck

2.7.2. Cell culture

All cell lines were grown at 37 °C and 7.5 % CO_2 (incubator from Labotect). In contrast, immortalized *TTL* knockout (I) cells were grown at 32 °C. All media used for cell culturing were prepared in a clean bench (SterilGARD® III Advance from Labotect) and stored at 4 °C. Before usage solutions were pre-warmed to 37 °C in a water bath (Grant Instruments). To transfer cells to a new culture dish, cells were washed with sterile PBS, detached from the dish by an incubation at 37 °C for 5 min in 0.25 % Trypsin/1 mM EDTA and finally diluted by adding fresh medium.

Medium for MEFs:

45 % DMEM (Dulbecco's Modified Eagle Medium) high glucose (4.5 g/l)
45 % F10 (Nutrient Mixture, Ham)
10 % (v/v) FCS lot 047K3395 from Sigma
2 mM Glutamine
50 U/ml Penicillin/Streptomycin

Medium for NIH3T3, PtK_2 and immortalized *TTL* knockout cells:

DMEM (Dulbecco's Modified Eagle Medium) low glucose (1 g/l)
10 % (v/v) FCS lot 101K3361 from Sigma
2 mM Glutamine
50 U/ml Penicillin/Streptomycin

Doxycycline was added to the medium in a final concentration of 2 µg/ml when *TTL* knockout (II) cells were cultured.

2.7.3. Isolation of mouse embryonic fibroblasts

To isolate primary mouse embryonic fibroblasts (MEFs) 13 day old embryos were used. First, the head and all red organs were removed and the tail was kept for genotyping (see chapters 2.4.3. and 2.4.5.). The remaining parts were transferred to 0.5 ml 0.25 % Trypsin/1 mM EDTA and cut in small pieces. After 30 min of incubation at 37 °C, 0.5 ml growth medium was added and aggregates solved by pipetting up and down. Then, cells were transferred to 10 cm plastic dishes that contained 9 ml growth medium. During the first few passages fibroblasts do overgrow other cell types.

2.7.4. Treatments

To reduce cell activity, cells were grown in FCS-free medium for two days, whereas *TTL* knockout (II) cells were cultured without doxycycline. If necessary, cells were re-activated by transfer to FCS- or doxycycline-containing medium, respectively. Cell starvation was used before wound-healing assays, immunofluorescence or Western blot analysis. More specific treatments are described below.

2.7.4.1. Reduction of tyrosinated tubulin levels

In this study, the effects of the absence of tyrosinated tubulin is examined. Since *TTL* knockout cells still contain tyrosinated tubulin due to ongoing tubulin synthesis, different treatments were tested to generate cells that are free of tyrosinated tubulin.

Cycloheximide:

To inhibit protein synthesis by blocking the translocation reaction on the ribosomes during translation, 0.25 mM cycloheximide was added to the growth medium (Slee *et.al.*, 1996). A 0.25 M stock solution was prepared in ethanol. Incubation times varied from 3 – 25 h. After that, cells were either fixed for immunofluorescence or lysed for Western blot analysis.

Forskolin:

To increase carboxypeptidase activity, cells were treated with 10 µM forskolin (10 mM stock solution in ethanol) for 8 – 24 h (Wehland & Weber, 1987b). After the treatment, cells were washed and fixed for immunofluorescent staining.

Mitomycin C:

For blocking the cell cycle, the DNA cross-linker mitomycin C was added to the growth medium in a concentration of 10 µg/ml (Celis, 1998). After 3 h, cells were washed three times with sterile PBS and kept in culture or lysed in 4x SDS sample buffer (see 2.5.6.) for Western blot analysis.

Nocodazole:

To reversibly block the cell cycle by depolymerization of microtubules, cells were treated with 0.4 µg/ml nocodazole for 2 – 24 h (Wehland & Weber, 1987b). After treatment cells were washed and used for immunofluorescence staining. The stock solution was prepared in DMSO with a concentration of 0.4 mg/ml nocodazole.

Taxol®:

Paclitaxel (Taxol®, 10 mM stock solution in DMSO) was used to block mitosis by stabilizing microtubules. Cells were grown in a concentration of 10 µM for 6 – 24 h (Wehland & Weber, 1987b), washed and fixed or kept in culture for further experiments.

Thymidine:

High concentrations of thymidine inhibit DNA synthesis by the reduction of the nucleotide precursor pool of dCTP. As cells are only affected when they are in S-phase, thymidine treatment can be used to synchronize cell populations (Celis, 1998).

Thymidine was added in a concentration of 2 mM to the medium for 24 h to stop the cell cycle. For a complete synchronization of the cells, a double thymidine block was performed. Therefore, cells were kept in medium containing 2 mM thymidine for 17 h. After two times washing with FCS-free medium 2 µM dCytidine was added for 9 h followed by another washing and 16 h incubation with 2 mM thymidine again. Finally, cells were washed and fixed for immunofluorescence or lysed for Western blotting.

2.7.4.2. Inhibition of protein kinases and phosphatases

To test if the observed phosphorylation-caused mass shift of CLIP-115 between wild type and *TTL*-/- MEFs is caused by a serine/threonine or tyrosine phosphorylation, cells were treated with different kinase and phosphatase inhibitors. Cells were washed with PBS and lysed in 2x destroyer buffer for Western blot analyses after the treatments. Control cells were treated with DMSO instead of an inhibitor.

Staurosporine:

To inhibit the activity of a broad range of protein kinases, cells were incubated with 0.5 µM staurosporine for 1 – 3 h (0.5 mM stock solution in DMSO, Bijur *et.al.*, 2000).

Genistein:

For the inhibition of tyrosine kinases, 100 µM genistein was added (100 mM stock solution in DMSO, Elliot *et.al.*, 2001) to the growth medium followed by an incubation of 1 – 3 h.

Calyculin A:

The activity of serine/threonine-phosphatases (type PP1) was inhibited in cells by incubation with 5 nM calyculin A for 20 min (stock solution of 5 µM in DMSO).

Okadaic acid:

Cells were treated with 25 nM okadaic acid (2 µM stock solution in DMSO) for 20 min to inhibit serine/threonin-phosphatase (type PP2) activity.

Vanadate:

To specifically inhibit tyrosine phosphatases, cells can be treated with ortho-sodium vanadate (Na_3VO_4). For that, 10 µl 100 mM Na_3VO_4 was mixed with 87 µl H_2O_{deion} and 3 µl 30 % H_2O_2 and incubated for 10 min at room temperature. Then, Na_3VO_4 was added to the growth medium at a final concentration of 100 µM and cells were incubated for 10 – 120 min.

2.7.5. Transfection

To test the transfection efficiency of cells, MEFs were transfected with the following transfection reagents FuGENE® 6 (Roche), Lipofectamine™ 2000 (Invitrogen), METAFECTENE™ (Biontex), SuperFect (Qiagen) and ICAFectin™ 441 (Eurogentec) as described by the manufacturers. Since FuGENE® 6 yielded the best transfection efficiency and was used in further experiments, the procedure is briefly described here. Cells were seeded 24 h before transfection. For the transfection of cells in 3.5

cm dishes, 2 µg of DNA was mixed with 6 µl of FuGENE® 6 in OPTI-MEM® growth medium followed by 30 min incubation at room temperature before adding the mixture to the cells. The recipe was doubled for transfecting cells grown in 6 cm dishes and expanded to 10 µg of DNA and 30 µl of FuGENE® 6 when cells were grown in 10 cm dishes. Cells were fixed for immunofluorescence or lysed for Western blotting 16 – 48 h after transfection.

2.7.6. Wound-healing assay

To observe cell polarization and migration after reducing levels of tyrosinated tubulin, cells were grown on glass coverslips until confluency followed by starvation for 2 d. A wound was introduced by scratching with a pipette tip followed by re-activating the cells by adding FCS-containing medium to the cells 20 min after wounding (Gundersen et al., 1994). Cells were fixed at different time points after wounding and analysed by immunofluorescence.

2.7.7. Cell lysis

To lyse cells for Western blot analysis, SDS-containing destroyer buffer was used. Therefore, cells were washed twice with PBS and harvested by scratching in 100 µl 2x destroyer buffer containing protease inhibitor cocktail (Roche). Next, lysates were boiled for 10 min at 99 °C and stored at -20 °C for later analysis.

Basic IP buffer was employed in cell lysis when lysates were subsequently used for enzyme-treatments (2.7.8.). In that case, cells were washed twice with PBS and scratched in 200 µl basic IP buffer containing protease inhibitor cocktail (Roche). For further lysis cells were kept on ice for 15 – 30 min followed by the enzyme treatment.

Destroyer buffer, pH 7.5:

25 mM Tris base

1 mM EDTA

1 mM EGTA

1 % (v/v) SDS

Basic IP buffer:

15 mM KCl

50 mM NaCl

8 mM Tris base

12 mM Hepes free base

3 mM $MgCl_2$

Before use addition of

1 tablet protease inhibitor cocktail, complete, EDTA-free (Roche) in 10 ml

1 % (v/v) Triton X100

2.7.8. SAP-treatment of cell lysates

To test if the observed difference of the molecular weight of CLIP-115 in wild type and *TTL*-/- MEFs was caused by phosphorylation, MEF lysates were treated with shrimp alkaline phosphatase (SAP; Roche). Total cell lysates (see 2.7.7.) were mixed with 20 U SAP. Dephosphorylation was started by transferring the mixtures to 37 °C. After 1 h incubation, samples were stored for further analysis at -20 °C.

2.7.9. Subcloning

To isolate a clone of the mouse antibody 1D5 against detyrosinated tubulin that shows a strong staining in immunofluorescence five stored hybridoma clones were thawed and subcloned. Therefore, the non-adherent hybridoma cells were transferred to tubes containing 9 ml of growth medium and centrifuged for 5 min at 1000 rpm. The supernatant was removed, the cell pellet re-suspended in 2 ml of medium and cells grown at 37 °C in 6-well plates overnight. Cells were then transferred to 10 cm dishes (Corning, untreated) containing 10 ml of medium. After three days, 1 ml culture supernatant of each well was centrifuged and tested in immunofluorescence on PtK_2 cells as described in 2.6.4. Cells of the 1D5 clone with the strongest staining were diluted 1:6 in medium and grown for another three days. Then, cells were counted in a Neubauer chamber and seeded in 96-well plates in concentrations of 50 cells/well, 10 cells/well, 2.5 cells/well (32 wells per concentration), 0.5 cells/well, and 0.25 cells/well (48 wells per concentration). After two weeks, the supernatant of each well containing a single clone was tested in immunofluorescence on PtK_2 and *TTL* knockout cells. Again, clones that showed a

strong specific staining were transferred to 6-well plates, grown in 3 ml of medium, and fed with another 3 ml after three days. Since different cell lines contain different levels of detyrosinated tubulin, PtK_2, *TTL* knockout and NIH 3T3 cells were used to gain more detailed information of the tested subclones. The clone, which gave the strongest and most specific staining, was expanded. After the addition of 0.02 % sodium azide, the supernatant was stored at 4 °C. Additionally, cells were frozen for later use.

Growth medium:

OPTI-MEM® I from Gibco
5 % (v/v) FCS lot 101K3361 from Sigma
2 mM Glutamine
50 U/ml Penicillin/Streptomycin

2.7.10. Epifluorescence Microscopy

Immunostained cells were analysed using an inverted microscope (Axiovert S100 TV or Axiovert 135 TV, both from Zeiss), which was equipped for epifluorescence and phase contrast microscopy. In general, a 63x/NA 1.4 plan-apochromatic objective (Zeiss) in combination with immersion oil (Immersol™ 518F, Zeiss) was employed. For epifluorescence, the microscopes were connected to a mercury lamp (HBO 100W/2 from Osram, later changeover to HXP 120 from Kübler). Images were acquired with a back-illuminated, cooled charge-coupled-device (CCD) camera, either driven by IPLab software from Scanalytics Inc. (camera: TE-CCD 800PB, Princeton Scientific Instruments) or by MetaMorph® software from Molecular Devices (camera: Cool Snap HQ^2, Visitron Systems). Images were then processed using Adobe Photoshop 7.0. Microtubule plus-end lengths were measured in ImageJ 1.42 (http://rsbweb.nih.gov/ij/download.html) with a scale of 9.800 pixels/µm. Data was further processed in Microsoft Excel 2000, and statistic analyses were performed using Minitab software.

2.7.11. Microinjection

Cells for microinjection were seeded on 12 mm glass coverslips and kept in the plastic dish at room temperature during the injection procedure. To control the flow

through the injection needle under UV light and to identify injected cells after fixation, the antibodies for microinjection were mixed with an Alexa Fluor 488-coupled antibody that was chosen to avoid cross-reactions. The antibody mix was centrifuged at 13000 rpm and 4 °C for a minimum of 10 min to remove aggregates that could clog the needle. Microinjections were performed using sterile capillaries (Femtotips I, Eppendorf), which were loaded from the backside with the antibody solution using a flexible pipette tip. To guarantee an undisturbed flow-through it was important to avoid air bubbles. The needle was transferred to an injection unit (Narishige, Nikon) connected to a Transjector 5246 (Eppendorf) that served as a pressure supply. The transjector provided a constant pressure up to 100 hPa. Microinjection was performed manually. The employed microscope (Axiovert S100 TV, Zeiss) was equipped with a 20x or 40x/LD Achroplan objective depending on the cell size. Cells were fixed 2 – 4 h after injection and analysed by immunofluorescence (see 2.6.4.).

3. Results

In this study, the physiological role of the α-tubulin tyrosination cycle was investigated by using fibroblasts that lack tubulin-tyrosine ligase (TTL). As reported previously, mitotic *TTL* knockout cells still contain tyrosinated (Tyr-) tubulin (Erck et al., 2005). Therefore, chemical treatments were employed to reduce Tyr-tubulin levels enabling the analysis of cellular processes in the absence of Tyr-tubulin. Furthermore, microinjection of antibodies that block the remaining C-terminal tyrosine residues of α-tubulin was performed as alternative approach to obtain cells without any functional Tyr-tubulin. In wound-healing assays the impact of reduced Tyr-tubulin amounts on cell polarization and migration was investigated.

As it was not possible to generate viable cells that completely lack Tyr-tubulin, freshly isolated *TTL* knockout mouse embryonic fibroblasts (MEFs) were used to characterize different tubulin pools. In a population of *TTL* knockout MEFs both Tyr-positive and Tyr-negative cells were present, which were separately analysed. Although it has been reported that the subcellular localisation of microtubule plus-end tracking proteins (+TIPs) is affected by TTL deficiency (Erck et al., 2005; Peris et al., 2006), the mechanism of microtubule binding of +TIPs and its regulation is still unknown. Therefore, the localisation and biochemical properties of several +TIPs were investigated in this study.

One of the analysed +TIPs, namely CLIP-115, showed differences in its localisation towards microtubules in wild type and Tyr-negative *TTL* knockout MEFs. Additionally, CLIP-115 appeared at a different molecular weight in the presence and absence of TTL. Since inhibitor treatments pointed to differential tyrosine phosphorylation of CLIP-115 in wild type and TTL-deficient MEFs, site-directed mutagenesis experiments were performed to identify potential phosphorylation sites. Subsequent mass spectrometry analysis of CLIP-115 was employed to validate the results obtained by the mutagenesis experiments and to identify putative additional phosphorylation sites that may reveal new aspects in the plus-end tracking mechanism of CLIP-115.

3.1. Depletion of tyrosinated tubulin in *TTL* knockout cells

Fibroblasts that lack the tubulin-tyrosine ligase still contain residual amounts of tyrosinated tubulin. This pool most probably results from ongoing protein biosynthesis. However, to investigate the effects of TTL deficiency on processes like cell migration and cell polarity, and on the intracellular distribution of microtubule-associated proteins, the aim was to obtain cells that were completely free of tyrosinated tubulin. For this purpose, different chemical treatments in cell culture were performed to inhibit transcription and/or translation. In addition, microinjection of antibodies was used to specifically block the extreme C-terminal tail of α-tubulin.

3.1.1. Chemical treatments

To interrupt transcription by cross-linking the DNA and thereby stop the production of Tyr-tubulin, immortalized *TTL* knockout (I) cells that only divide at 32 °C (see Tab. 8 in chapter 2.7.1.) were treated with mitomycin C. Cells were then tested for the presence of tyrosinated (Tyr-), detyrosinated (Glu-) and Δ2-Glu-tubulin by immunofluorescence. Mitomycin-treated cells were also kept in culture for a total duration of 10 days after treatment. Although the cells showed high amounts of Glu- and Δ2-Glu-tubulin, microtubules were still labelled by antibodies against Tyr-tubulin (not shown). In addition, translation was inhibited by cycloheximide, which blocks the translocation reaction on eukaryotic ribosomes. Therefore, cells were incubated with cycloheximide alone or subsequent to the mitomycin C treatment for different time intervals. During treatments, the temperature-sensitive cells were transferred to 37 °C to additionally inhibit mitosis. Western blot analysis using YL1/2 antibody revealed a strong reduction of Tyr-tubulin after cycloheximide treatment, whereas treatments with mitomycin C alone or followed by a cycloheximide treatment did not efficiently decrease the Tyr-tubulin levels (not shown). However, the cell viability was severely impaired by treatments with cycloheximide.

Furthermore, thymidine, nocodazole, taxol and forskolin were alternatively applied to the cells (as described in chapter 2.7.4.). Thymidine and nocodazole were both employed to inhibit mitosis and additionally combined with a cycloheximide treatment of 16 h. Thymidine reduces the nucleotide precursor pool of dCTP and by that blocks DNA synthesis. Hence, a doublefold thymidine block was performed to synchronize and arrest the cells in mitosis. In addition to the treatment with thymidine, the

cytotoxin nocodazole was applied in order to block the cell cycle by its depolymerizing effect on microtubules. Both the thymidine treatment as well as the depolymerization of microtubules by nocodazole only reduced Tyr-tubulin levels in combination with cycloheximide (not shown). Again, all studied cells were in poor condition after treatments. Another approach to inhibit mitosis was the application of the microtubule-stabilizing drug taxol. Taxol was also used in conjunction with forskolin, which activates carboxypeptidases (Wehland & Weber, 1987b) and, thus, should further decrease Tyr-tubulin levels in *TTL* knockout cells. Moreover, cells were subsequently treated with cycloheximide. However, none of these treatments turned out to be effective to lower Tyr-tubulin amounts (not shown).

Additionally, another immortalized *TTL* knockout cell line (*TTL* knockout (II), see Tab. 8 in chapter 2.7.1.) was used. *TTL* knockout (II) cells only divide in medium containing 2 µg/ml doxycycline. All treatments were performed as described above. In summary, the treatments failed in an efficient reduction of Tyr-tubulin levels (not shown). Interestingly, *TTL* knockout (II) cells reacted more sensitive to the treatments than the temperature-sensitive *TTL* knockout (I) cells. As many of the *TTL* knockout (II) cells died after the mentioned treatments, it was also tested whether starvation already reduces Tyr-tubulin levels. Therefore, cells were cultivated for two days without FCS and doxycycline before analysing the Tyr-tubulin levels in immunofluorescence and Western blotting. The withdrawal of either FCS or doxycycline itself did not evoke any obvious reduction in Tyr-tubulin, whereas culturing without both additives resulted in lower Tyr-tubulin levels. However, again many cells did not survive starvation. Results of all chemical treatments are summarized in Table 9.

Table 9: Chemical treatments of immortalized *TTL* knockout cells to reduce Tyr-tubulin levels.

Treatment	Reduction of Tyr-tubulin in	
	TTL knockout (I) cells	*TTL* knockout (II) cells
Cycloheximide (CHX)	**++**	-
Forskolin	-	-
Forskolin + Taxol	-	-
Forskolin + Taxol + CHX	-	-
Mitomycin C	-	-
Mitomycin C + CHX	-	-
Nocodazole	-	-
Nocodazole + CHX	**+**	**+**
Starvation:		
- Doxycycline	n. d.	-
- FCS	-	-
- FCS - Doxycycline	n. d.	**+**
Taxol	-	-
Thymidine	-	-
Thymidine + CHX	**+**	**+**

++ Strong reduction of Tyr-tubulin level

+ Moderate reduction of Tyr-tubulin levels

- No reduction of Tyr-tubulin levels

n. p. not determined

3.1.2. Investigation of cell migration and cell polarity

To reveal a potential effect of the reduced Tyr-tubulin amount on cell polarity, starved *TTL* knockout (II) cells were studied in wound-healing assays. In this assay, a confluent layer of serum-starved cells is wounded by scratching with a pipette tip. After the addition of serum, cells at the wound edge start to polarize by reorientation of their microtubule organizing centre (MTOC) in the direction of the wound (green area in Fig. 14a). In parallel, stabilized microtubules are formed in the leading edge, whereas the cells start to migrate into the wound in order to close it. As the Golgi apparatus is closely associated with the MTOC it can be used to visualize cell polarity (Palazzo et al., 2001).

In this study, *TTL* knockout (II) cells were grown on coverslips until confluency and kept in serum- and doxycycline-free medium for two days before a wound was introduced into the cell layer. Twenty minutes later, the medium was substituted by normal growth medium for cell re-activation as described in chapter 2.7.6. Cells were fixed 0, 1, 2, 3 and 4 h after changing the medium and stained with a Golgi-marker to visualize cell polarity. One hour after wounding, cells started to orient the Golgi towards their leading edge at the cell-free wounding area. After 2 h, all cells at the wound edge showed a localisation of the Golgi between nucleus and leading edge. Apparently, the induced reduction of Tyr-tubulin in starved *TTL* knockout (II) cells had no influence on the ability of cells to polarize (Fig. 14b). Furthermore, the cells closed the wound without being hindered in migration (not shown).

a) **b)**

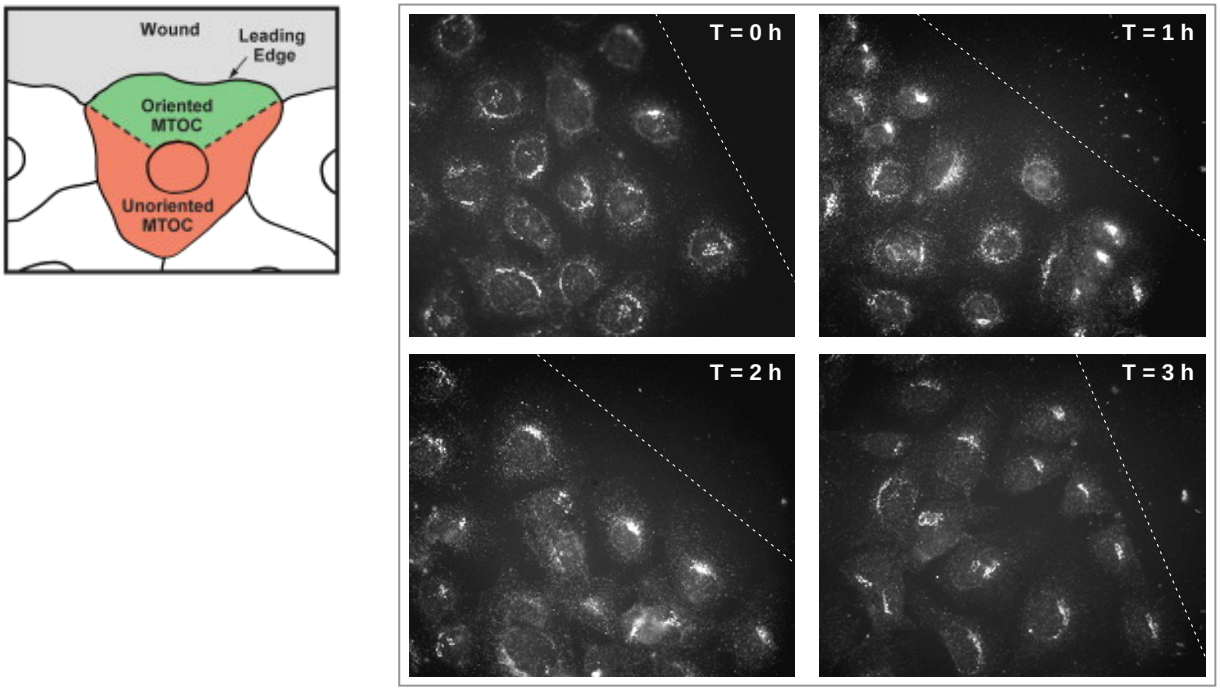

Fig. 14: Wound-healing assay with *TTL* knockout (II) cells after 2 days of starvation. a) Scheme to show MTOC reorientation in fibroblasts (from Palazzo et al., 2001). In polarized cells the MTOC is localised in the green area facing the wound, whereas an unoriented MTOC would be located in the red area. **b)** Starved *TTL* knockout (II) cells at time point T after wounding and transfer to FCS-containing medium (the dashed line marks the wound edge). Cell polarity was analysed using the Golgi-specific antibody golgin 97. All peripheral cells showed polarization 2 h after wounding.

In summary, the aim was to obtain TTL-deficient fibroblasts without any residual tyrosinated tubulin. Unfortunately, all chemical treatments used in this study did only result in slightly decreased levels of tyrosinated tubulin and therefore had no obvious effects on cellular processes such as cell polarization.

3.1.3. Microinjection of antibodies

Since, as described above, chemical treatments of TTL-deficient fibroblasts did not result in the complete loss of tyrosinated tubulin levels, microinjection of antibodies that specifically recognize the α-tubulin C-terminus containing the ultimate tyrosine was used to block the remaining tyrosinated tubulin.

To obtain pure antibodies that could be used for microinjection, the murine antibody 20C6 was successfully purified from hybridoma supernatants using protein G affinity chromatography (see 2.5.2.1.). Since rat antibodies possess a very weak affinity for protein A or G, the rat monoclonal antibody YL1/2 was purified from ascites (Biotem, France) by ammonium sulfate precipitation and FPLC (see 2.5.2.2.). Both the precipitation and the FPLC-mediated purification were successful as observed by SDS-PAGE and subsequent Coomassie-staining (not shown). Antibody-containing FPLC fractions were pooled and used for microinjection.

First, different purified YL1/2 antibody concentrations, ranging from 0.5 mg/ml to 3.0 mg/ml, were tested in manually performed microinjections on immortalized *TTL* knockout (II) cells to determine an appropriate antibody concentration. After microinjection, cells were kept in culture for an additional 2 – 4 h followed by methanol/PFA fixations and analysis by immunofluorescence. Non-injected cells showed a normal cellular distribution of tyrosinated microtubules. In contrast, cells that were microinjected with 0.5 mg/ml YL1/2 antibody showed the appearance of thicker microtubules indicating the presence of microtubule bundles. This effect became more prominent with increasing antibody concentrations (not shown) as previously described (Wehland et al., 1983). Since antibodies possess two epitope binding sites, one on each F_{ab} fragment, they can in principle bind two separate microtubules resulting in the observed microtubule bundles.

To avoid this cross-linking of microtubules by the injected antibody, F_{ab} fragments of both 20C6 and YL1/2 antibodies were digested from the respective F_c parts followed by purification. For that, a specific papain-mediated digest was performed using the

ImmunoPure® Fab Preparation Kit from Pierce (see chapter 2.5.3.). To ensure the exclusive presence of F_{ab} fragments, additional purification steps were performed.

In case of the murine 20C6 antibody, remaining F_c-fragments were depleted from purified F_{ab} fractions by a subsequent purification step using protein A. The success of the procedure was validated by SDS-PAGE in reducing and non-reducing conditions followed by Coomassie-staining. After papain digestion, F_{ab} fragments of a molecular weight of about 25 kDa could be detected. In non-reducing conditions, the purified F_{ab} fragments gave a clean band at about 40 kDa (not shown).

Also the generation of YL1/2 F_{ab} fragments was documented by SDS-PAGE in both reducing and non-reducing conditions. After papain digest, F_{ab} and F_c fragments were visible as a double band at about 25 kDa and a single band at about 28 kDa, respectively (not shown). To achieve separation of YL1/2 F_{ab} from F_c fragments, an additional purification by FPLC using anion exchange chromatography was performed. F_c fragment-depleted fractions of F_{ab} fragments were then pooled, concentrated in PBS and employed in microinjection.

In parallel, commercial purification of F_{ab} fragments of both 20C6 and YL1/2 antibodies by the Pineda Antibody Service (Berlin) was performed to obtain larger amounts of F_{ab} fragments. Unfortunately, SDS-PAGE analysis of the received samples revealed that these samples were contaminated and could not be used for further analysis.

Although only little amounts of self-purified F_{ab} fragment were obtained, still a few initial experiments could be performed. Freshly isolated wild type and *TTL* knockout primary mouse embryonic fibroblasts were employed (see chapters 2.7.3.). Cells were fixed 2 h after microinjection and stained for the microtubule plus-end tracking protein CLIP-170 that was reported to be mislocalised in cells lacking Tyr-tubulin (Peris et al., 2006). Indeed, about 25 % of microinjected wild type and *TTL* knockout MEFs showed CLIP-170 bound to very few microtubule plus-ends. In non-injected MEFs, CLIP-170 normally localised at microtubule plus-ends. However, the differences in the localisation of CLIP-170 in wild type and *TTL* knockout MEFs described by Peris and colleagues (2006) could not be confirmed.

In summary, microinjection of both undigested antibodies as well as isolated F_{ab} fragments did not give clear results in our experimental set-up. Since the aforementioned experiments did not sufficiently reduce Tyr-tubulin levels in

immortalized *TTL* knockout MEFs, it was decided to focus further studies on a detailed characterization of primary *TTL* knockout mouse embryonic fibroblasts in order to gain deeper insight into the impact of TTL deficiency.

3.2. Characterization of tubulin pools in TTL-deficient mouse embryonic fibroblasts

To unravel the physiological meaning of the α-tubulin tyrosination cycle, the lack of the tubulin-tyrosine ligase was investigated on cellular level in this study. Besides morphological anomalies, Erck et al. (2005) reported a mislocalisation of the microtubule plus-end tracking protein CLIP-170 in *TTL*-/- neurons. To identify potential effects of TTL deficiency in another cell type we chose primary mouse embryonic fibroblasts (MEF) for our investigations. Compared to neurons, fibroblasts are much easier to culture and for that suitable for the experiments of this study.

By crossing heterozygous *TTL*+/- mice (Erck et al., 2005) and isolating 13 days old embryos MEFs could be established (see chapter 2.7.3.). After confirmation of the genotype by PCR (described in chapter 2.4.5.), MEF cell lines were starved for two days to enhance potential differences in tubulin pools. Subsequently, wild type, *TTL*+/- and *TTL*-/- MEFs were analysed by immunofluorescence to show different pools of α-tubulin, whereas β-tubulin was used as a control to check microtubule integrity. Images were acquired with the same exposure times and settings by IPLab software to enable a comparison of the specific tubulin pools in different genotypes. Representative images are shown in Figure 15. As expected, the presence of β-tubulin was independent of the genotype and showed an intact microtubule network. Similar intensities of tyrosinated tubulin were only recognizable in wild type and *TTL*+/- MEFs. In *TTL*-/- MEFs, stainings of Tyr-tubulin exhibited only pale microtubule structures. Beside TTL-dependent changes in the amount of Tyr-tubulin, levels of detyrosinated tubulin considerably differed between the studied cell lines. Whereas the level of Glu-tubulin was low in wild type and heterozygous MEFs, TTL-deficient MEFs possessed a highly enriched amount of Glu-tubulin. Moreover, *TTL*-/- MEFs were the only cells containing Δ2-Glu-tubulin.

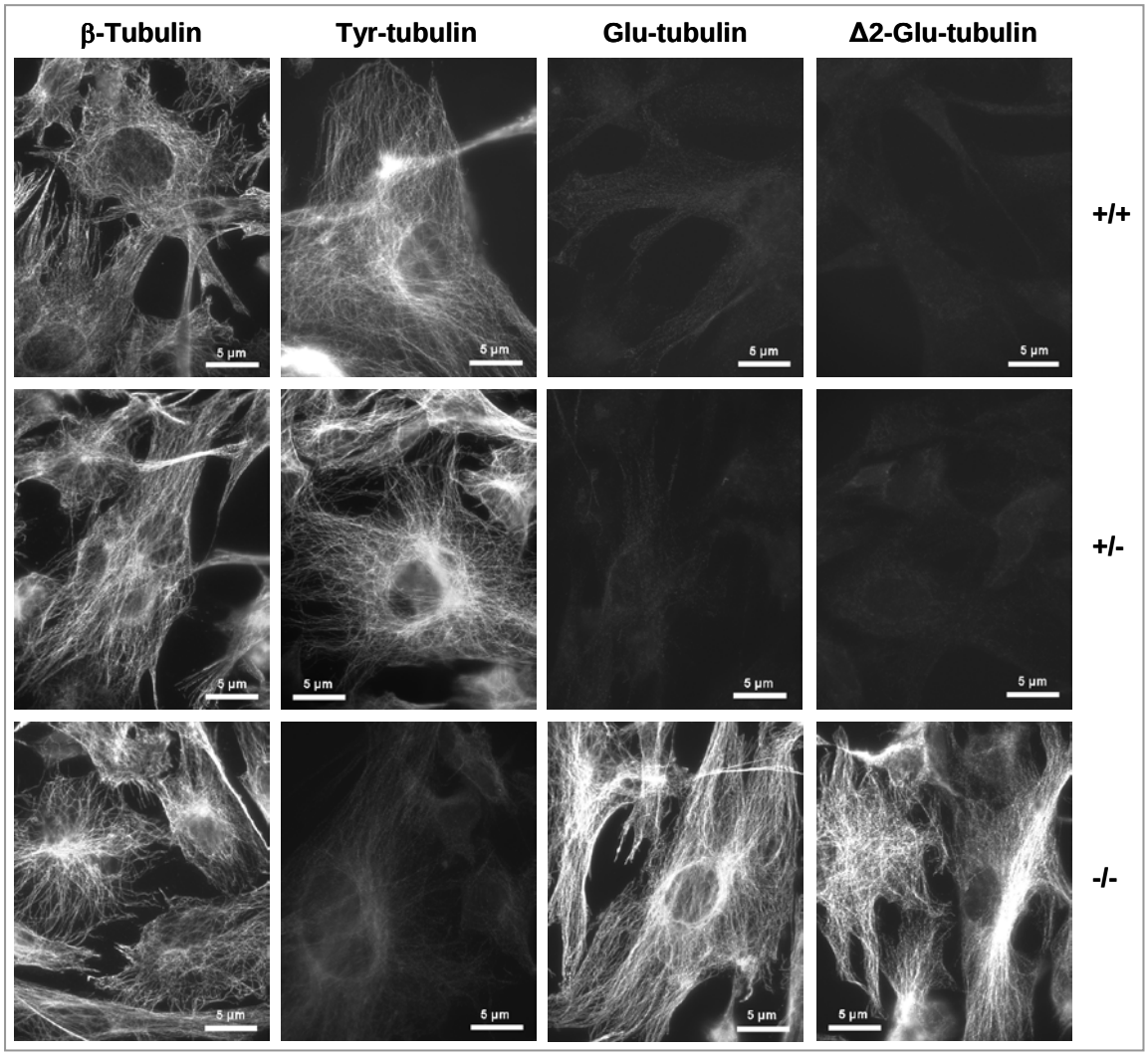

Fig. 15: Tubulin staining in wild type (+/+), *TTL*+/- and *TTL*-/- MEFs. Immunofluorescence of β-tubulin, Tyr-tubulin, Glu-tubulin and Δ2-Glu-tubulin using antibodies 2.3B11, YL1/2 cell culture supernatant, 1D5 clone H4 cell culture supernatant and antibody L4, respectively. Note the clear differences in tubulin pools in wild type and *TTL*+/- MEFs compared to TTL-deficient MEFs.

To confirm the results of the immunofluorescence studies, Western blot analyses were additionally performed by using the same set of antibodies. Actin served as an additional loading control besides β-tubulin (Fig. 16). Consistent with the results of the immunofluorescent stainings, tyrosinated tubulin could only be identified in wild type and heterozygous MEFs (cell lines 1, 2, 7 and 9), whereas detyrosinated and Δ2-Glu-tubulin were exclusively found in TTL-deficient MEFs (cell lines 3, 8, 21 and 22). As expected, the amounts of β-tubulin and actin appeared to be independent of the presence or absence of the TTL gene.

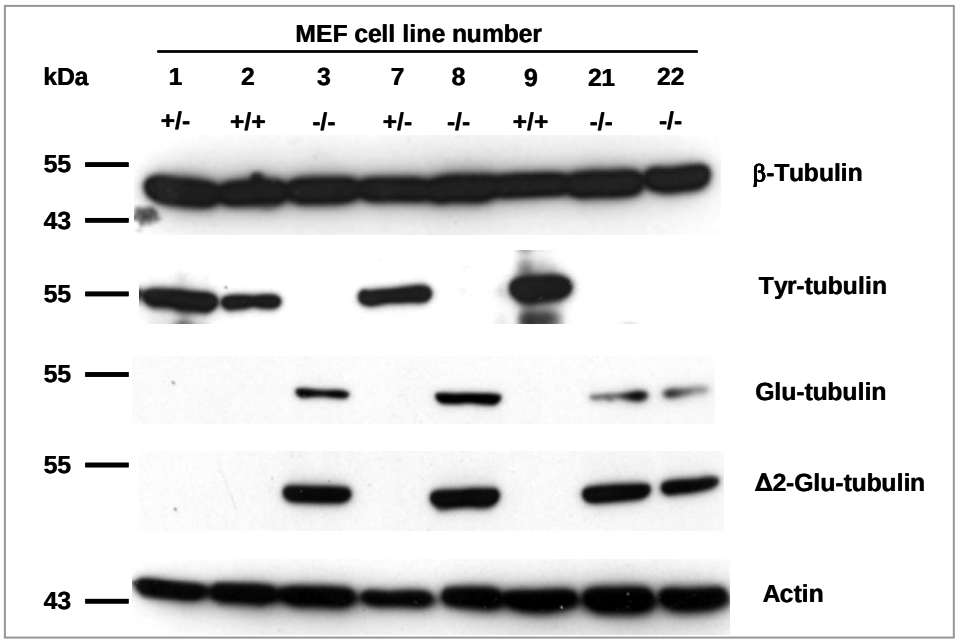

Fig. 16: Tubulin amounts in wild type (+/+), *TTL*+/- and *TTL*-/- MEFs. Western blot analysis of β-tubulin (2.3B11), Tyr-tubulin (YL1/2 hybridoma supernatant), Glu-tubulin (1D5 clone H4 hybridoma supernatant), Δ2-Glu-tubulin (L4) and actin (A5060) in wild type, *TTL*+/- and *TTL*-/- MEF lysates. Cells were serum-starved for 2 d before lysis.

Although Tyr-tubulin could neither be recognized by immunofluorescence nor by Western blotting with YL1/2 hybridoma supernatant, labelling with highly concentrated YL1/2 antibody revealed a heterogeneous population of *TTL*-/- MEFs as described by Peris et al. (2006). A small percentage of cells still contained Tyr-tubulin, while the majority of cells were negative for Tyr-tubulin in immunofluorescent stainings. In our cell culture, the amount of Tyr-negative MEFs increased with numerous passages, whereas most of the freshly isolated *TTL*-/- MEFs were still positive for Tyr-tubulin.

3.3. Microtubule plus-end tracking proteins in MEFs

For further analysis of TTL deficiency, the characterization of wild type and *TTL* knockout MEFs was subsequently focussed on microtubule plus-end tracking proteins (+TIPs). In previous studies, Erck et al. (2005) demonstrated a mislocalisation of the microtubule plus-end tracking protein CLIP-170 in *TTL*-/- neurons. Additionally, Peris et al. (2006) published binding of CAP-Gly domain-containing proteins such as CLIP-170, CLIP-115 and p150^{Glued} only to plus-ends of

tyrosinated microtubules in fibroblasts. Therefore, we investigated microtubule plus-end tracking proteins by immunofluorescence and Western blot analyses regarding their localisation and biochemical properties. Since heterozygous MEFs showed the same phenotype as wild type MEFs, further experiments were focussed only on wild type and TTL-deficient MEFs.

3.3.1. Localisation of microtubule plus-end tracking proteins

The end-binding protein 1 (EB1) was reported to bind microtubule plus-ends independently of the tyrosination state of the microtubule and is therefore unaffected by the presence or absence of the TTL gene (Peris et al., 2006). As expected, stainings of EB proteins labelled the microtubule plus-ends in wild type MEFs and in Tyr-positive as well as Tyr-negative *TTL*-/- MEFs (Fig. 17, third panel). Consequently, EB staining could be used as a plus-end marker in further experiments.

In contrast, CLIP-170 localisation was reported to be dependent on tyrosinated α-tubulin in neurons (Erck et al., 2005) and fibroblasts (Peris et al., 2006). However, in this study, staining of CLIP-170 showed a persistent localisation at microtubule plus-ends in MEFs, independently from the presence or absence of Tyr-tubulin (Fig. 17, second panel). Merged images demonstrate the co-localisation of CLIP-170 and EB1 not only in wild type MEFs, but also in both Tyr-positive and Tyr-negative *TTL*-/- MEFs (Fig. 17, right panel). The length of CLIP-170 plus-end comets was not influenced by the presence or absence of Tyr-tubulin.

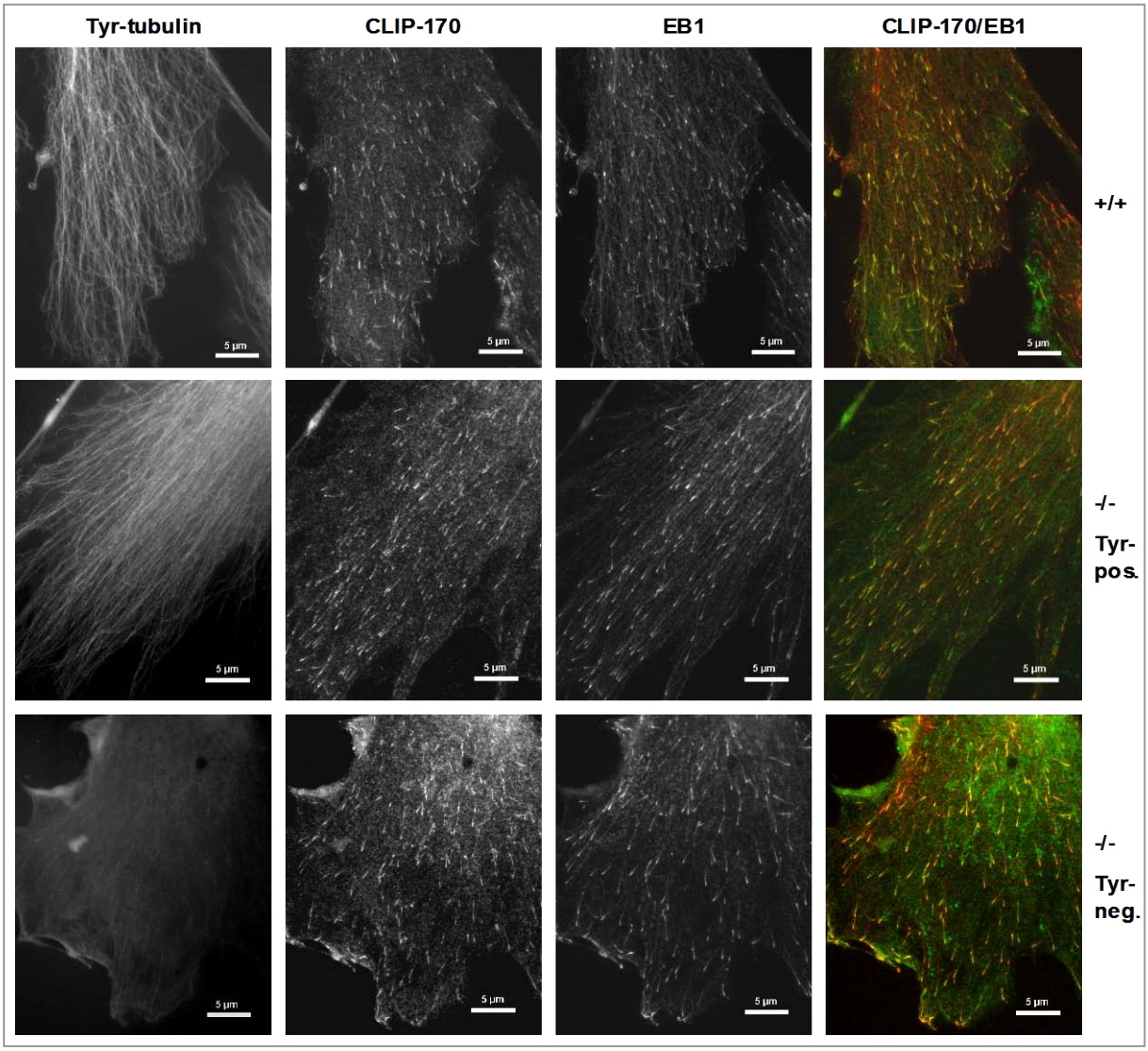

Fig. 17: CLIP-170 localisation in wild type and *TTL*-/- MEFs. Wild type (+/+), Tyr-positive *TTL* knockout (-/- Tyr-pos.) and Tyr-negative *TTL* knockout MEFs (-/- Tyr-neg.) were immunostained for Tyr-tubulin using purified YL1/2, CLIP-170 using #2360 antibody and EB1 using clone 5 antibody. Merged images show co-localisation of CLIP-170 (green) and EB1 (red).

Interestingly, the localisation of CLIP-115, which is a close family member of CLIP-170, appeared to be different in Tyr-positive and Tyr-negative MEFs. In both cell types, CLIP-115 was bound to the microtubule plus-ends but showed significantly longer plus-end comets in *TTL*-/- MEFs lacking Tyr-tubulin. In contrast, *TTL*-/- MEFs that still contained Tyr-tubulin resembled wild type MEFs in the CLIP-115 phenotype (Fig. 18).

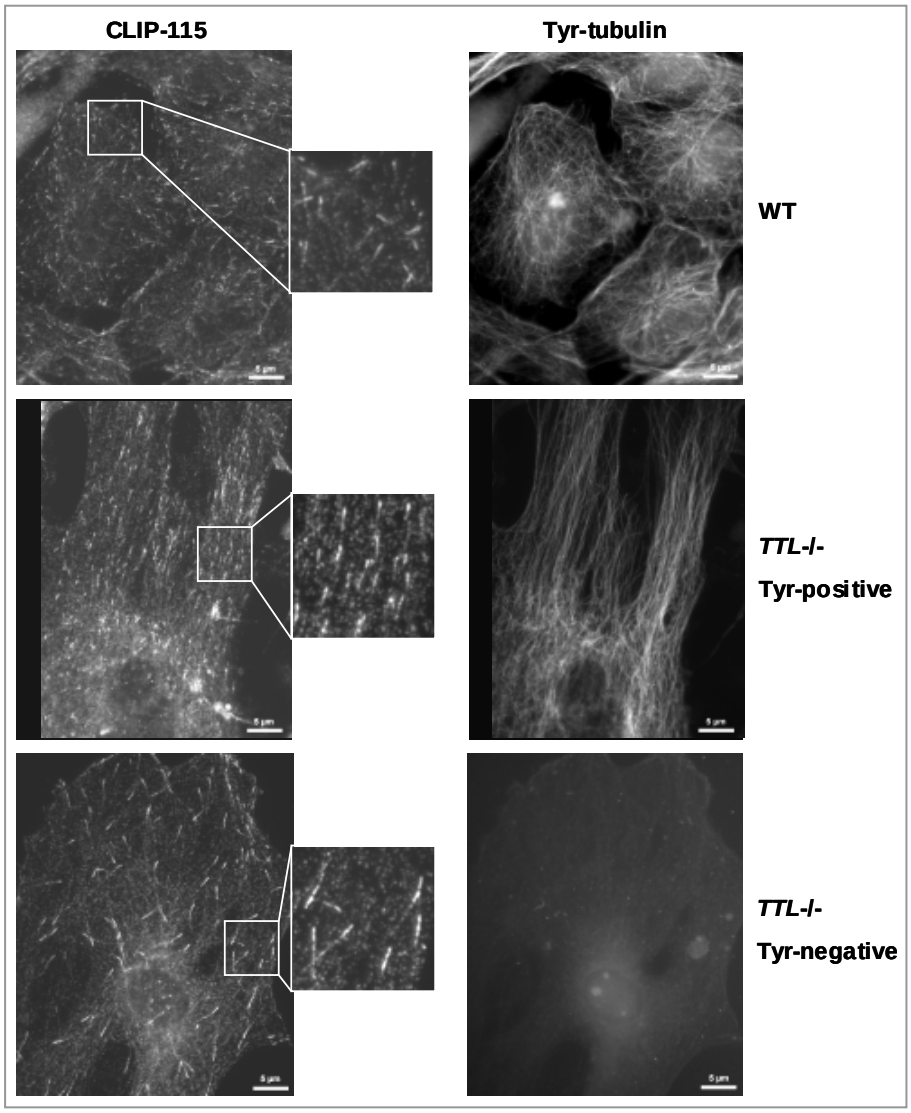

Fig. 18: Elongated CLIP-115 plus-end comets in Tyr-negative *TTL*-/- MEFs. CLIP-115 and Tyr-tubulin immunostaining in wild type, Tyr-positive and Tyr-negative *TTL*-/- MEFs using antibodies #2163 and purified YL1/2, respectively.

Although it was reported for the dynactin complex component p150^{Glued} to exclusively bind to plus-ends of tyrosinated microtubules (Peris et al., 2006), in this study stainings of p150^{Glued} did not reveal any difference between wild type and *TTL*-/- MEFs. Instead, p150^{Glued} co-localised with CLIP-170 (not shown). As stainings were very weak and did not differ in the studied MEF cell lines, p150^{Glued} was not further analysed.

3.3.2. Length of CLIP-170 and CLIP-115 plus-end comets

To quantify the length of CLIP-170 and CLIP-115 plus-end comets, images were reversed and brightened in Adobe Photoshop (“Input Levels” set to 50 – 1.00 – 230) to decrease background signal. Furthermore, the nucleus and the flanking perinuclear space of 2 µm were marked and excluded in following measurements. By that, an artificial shortening of the comets caused by the angle of the plus-ends was minimized (Fig. 19a). Measurements were then performed manually in the peripheral, flat cell area using ImageJ 1.42 software. Images were acquired from two wild type and two *TTL*-/- MEF cell lines in two independent experiments. 500 plus-end comets per cell line and experiment were measured in wild type, Tyr-positive and Tyr-negative *TTL*-/- MEFs giving 1000 values that were taken together for statistical analysis. Measurements revealed CLIP-170 plus-end comets to be of similar length in wild type, Tyr-positive and Tyr-negative *TTL*-/- MEFs with medians between 0.64 µm and 0.70 µm (Fig. 19b). In contrast, CLIP-115 plus-end comets are significantly longer in Tyr-negative *TTL*-/- MEFs with a median of 1.06 µm compared to 0.61 µm in Tyr-positive *TTL*-/- and 0.60 µm in wild type MEFs (Fig. 19c). According to the Anderson-Darling normality test the data set did not show a Gaussian distribution due to a higher percentage of plus-ends shorter than the average. Consequently, a student’s t-test would not be legitimate for statistical analysis and therefore, the Mann-Whitney-Rank sum test was alternatively chosen using MiniTab 10.5 software.

a)

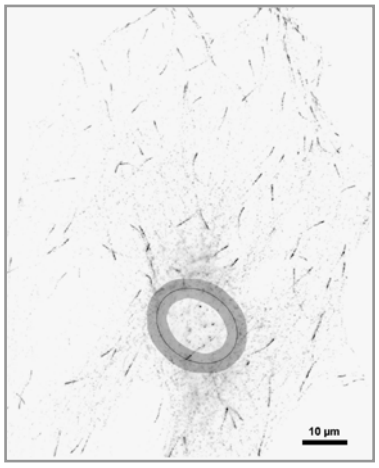

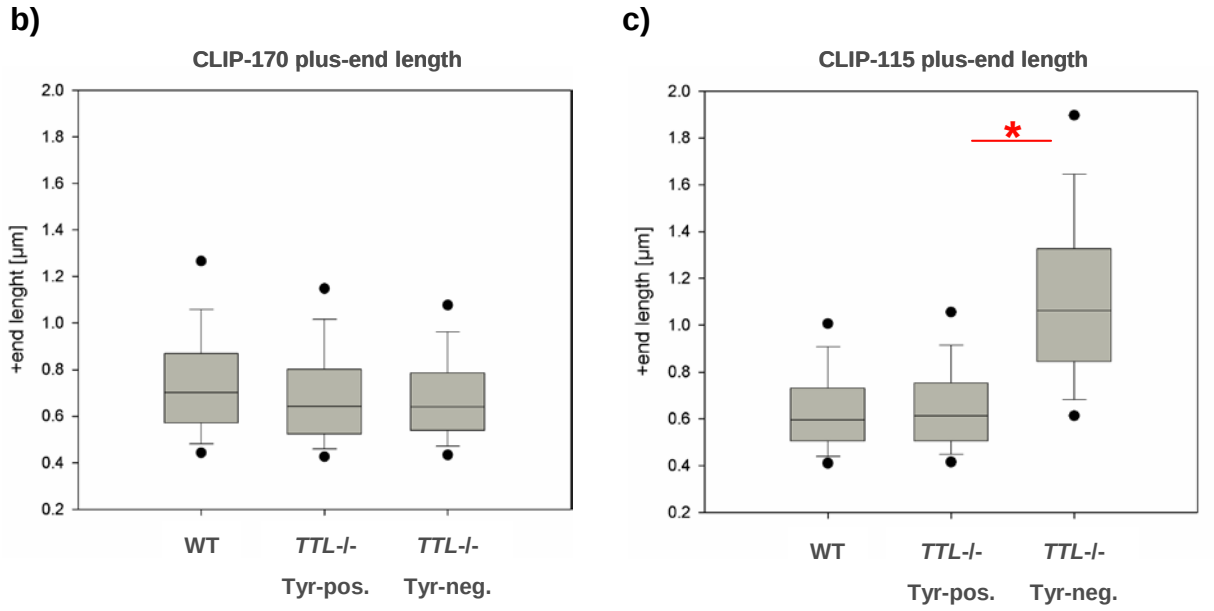

Fig. 19: Analysis of CLIP-170 and CLIP-115 plus-end length. a) Representative image of CLIP-115 localisation in a Tyr-negative *TTL*-/- MEF processed in Adobe Photoshop for measuring the lengths of plus-end comets. The circle marks the nucleus and the grey zone outside the nucleus correlates with a 2 µm perinuclear space. Only plus-end comets outside this area were measured. **b)** Box plot diagram of the CLIP-170 plus-end lengths. The horizontal line marks the median, the boxes include 50 % of all values from 25th to 75th percentile (interquartile range IQR), the whiskers include the 1.5x IQR, and the dots mark the 5th and 95th percentile, respectively. Each box plot implies the lengths of 1000 plus-end comets, the numbers of cells are n = 18 (wild type), n = 20 (Tyr-pos.) and n = 13 (Tyr-neg.). **c)** Box plot diagram of the CLIP-115 plus-end lengths as described for CLIP-170. Each box plot implies the lengths of 1000 plus-end comets; the numbers of analysed cells are n = 14 (wild type), n = 21 (Tyr-pos.) and n = 20 (Tyr-neg.). *Statistical analysis with Mann-Whitney-Rank sum test gave significantly longer CLIP-115 plus-end comets in Tyr-negative MEFs ($P < 0.001$).

To verify the elongation of CLIP-115 plus-end comets in the absence of Tyr-tubulin, *TTL*-/- MEFs were transfected with an expression vector containing the *TTL* cDNA to reconstitute the wild type phenotype. The *TTL* cDNA was cloned into a pIRES2-EGFP vector resulting in a bicistronic construct that allowed the translation of the exogenous TTL and the GFP reporter independent of each other. As a control, cells were also transfected with the same vector containing the *TTL* cDNA in antisense direction. Wild type MEFs were transfected with both constructs as well. Cells were fixed 16 – 24 h after transfection and stained for Tyr-tubulin, Glu-tubulin, CLIP-115 and GFP that lost most of its autofluorescence during methanol fixation. Expression of an exogenous TTL in TTL-deficient cells leads to an increase of the Tyr-tubulin

level, whereas the amount of detyrosinated tubulin decreases. In contrast, cells expressing the antisense construct do not change their levels of Tyr- and Glu-tubulin (Fig. 20a). Consistently, all studied *TTL* knockout MEFs overexpressing exogenous TTL exhibit a significant shortening of the CLIP-115 plus-end comets with a median length of 0.54 µm. Overexpression of the antisense construct did not evoke any effect on the CLIP-115 plus-end length. The expression of both the sense as well as the antisense construct did not cause any effect in wild type MEFs (Fig. 20b). Hence, the shortening of plus-end comets in *TTL*-/- MEFs overexpressing the TTL gene was obviously based on the reappearance of Tyr-tubulin.

For quantification, images were acquired and processed as described above followed by measuring the length of CLIP-115 plus-end comets. Again, experiments were performed independently with two different wild type and *TTL*-/- MEF cell lines. As mentioned above, quantification of CLIP-115 plus-end length illustrates a significant shortening in *TTL*-/- MEFs expressing an exogenous TTL (Fig. 20c).

a)

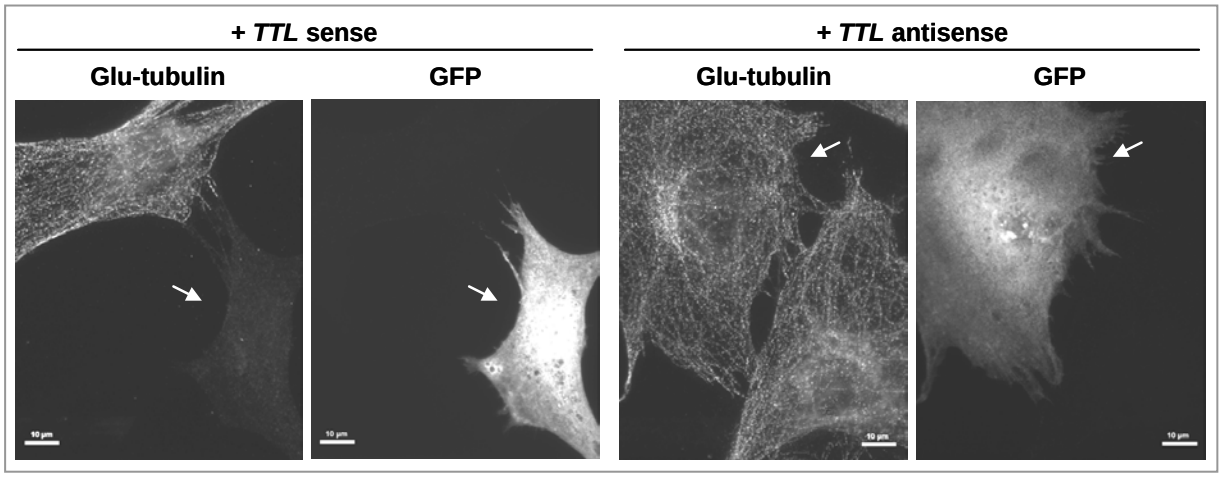

b)

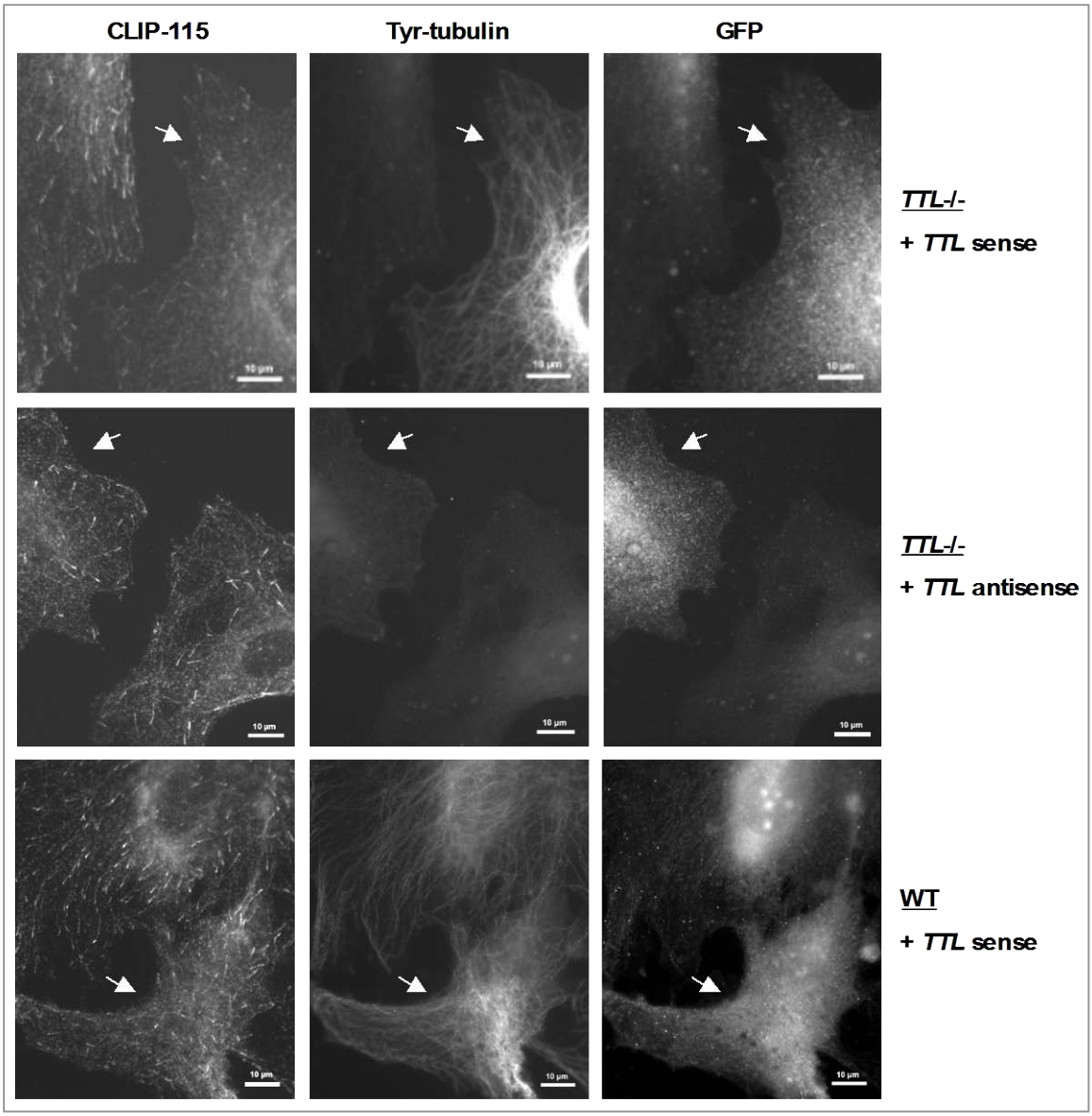
CLIP-115
Tyr-tubulin
GFP
TTL-/-
+ TTL sense
TTL-/-
+ TTL antisense
WT
+ TTL sense

c)

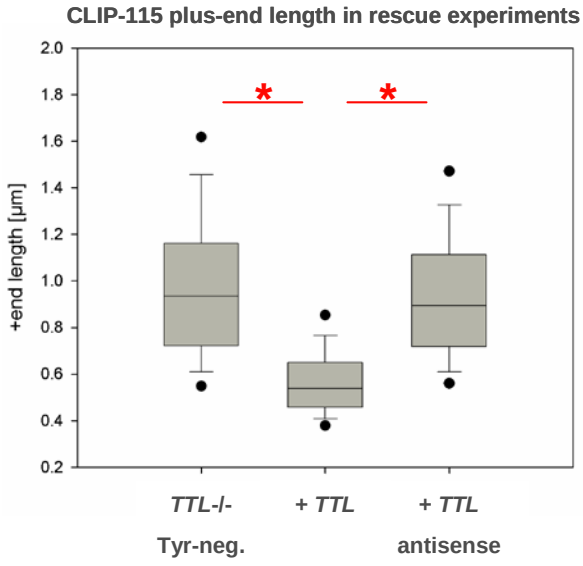
CLIP-115 plus-end length in rescue experiments
+end length [µm]
2.0
1.8
1.6
1.4
1.2
1.0
0.8
0.6
0.4
0.2
*
*
TTL-/-
+ TTL
+ TTL
Tyr-neg.
antisense

Fig. 20: Shortening of CLIP-115 plus-end comets in *TTL*-/- MEFs overexpressing TTL. a) Staining of Glu-tubulin using 1D5 clone H4 hybridoma supernatant and GFP using antibody MAB3580 in *TTL*-/- MEFs expressing the sense or antisense *TTL*-construct, respectively. White arrows mark transfected cells. **b)** CLIP-115, Tyr-tubulin and GFP stained in *TTL*-/- and wild type MEFs using antibodies #2163, purified YL1/2 and MAB3580, respectively. Cells were transfected with the TTL gene cloned in sense and antisense direction (wild type transfected with *TTL* antisense not shown). White arrows mark transfected cells. Note the shorter CLIP-115 plus-end comets in a *TTL*-/- MEF overexpressing TTL compared to a non-transfected *TTL*-/- MEF. **c)** Box plot diagram of the CLIP-115 plus-end lengths in *TTL*-/- MEFs either untransfected and Tyr-negative, transfected with the TTL gene or transfected with a *TTL* antisense construct. Each box plot implies the lengths of 1000 plus-end comets, the numbers of cells are n = 8 (untransfected, Tyr-negative *TTL*-/- MEFs), n = 12 (expressing TTL) and n = 17 (expressing *TTL* antisense). * Statistical analysis with Mann-Whitney-Rank sum test gave significantly shorter CLIP-115 plus-end comets in TTL-overexpressing *TTL*-/- MEFs ($P < 0.001$).

Additionally, CLIP-170 and EB1 were analysed in the above described TTL rescue experiments (Fig. 21a, b; *TTL* antisense construct and wild type MEFs not shown). All studied wild type and *TTL*-/- MEFs possessed the same subcellular distribution of both CLIP-170 and EB1. The overexpression of the TTL gene did neither influence CLIP-170 nor EB1 localisation or plus-end length (Fig. 21a and b).

a)

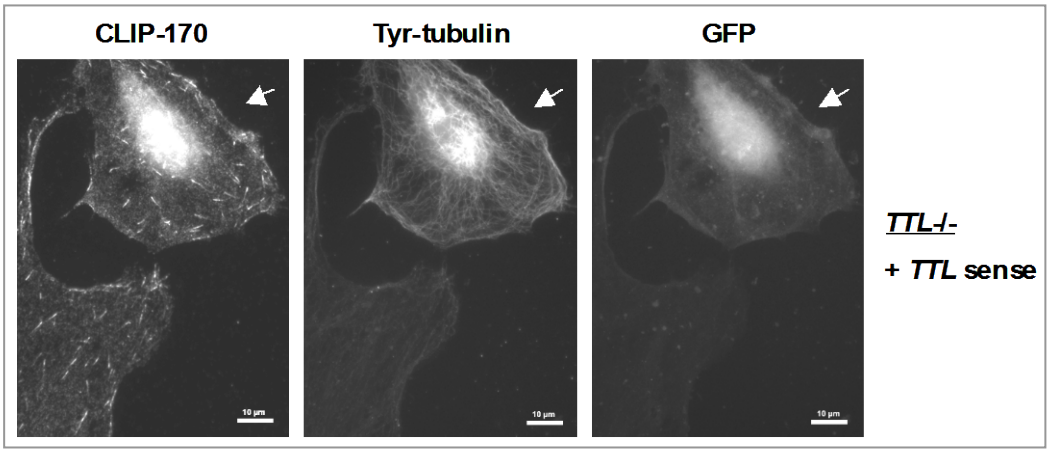

b)

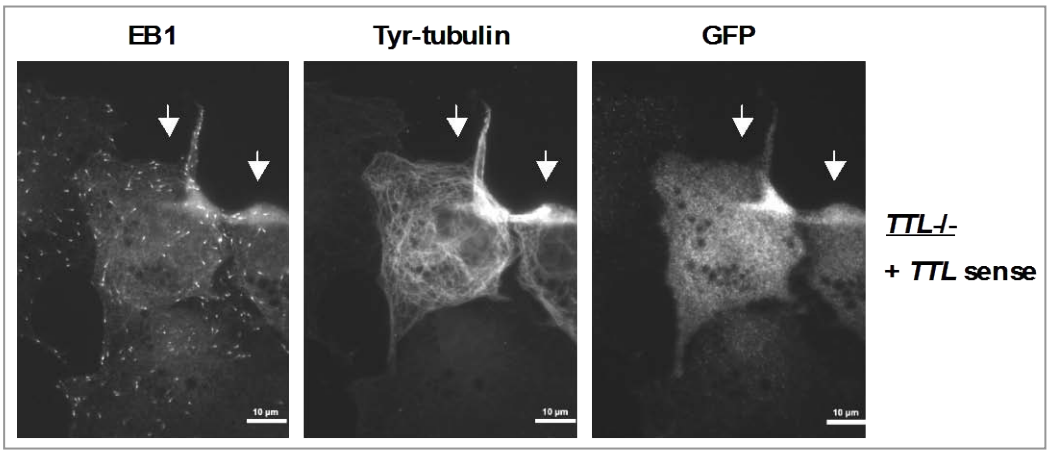

Fig. 21: CLIP-170 and EB1 in *TTL*-/- MEFs transfected with TTL. *TTL*-/- MEFs were transfected with the sense *TTL*-construct and immunostained for **a)** CLIP-170 (#2360) and **b)** EB1 (clone 5 antibody). Cells were co-stained for Tyr-tubulin (purified YL1/2) and GFP (MAB3580) to show functionality of the *TTL*-construct. White arrows mark transfected cells. Both CLIP-170 and EB1 plus-end lengths were not influenced by TTL expression.

In summary, the absence of Tyr-tubulin led to elongated plus-end comets of CLIP-115, as demonstrated in immunofluorescence analysis and rescue experiments of TTL-deficient MEFs. In contrast, neither the close family member CLIP-170 nor EB1, which belongs to a completely different +TIP family, were affected by the lack of Tyr-tubulin.

3.3.3. Biochemical analysis of microtubule plus-end tracking proteins

Besides analysing their localisation, the microtubule plus-end tracking proteins CLIP-115, CLIP-170 and EB1 were biochemically investigated by Western blotting. Signal intensities of the investigated +TIPs did not differ between the genotypes. Surprisingly, CLIP-115 possessed a slightly smaller molecular weight in lysates obtained from *TTL*-/- MEFs compared to heterozygous and wild type MEFs indicating a genotype-depending modification (compare CLIP-115 signal of cell lines 7, 8 and 9 in Fig. 22). Again, heterozygous MEF cell lines revealed a comparable phenotype to wild type MEFs. As CLIP-170 is expressed in two splice variants (Griparic & Keller, 1998) it gave a double band in Western blotting. Within each sample both bands showed the same intensity. Furthermore, CLIP-170 signals appeared to be similar in all studied genotypes (Fig. 22, middle blot). Analogously, the EB1 signal did not

reveal any difference between wild type, heterozygous and TTL-deficient MEFs (Fig. 22, lower blot).

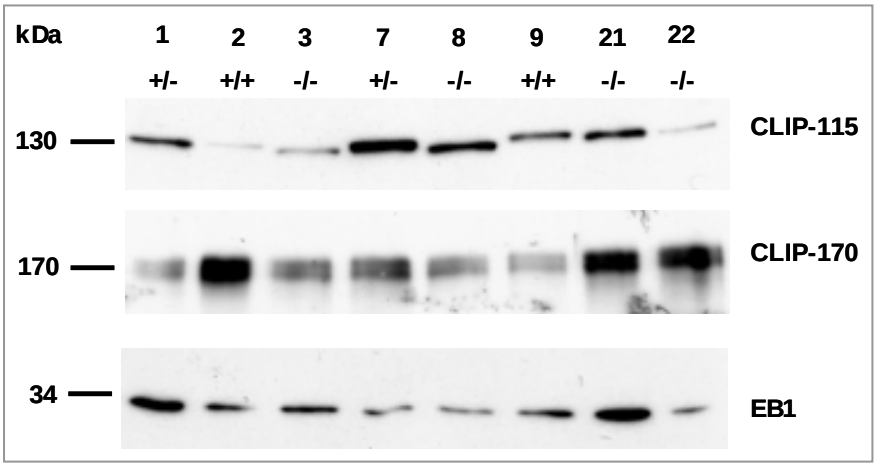

Fig. 22: CLIP-115 mass shift in MEFs. Western blot analysis of wild type, *TTL*+/- and *TTL*-/- MEF lysates using antibodies against CLIP-115 (#2238), CLIP-170 (#2360) and EB1 (clone 5). Obviously, CLIP-115 appears at a lower molecular weight in *TTL*-/- MEF lysates. Different signal intensities between the MEF cell lines are due to unequal loading.

The different molecular weights of CLIP-115 in MEFs containing or lacking the TTL gene could be a consequence of differential posttranslational modifications. Among these modifications, phosphorylation is very common and, as previously reported, involved in binding of microtubule-associated proteins like CLIP-170 (Rickard & Kreis, 1991) or CLASP (Kumar et al., 2009). Hence, it was conceivable that phosphorylation could evoke the observed shift of CLIP 115 in SDS-PAGE. To test this, wild type and *TTL*-/- MEF lysates were treated with the unspecific shrimp alkaline phosphatase (SAP). After the treatment, cell lysates were separated by SDS-PAGE and analysed by Western blotting. Indeed, the phosphatase treatment reduced the molecular weight of CLIP-115 in wild type MEF lysates to the level observed in the *TTL* knockout lysates. In contrast, this treatment did not show any effect on the molecular weight of CLIP-115 in *TTL*-/- MEF lysates and, therefore, indicated a less phosphorylated occurrence of CLIP-115 in the absence of TTL (Fig. 23, upper blot). Control blots stained for CLIP-170, EB1, Tyr-tubulin and actin did not reveal any shifts in molecular weight after phosphatase treatment (Fig. 23, Tyr-tubulin and actin not shown).

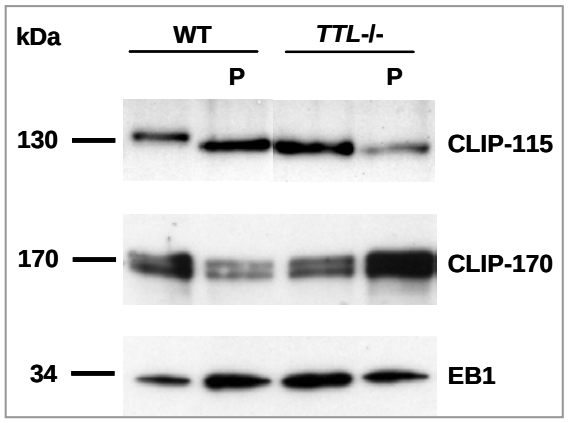

Fig. 23: CLIP-115 is less phosphorylated in *TTL*-/- MEFs. Western blot analysis of wild type and *TTL*-/- MEF lysates using antibodies against CLIP-115 (#2238), CLIP-170 (#2360) and EB1 (clone 5). Lysates that were treated with shrimp alkaline phosphatase (SAP) are marked with "P". Note the shift of the CLIP-115 molecular weight in wild type MEF lysate after SAP-treatment. Different signal intensities result from unequal loading.

Since the observed mass shift in CLIP-115 could be the product of a single or multiple phosphorylation events, 2-dimensional SDS-PAGE was employed to reveal a phosphorylation-dependent shift of CLIP-115 from its isoelectric point (pI). An observed shift is indicative for the number of additional phosphate residues. Non-phosphorylated CLIP-115 has a pI of 6.13 as calculated using online calculation facilities from Scansite (http://scansite.mit.edu/index.html). According to that, each phosphorylation should cause a pI reduction of 0.03 – 0.05 units (Tab. 10).

Table 10: Number of phosphate residues with corresponding calculated molecular weight and isoelectric point of CLIP-115.

Number of phosphates	Molecular weight [Da]	Isoelectric point
0	111868.5306	6.13
1	111946.4946	6.08
2	112024.4586	6.04
3	112102.4226	6.00
4	112180.3866	5.96
5	112258.3506	5.92
6	112336.3146	5.88
7	112414.2786	5.85
8	112492.2426	5.81

Two-dimensional SDS-PAGE starts with an isoelectric focussing of the sample proteins in a pH gradient followed by a mass-dependent separation using SDS-PAGE. Therefore, 24 cm Immobiline™ Dry Strips (GE Healthcare) with a pH gradient from 5.5 – 6.7 were employed guaranteeing a resolution of 0.05 pH units/cm. Total protein samples from wild type and *TTL*-/- MEF lysates were loaded on the gel strips and focussed by an applied current gradient. After the subsequent SDS-PAGE, gels were stained with Coomassie to control correct protein focussing or analysed by Western blotting. In Coomassie-stained SDS gels proteins were visible as focussed dots ensuring a successful isoelectric focussing of the samples. In contrast to that, Western blots probed with anti-CLIP-115 antibody showed a signal distributed over the whole pH range resulting from a failed isoelectric focussing of CLIP-115 (not shown). Variation of loaded protein amounts as well as different loading techniques did not improve CLIP-115 focussing.

Alternatively, non-equilibrium pH gel electrophoresis (NEPHGE; Klose & Kobalz, 1995) was employed. In this method, the pH gradient for isoelectric focussing is established after current application. By that, the focussing of sample proteins can be improved. The first dimension was run in a 9 M urea gel while building up a gradient from pH 2 – 11 followed by SDS-PAGE for the second dimension. The 2-dimensional SDS gels were then blotted and probed with an anti-CLIP-115 antibody followed by Coomassie-staining of the membranes. Whereas the isoelectric focussing of most sample proteins was successful, as demonstrated on the Coomassie-stained membranes, this method also failed to focus CLIP-115 (not shown).

In summary, both the traditional 2-dimensional gel electrophoresis as well as NEPHGE failed in isoelectric focussing of the CLIP-115 polypeptide. Since other proteins were focussed in the different experimental set-ups, the inability of CLIP-115 focussing must be based on the molecular protein properties. Therefore, we were unfortunately not able to predict the number of CLIP-115 phosphorylation sites, which was indicated to depend on *TTL* genotype.

3.3.4. Effects of phosphatase and kinase inhibition on CLIP-115

As Western blot analysis unravelled different molecular weights of CLIP-115 in wild type and *TTL*-/- MEFs resulting from differential phosphorylation states, cells were then treated with phosphatase inhibitors to reveal the engaged amino acids.

Therefore, sodium vanadate was employed to inhibit tyrosine phosphatases, and calyculin A and okadaic acid were used as inhibitors of serine/threonine phosphatases (types PP1 and PP2, respectively). Furthermore, MEFs were treated with the broad range kinase inhibitor staurosporine as well as the tyrosine kinase inhibitor genistein. After the treatments, total MEF lysates were obtained and analysed by Western blotting. Wild type MEFs did not show any effect of any treatment. In contrast, after treatment of *TTL*-/- MEFs with sodium vanadate (V), a second CLIP-115 band appeared on the level similar to that observed in wild type (Fig. 24a, second lane from left side). Okadaic acid (OA) and calyculin A (CA) treatments did not result in an obvious effect, only a smear above the primary CLIP-115 signal was visible (Fig. 24a, third and fourth lane from left side). These results indicate a tyrosine phosphorylation to be involved in the observed difference of CLIP-115 molecular weight in wild type and *TTL*-/- MEFs. In contrast to the treatments with phosphatase inhibitors, protein kinase inhibition did not influence the molecular weight of CLIP-115 in MEFs (Fig. 24b). Additionally, blots were probed with an anti-CLIP-170 antibody but the molecular weight of CLIP-170 was not affected by any inhibitor treatment (Fig. 24a; blots after kinase inhibition not shown).

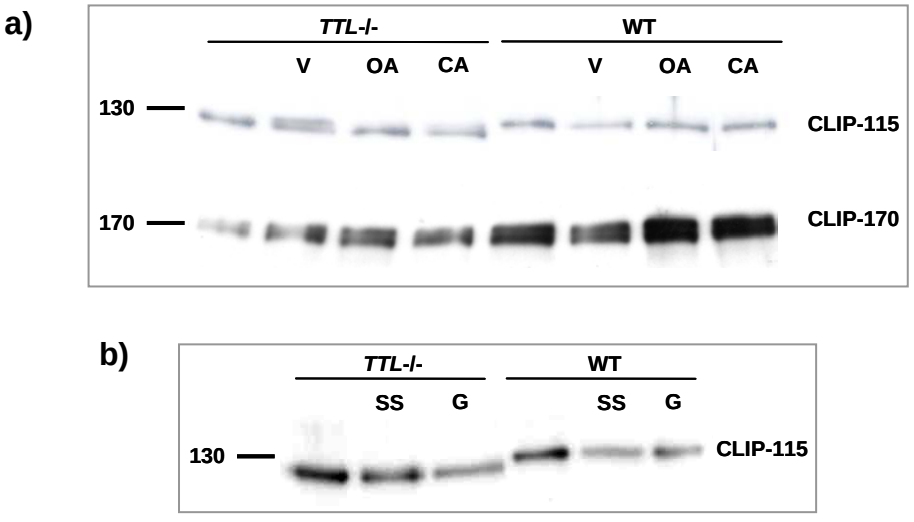

Fig. 24: Inhibition of tyrosine phosphatases leads to a mass shift of CLIP-115 in *TTL*-/- MEFs.
a) Western blot analysis of *TTL*-/- and wild type MEF lysates using antibodies against CLIP-115 (#2238) and CLIP-170 (#2360). MEFs were either untreated or treated with sodium vanadate (V), okadaic acid (OA) or calyculin A (CA). **b)** Western blot of *TTL*-/- and wild type MEF lysates stained for CLIP-115 using antibody #2238. MEFs were untreated, treated with staurosporine (SS) or treated with genistein (G) before lysis. Different signal intensities result from unequal loading.

In order to receive a complete phosphorylation of CLIP-115 in *TTL*-/- MEF lysates, sodium vanadate treament was optimized by cultivating cells in vanadate-containing medium for up to 2 h. Subsequently, cell lysates were obtained and analysed by Western blotting. Unfortunately, these experiments failed to reveal an obvious change in the molecular weight of CLIP 115. Additionally, wild type and *TTL*-/- MEFs were analysed by immunofluorescence after increasing incubation times with sodium vanadate. As expected, stainings of CLIP-115 showed a decrease of microtubule plus-end comets with increasing duration of the vanadate exposure in wild type and TTL-deficient MEFs. After 1 h incubation in vanadate-containing medium, CLIP-115 completely disappeared from microtubule plus-ends in wild type MEFs (Fig. 25b). In general, TTL-deficient MEFs reacted less sensitive to the treatment with a few CLIP-115-stained plus-ends still present after 1 h of vanadate exposure (Fig. 25b). Nevertheless, inhibition of tyrosine phosphatase activity by sodium vanadate obviously eliminated most of CLIP-115 binding at microtubule plus-ends. In addition, localisation studies of CLIP-170 and EB1 revealed a removal from microtubule plus-ends after 15 min and 30 min of vanadate treatment in wild type MEFs, respectively. In contrast, even after 1 h of treatment only a reduction of CLIP-170 and EB1 plus-ends was visible in *TTL*-/- MEFs (not shown). Longer treatment predominantly destroyed the microtubule network, as observed in β-tubulin staining (not shown).

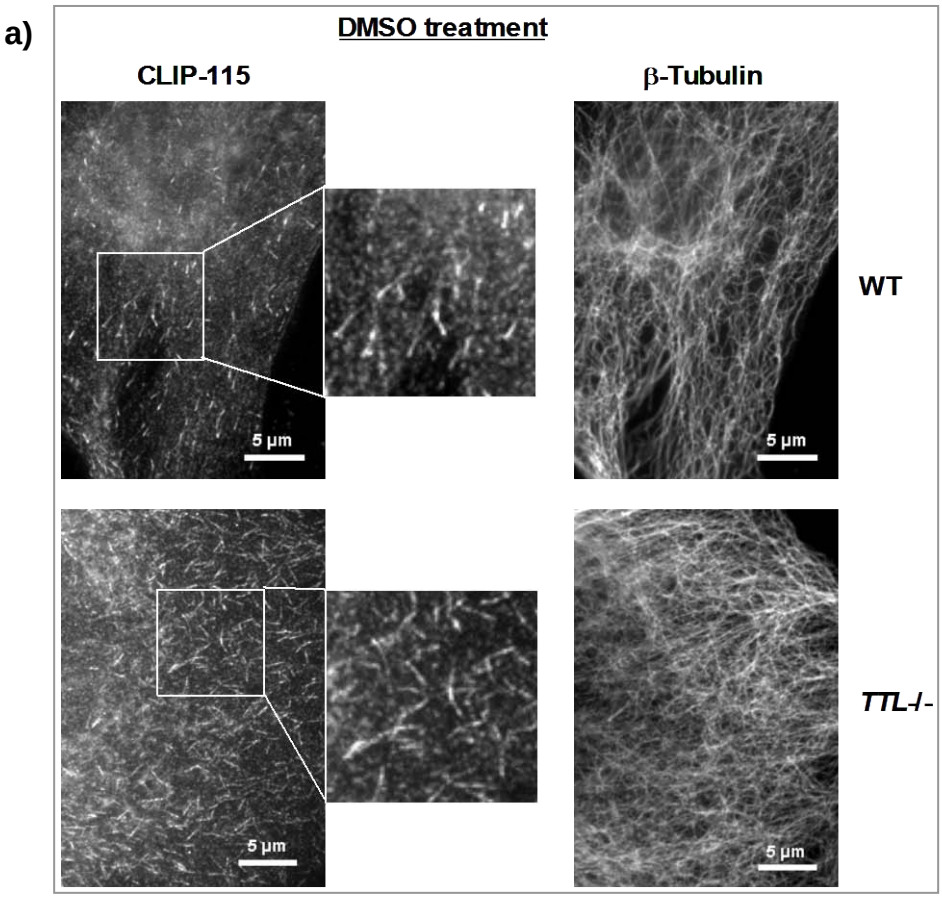
a)
DMSO treatment
CLIP-115
β-Tubulin
WT
TTL-/-
5 µm

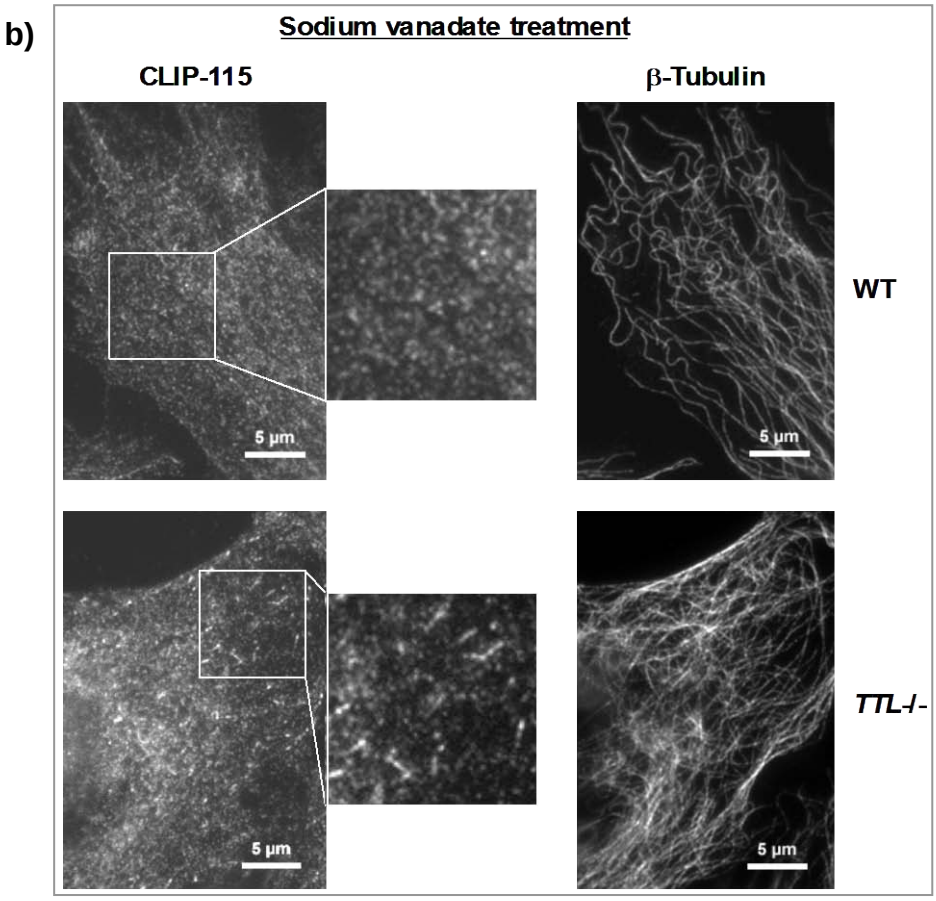
b)
Sodium vanadate treatment
CLIP-115
β-Tubulin
WT
TTL-/-
5 µm

Fig. 25: Reduction of CLIP-115 at microtubule plus-ends after vanadate treatment. CLIP-115 and β-tubulin stained in wild type and *TTL*-/- MEFs either treated with DMSO as control (**a**) or after 1 h of sodium vanadate treatment (**b**) using antibodies #2238 and T4026, respectively. In wild type MEFs, CLIP-115 was completely released from microtubule plus-ends (b, upper panel), whereas CLIP-115 binding to plus-ends was only reduced in *TTL*-/- MEFs (b, lower panel).

Furthermore, it could be demonstrated that the vanadate effects were reversible. In washout experiments CLIP-115, CLIP-170 and EB1 reappeared at microtubule plus-ends after 2 – 4 h cultivation in vanadate-free medium. Representative images of CLIP-115 in wild type and *TTL*-/- MEFs after 30 min of sodium vanadate treatment and 4 h after vanadate washout are shown in Fig. 26 (CLIP-170 and EB1 not shown).

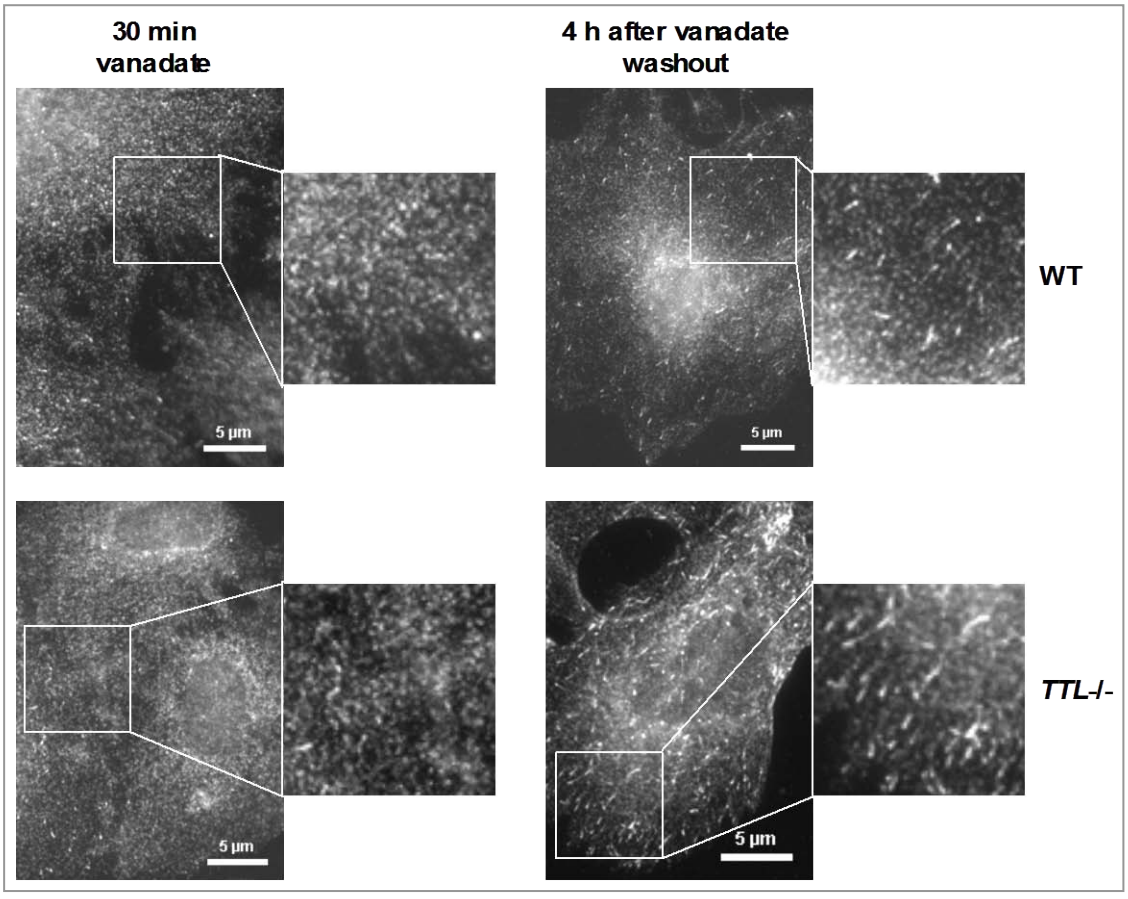

Fig. 26: CLIP-115 reappears at microtubule plus-ends after vanadate washout. CLIP-115 immunostaining of wild type and *TTL*-/- MEFs using antibody #2238. Cells were treated with sodium vanadate for 30 minutes resulting in a reduced CLIP-115 localisation at microtubule plus-ends (left panel). Four hours after vanadate washout, CLIP-115 reappeared at microtubule plus-ends (right panel).

Taken together, only vanadate treatment had an effect on the localisation and biochemical properties of CLIP-115, whereas okadaic acid and calyculin A as well as kinase inhibition did not show any effect. This data support tyrosine phosphorylation as a mechanism to modulate the binding of CLIP-115 to microtubule plus-ends.

3.3.5. Identification of putative phosphorylation sites in CLIP-115

As described in chapters 3.3.3. and 3.3.4., the apparent shift in molecular mass of CLIP-115 obviously depends on its phosphorylation status. To identify potential phosphorylation sites in the CLIP-115 amino acid sequence, the online NetPhosK 1.0 as well as the NetPhos 2.0 Server (Technical University of Denmark) was used. Inhibitor experiments already indicated that most probably tyrosine phosphorylation results in the differences in the molecular mass of CLIP-115 in wild type and *TTL*-/- MEF lysates. By using both the general as well as the kinase-based scanning modus, six tyrosines in the CLIP-115 polypeptide were revealed as putative phosphorylation targets with a higher score than 0.5 (listed in Tab. 11). The scores give the probability of a phosphorylation at the respective amino acid predicted by the servers NetPhosK 1.0 and NetPhos 2.0.

Table 11: Putative CLIP-115 tyrosine phosphorylation sites with potential kinases and probability score as predicted by the NetPhosK 1.0 and the NetPhos 2.0 Servers (Technical University of Denmark).

Tyrosine residue	Predicted kinase	Score (NetPhosK/NetPhos)
Y-270	EGFR*	**0.52** / 0.299
Y-348	INSR**	**0.51** / 0.287
Y-407	-	- / **0.841**
Y-533	-	- / **0.816**
Y-554	-	- / **0.938**
Y-732	EGFR* INSR**	**0.52** / **0.910** **0.50** / **0.910**

*Epidermal Growth Factor Receptor

**Insulin Receptor

All identified tyrosines, except for tyrosine 270, are located in the coiled-coil domain of CLIP-115. The tyrosine at position 270 is part of the second CAP-Gly domain that is responsible for microtubule binding (Mishima et al., 2007). Closer identification of all CAP-Gly domain-containing proteins revealed this tyrosine to be conserved in all proteins indicative for a crucial role in domain structure and/or microtubule binding. The position of all tyrosines identified as possible phosphorylation sites are schematically shown in Figure 27. All six tyrosines were used in mutation analysis to be described in chapter 3.3.5.2.

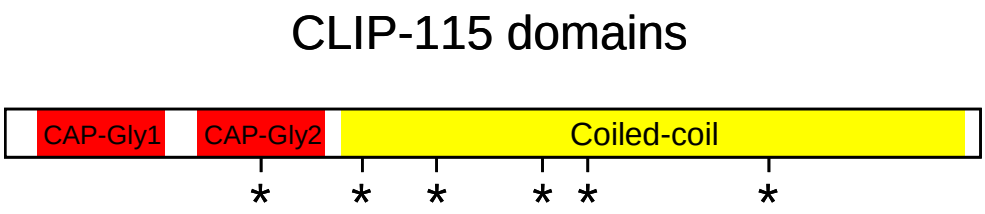

Fig. 27: Scheme of CLIP-115 domains and location of potentially phosphorylated tyrosines. Schematic drawing of CLIP-115 with the CAP-Gly domains in red and the coiled-coil domain in yellow. Asterisks mark the positions of the putative tyrosine phosphorylation sites Y270, Y348, Y407, Y533, Y554 and Y732 (from left to right).

3.3.5.1. Cloning of CLIP-115

To study the influence of a putative phosphorylation of the predicted tyrosine residues, CLIP-115 mutants were generated as GFP fusion proteins. Therefore, the respective tyrosines were substituted either with glutamic acid mimicking phosphorylation or with phenylalanine blocking phosphorylation. By overexpression in multiple cell lines GFP-CLIP-115 fusion proteins were tested for their ability to bind microtubule plus-ends.

For cloning of CLIP-115, forward and reverse primers were designed to amplify the full length CLIP-115 sequence while introducing an *Xho* I and an *Eco* RI restriction site for directed ligation in pEGFP-C3 vector (primers M64 and M57, respectively). Full length CLIP-115 coding sequence was purchased from ImaGenes GmbH (AccNo BC053048). Sequencing using T7 primer confirmed the received sequence to be CLIP-115 isoform B. Compared to isoform A, the coiled-coil domain of isoform B is 35 amino acids shorter and consequently consists of 1012 amino acids corresponding to 3036 bp. An additional primer was designed to introduce an *Xho* I

restriction site and a kozak sequence upstream of the CLIP-115 start codon (primer M97). Moreover, sequencing primers for CLIP-115 were designed using “Primer3” software (Geneious). Next, the CLIP-115 full length sequence was amplified by PCR resulting in 3 kb fragments as confirmed by agarose gel electrophoresis. After extracting the PCR products from the agarose gel they were digested with the restriction enzymes *Xho* I and *Eco* RI to generate correct fragment ends for directed cloning. In addition, the vector pEGFP-C3 was linearised using *Xho* I and *Eco* RI enzymes as well. After purification of the digested DNA fragments by agarose gel electrophoresis, the PCR product was ligated into pEGFP-C3 resulting in CLIP-115 with an N-terminal EGFP. Additionally, a CLIP-115 construct with a C-terminal EGFP was generated by cloning into the pEGFP-N2 vector. Therefore, a primer to remove the *CLIP-115* stop codon while introducing an *Eco* RI site was designed (primer M98). Ligation mixes were used in *E. coli* transformation followed by plasmid DNA mini-preparation from grown colonies in order to select constructs containing inserts. The isolated plasmid DNA was tested by restriction analysis using *Xho* I and *Eco* RI to select for constructs carrying an insert. DNA from midi-preparations of the identified clones was then sent for sequencing. Verified CLIP-115 constructs with EGFP either at the N- or the C-terminus were overexpressed in NIH 3T3 cells, which were either fixed for immunofluorescence or lysed for Western blot analyses. Total cell lysates of transfected NIH 3T3 fibroblasts were separated by SDS-PAGE and investigated by Western blotting using both anti-GFP as well as anti-CLIP-115 antibodies. As expected, both antibodies revealed signals at a molecular weight of approximately 150 kDa corresponding to the fusion protein of CLIP-115 and EGFP. Consistent with endogenous CLIP-115, both fusion proteins localised at microtubule plus-ends when expressed at a low level. When expressed at higher levels, exogenous CLIP-115 proteins decorated the whole microtubule network (not shown; Hoogenraad et al., 2000).

In summary, cloning of full length CLIP-115 into pEGFP-vectors was successful and resulted in fusion proteins of the expected molecular weight and localisation at microtubule plus-ends.

3.3.5.2. Mutation of CLIP-115 tyrosines

For the introduction of either a glutamic acid as phosphomimic or a phenylalanine as non-phosphomimic at the position of the above-mentioned potential CLIP-115 phosphosites (Tab. 11) the pEGFP-C3-CLIP-115 (see 3.3.5.1.) construct was used as template DNA in site-directed mutagenesis (see 2.4.7.). Primers carrying the respective mutation were designed from the CLIP-115 sequence. Following the mutagenesis reaction, PCR products were transformed into *E. coli* and selected on Kanamycin-containing LB agar plates. Colonies were picked, plasmid DNA was isolated and sent for sequencing. Constructs with a correct sequence including the targeted mutation were then used in midi-preparations. The isolated constructs were overexpressed in NIH 3T3 cells as well as in wild type and TTL-/- MEFs to investigate their ability to bind microtubules. Additionally, the localisation of mutant fusion proteins was examined in *CLIP-115* knockout and *CLIP-115/CLIP-170* double knockout MEFs (kind gift of N. Galjart) to eliminate the endogenous CLIP-115 and CLIP-170 background. Representative images of Tyr-tubulin, CLIP-115, CLIP-170, EB1 and $p150^{Glued}$ stained in *CLIP-115/CLIP-170* double knockout MEFs are shown in Figure 28. CLIP-115 and CLIP-170 labelling revealed a slight background confirming the genotype of the cells. Endogenous EB1 decorated the microtubule plus-ends and demonstrated the existence of an intact microtubule network (Fig. 28, upper panel). Immunofluorescent staining of Tyr-tubulin revealed areas in a number of *CLIP-115/CLIP-170* double knockout MEFs, which were free of microtubules. In these areas, $p150^{Glued}$ appeared to be accumulated (Fig. 28, lower panel).

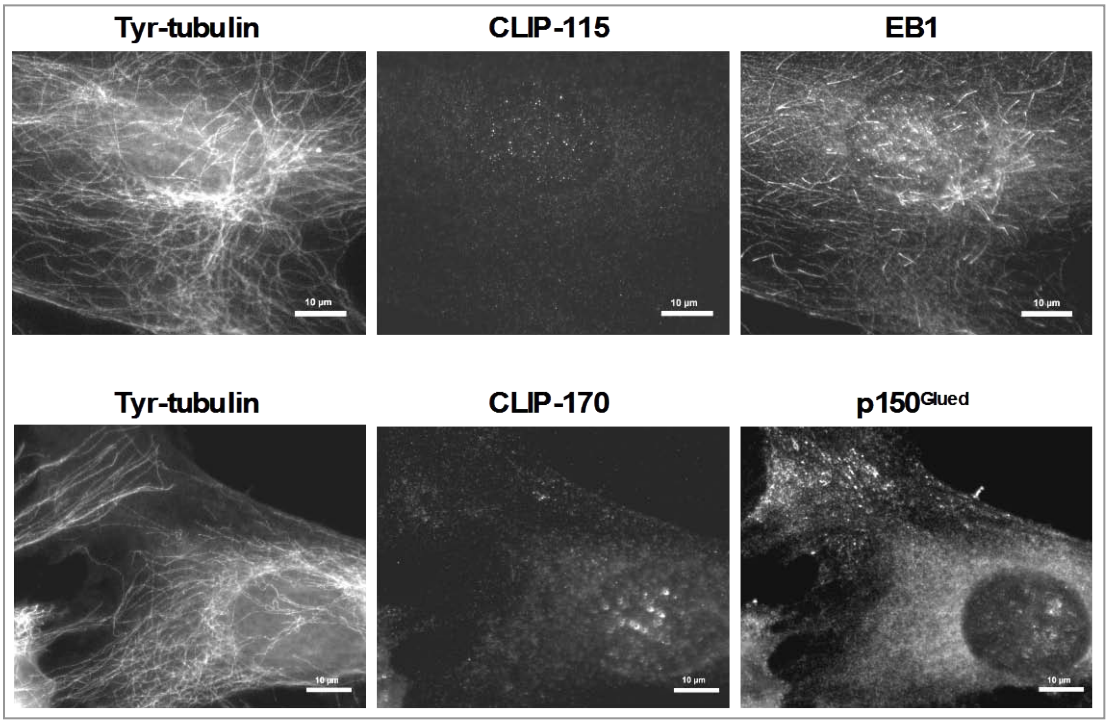

Fig. 28: Characterization of *CLIP-115/CLIP-170* double knockout MEFs. Immunostainings of *CLIP-115/CLIP-170* double knockout MEFs using antibodies against Tyr-tubulin (YL1/2), CLIP-115 (#2163), EB1 (clone 5), CLIP-170 (#2360) and p150^{Glued} (610474).

Except for CLIP-115 Y270E, all mutant CLIP-115 variants showed a localisation at microtubules comparable to the wild type protein (Fig. 29). Hence, it is conceivable that these mutations did not affect the binding ability of CLIP-115 to microtubule plus-ends at all. When overexpressed on a high level, EGFP-CLIP-115 even decorated the whole microtubule network. In contrast, the mutation of tyrosine 270 into glutamic acid strongly reduced microtubule binding of CLIP-115 and resulted in a severely reduced number of plus-end comets and microtubule structures. Instead of a distinct localisation on microtubules, the CLIP-115 mutant tended to a predominantly cytoplasmatic distribution. These experiments indicate that a phosphorylation at tyrosine 270 could hinder CLIP-115 microtubule binding.

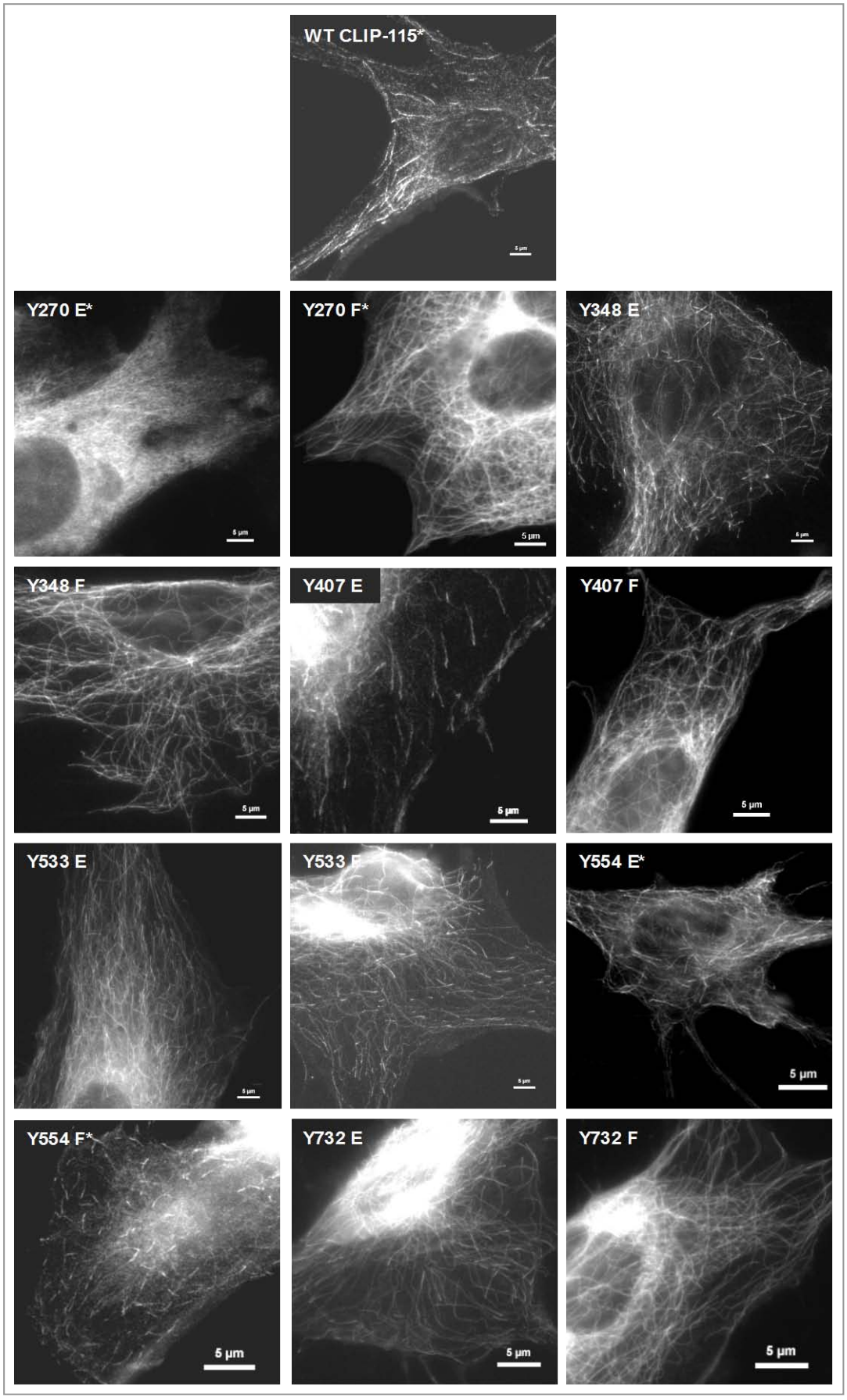
WT CLIP-115*
Y270 E*
Y270 F*
Y348 E
Y348 F
Y407 E
Y407 F
Y533 E
Y533 F
Y554 E*
Y554 F*
Y732 E
Y732 F
5 µm

Fig. 29: Substitution of CLIP-115 tyrosine 270 by glutamic acid strongly reduced binding to microtubule plus-ends. Wild type and mutant EGFP-CLIP-115 overexpression in *CLIP-115/CLIP-170* double knockout MEFs. The respective tyrosines (Y) were either substituted by glutamic acid (E) or by phenylalanine (F). Images marked with an asterisk show cells immunostained for CLIP-115 using antibody #2163 to enhance the fluorescent signal of the fusion protein. All other images show GFP autofluorescence.

As already mentioned, the tyrosine residue 270 is located within the second CAP-Gly domain of CLIP-115 and is conserved through CAP-Gly domain sequences of other proteins. Analogous to tyrosine 270, tyrosine 130 is present in the first CAP-Gly domain of CLIP-115. To verify an effect on the microtubule binding capacity of CLIP-115, tyrosine 130 was also substituted either with glutamic acid or phenylalanine, although it was not predicted to be a putative phosphorylation site. In addition, tyrosines 130 and 270 of CLIP-115 were simultaneously mutated resulting in four different constructs. To validate the results obtained by the mutation Y270E, tyrosine 270 was additionally mutated in alanine as an independent mimic of non-phosphorylation. Representative images of *CLIP-115/CLIP-170* double knockout MEFs overexpressing the mutant EGFP-CLIP-115 constructs are shown in Figure 30. In multiple experiments, specific antibodies against either CLIP-115 or GFP were used to enhance the signal of the overexpressed fusion proteins as methanol fixation could decrease GFP autofluorescence.

The mutation of tyrosine 130 into glutamic acid only slightly reduced the binding capacity of CLIP-115 to microtubules. However, microtubule binding was completely disrupted by the double mutants Y130E-Y270E and Y130E-Y270A (Fig. 30a, c and h). In contrast, the single Y130F mutant did not show any effect on the CLIP-115 localisation (Fig. 30b). The mutation of tyrosine 270 into alanine also slightly reduced the binding efficiency of CLIP-115 to microtubules as indicated by an increased cytoplasmic localisation (Fig. 30g). The introduction of phenylalanine at position 130 either combined with glutamic acid or alanine at position 270 led to the identical effects on CLIP-115 microtubule binding as observed for the CLIP-115 mutant Y270E (Fig. 30e and i).

In summary, only the mutations of tyrosine 270 into glutamic acid or alanine combined with a simultaneous substitution of tyrosine 130 with glutamic acid entirely abolished the binding of CLIP-115 to microtubules. The fact that also the CLIP-115

mutant Y270A binds microtubules with less affinity indicates severe conformational changes as a result of this mutation. Results from all overexpression experiments of CLIP-115 mutations in the employed cell lines are summarized in Table 12.

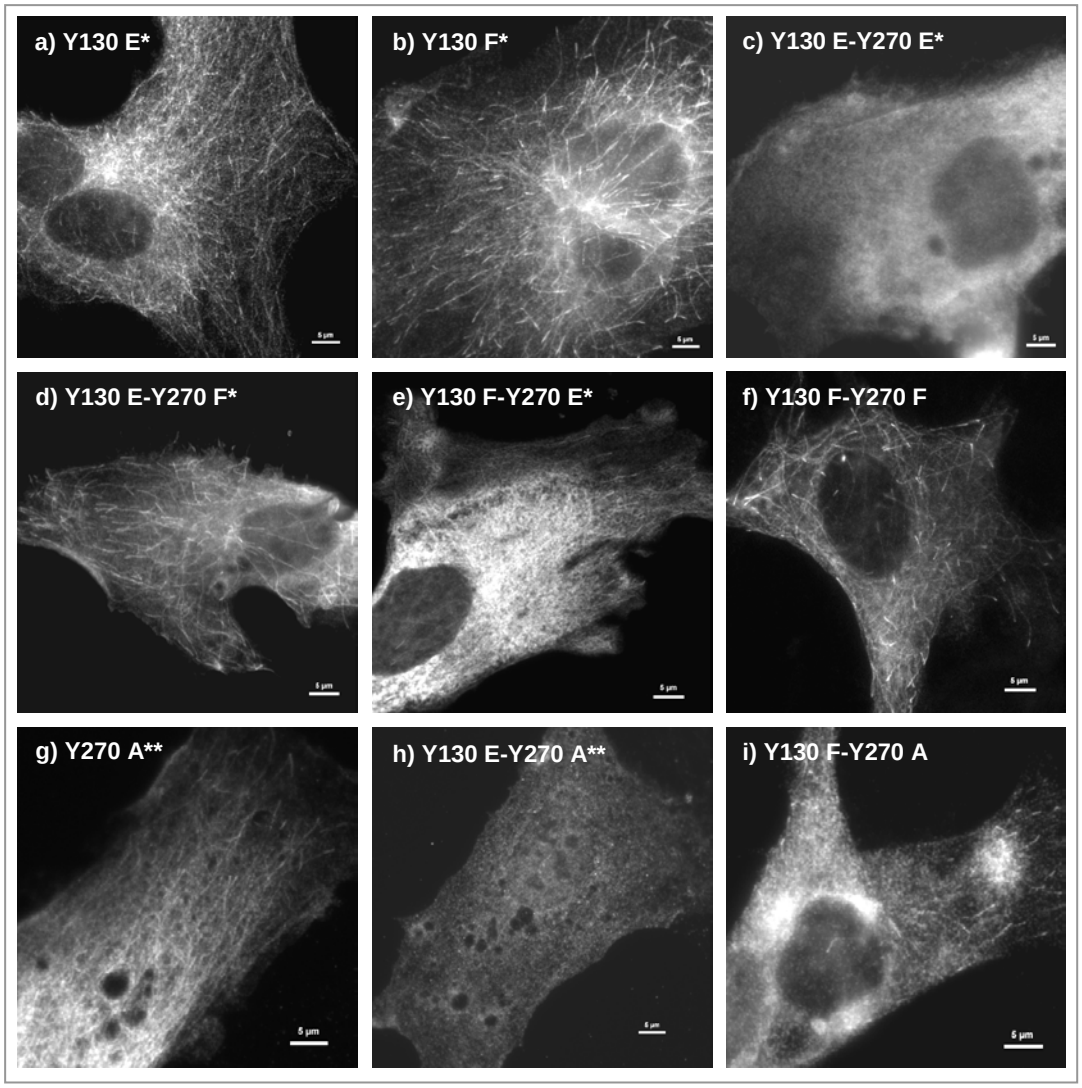

Fig. 30: Characterization of CLIP-115 double mutants. Mutant EGFP-CLIP-115 overexpression in *CLIP-115/CLIP-170* double knockout MEFs. The respective tyrosines (Y) were either substituted by glutamic acid (E) or by phenylalanine (F). Note that the substitution of CLIP-115 tyrosine 270 by glutamic acid or alanine in combination with the mutation of tyrosine 130 into glutamic acid completely disrupted binding to microtubules. Images marked with one asterisk show cells stained for CLIP-115 (#2163), whereas two asterisks mark cells stained for GFP (270F3). Images without asterisk show GFP autofluorescence.

Table 12: Microtubule binding of mutant EGFP-CLIP-115 overexpressed in *CLIP-115/CLIP-170* double knockout MEFs, *CLIP-115* knockout MEFs, NIH 3T3 cells, wild type and *TTL*-/- MEFs. Mutations with reduced binding to microtubules are in bold.

Mutation	***CLIP-115/ CLIP-170-/-***	***CLIP-115-/-***	**NIH 3T3**	**WT MEFs**	***TTL*-/- MEFs**
Y130 E	**+**	**+**	n. d.	**+**	**+**
Y130 F	++	++	n. d.	++	++
Y130 E – Y270 A	**-**	**-**	n. d.	**-**	**-**
Y130 E – Y270 E	**-**	**-**	n. d.	**-**	**-**
Y130 E – Y270 F	**+**	**+**	n. d.	**+**	**+**
Y130 F – Y270 A	**+**	**+**	n. d.	**+**	**+/-**
Y130 F – Y270 E	**+/-**	**+/-**	n. d.	**+/-**	**-**
Y130 F – Y270 F	++	++	n. d.	++	++
Y270 A	**+**	**+**	n. d.	**+**	**+**
Y270 E	**+/-**	**+/-**	**+/-**	**+**	**+/-**
Y270 F	++	++	++	++	++
Y348 E	++	++	++	++	++
Y348 F	++	++	++	++	++
Y407 E	++	++	++	++	++
Y407 F	++	++	++	++	++
Y533 E	++	++	++	++	++
Y533 F	++	++	++	++	++
Y554 E	++	++	++	++	++
Y554 F	++	++	++	++	++
Y732 E	++	++	++	++	++
Y732 F	++	++	++	++	++

++ Wild type-like binding to microtubules

+ Reduced binding to microtubules

+/- Strongly reduced binding to microtubules with cytoplasmic background

- No binding to microtubules, only cytoplasmic

n. d. not determined

In comparable experiments, mutation analysis of CLASP2 phosphorylation sites resulted in a shift of the molecular weight in SDS-PAGE (Kumar et al., 2009). Analogously, mutant EGFP-CLIP-115 fusion proteins were investigated in Western blot analysis. Therefore, lysates were obtained from MEFs and NIH 3T3 cells overexpressing EGFP-CLIP-115 constructs and analysed by Western blotting using either an anti-CLIP-115 or an anti-GFP antibody. However, Western blot analysis did not reveal any mass shift caused by tyrosine substitutions. All mutant CLIP-115 fusion proteins possessed the same molecular weight as wild type CLIP-115 fused to EGFP (Fig. 31). The mutation of tyrosine 270 into alanine and the double mutations of tyrosines 130 and 270 did not change the molecular weight of the EGFP-fused CLIP-115 as well (not shown).

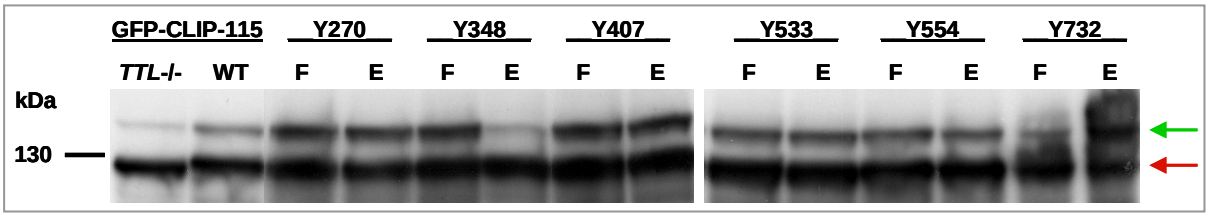

Fig. 31: EGFP-CLIP-115 fusion proteins show the same molecular weight.
Western blot analysis using antibody #2163 against CLIP-115 show endogenous CLIP-115 (approximately 130 kDa, red arrow) and exogenous EGFP-CLIP-115 (approximately 150 kDa, green arrow). Overexpression of EGFP-CLIP-115 in *TTL*-/- and wild type MEFs did not reveal any difference regarding the molecular weight (first two lanes on the left side), whereas endogenous CLIP-115 appeared at a smaller molecular weight in *TTL*-/- MEFs. Mutant EGFP-CLIP-115 proteins were overexpressed in NIH 3T3 cells. The respective tyrosines (Y) were substituted either by phenylalanine (F) or glutamic acid (E). Again, no differences in molecular mass could be observed.

3.3.5.3. Mutation of tyrosines in CLIP-170 CAP-Gly domains

Analogous to CLIP-115, the CAP-Gly domains of the closely related protein CLIP-170 contain conserved tyrosines at corresponding positions (tyrosines 108 and 261). Therefore, also CLIP-170 mutations were analysed in further studies. To investigate the impact of the conserved tyrosines on microtubule binding, the residues were substituted either by glutamic acid or phenylalanine in EGFP-CLIP-170 expression constructs. EGFP fusion proteins containing wild type or mutant CLIP-170 were overexpressed in *CLIP-115/CLIP-170* double knockout, wild type and *TTL*-/- MEFs followed by investigating their subcellular localisation. In contrast to CLIP-115

mutants, only the combined mutation of both CLIP-170 tyrosines into glutamic acid decreased the microtubule-binding efficiency. Interestingly, disruption of microtubule binding could only be observed in a few cells, whereas the majority of overexpressing cells still show binding of CLIP-170 to microtubules, although an increasing cytoplasmic localisation was present (Fig. 32d). Again, this effect was more drastic in *TTL*-/- MEFs. All results for CLIP-170 mutations are summarized in Table 13.

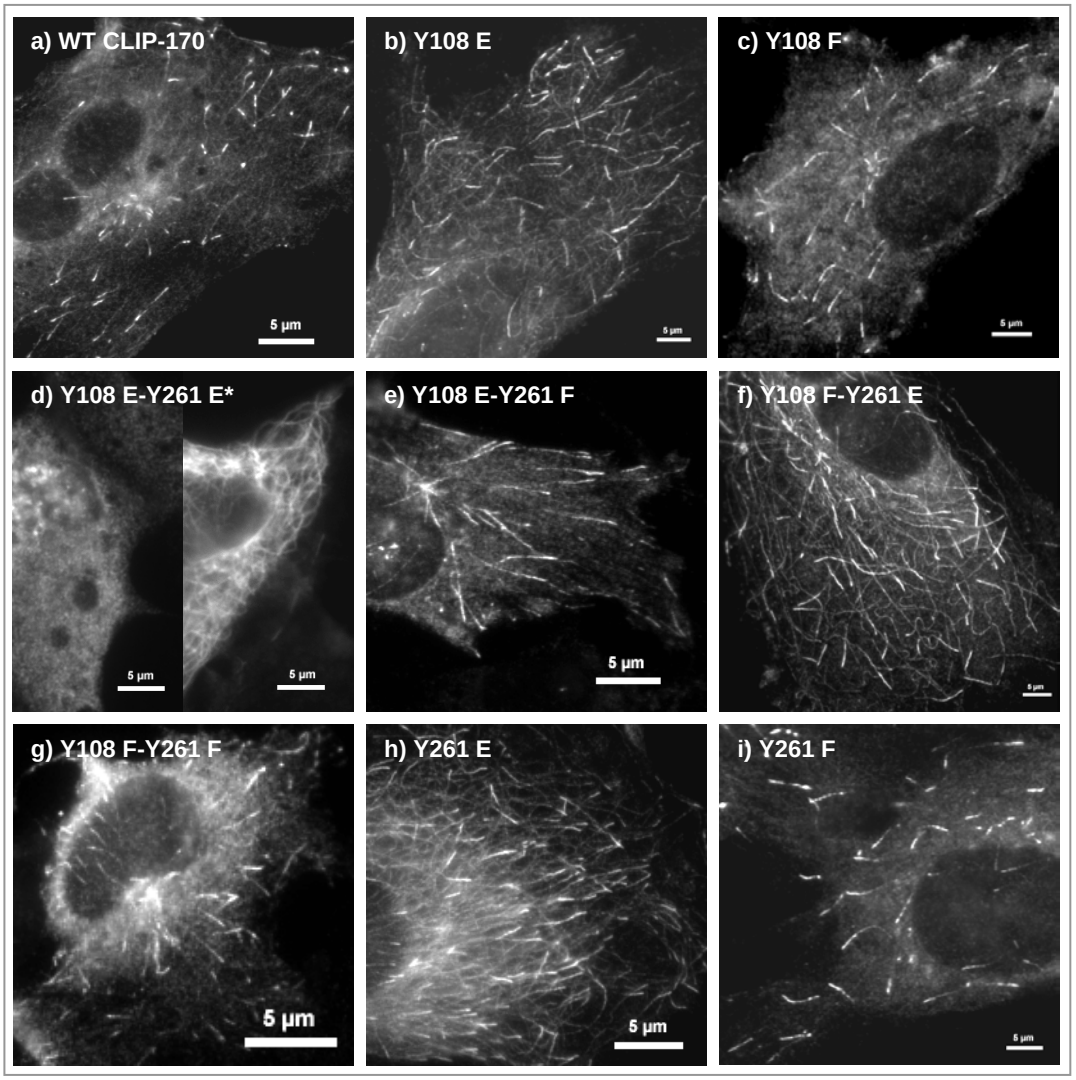

Fig. 32: Characterization of CLIP-170 mutants in MEFs. Wild type and mutant GFP-CLIP-170 overexpression in *CLIP-115/CLIP-170* double knockout MEFs. The respective tyrosines (Y) were either substituted by glutamic acid (E) or by phenylalanine (F). Cells were stained for CLIP-170 using antibody #2360. Note the clear reduction of microtubule association of the CLIP-170 double mutant Y108E-Y261E (*). Expression of this mutant revealed different subcellular distributions, i. e. variation from plus-end localisation to complete loss of microtubule binding. Therefore, two representative images are shown.

Table 13: Microtubule binding of mutant EGFP-CLIP-170 overexpressed in *CLIP-115/CLIP-170* double knockout MEFs, wild type and *TTL*-/- MEFs. For codings see Table 11.

Mutation	*CLIP-115/ CLIP-170-/-*	WT MEFs	*TTL*-/- MEFs
Y108 E	++	++	++
Y108 F	++	++	++
Y108 E – Y261 E	**+**	**+**	**+/-**
Y108 E – Y261 F	++	++	++
Y108 F – Y261 E	++	++	++
Y108 F – Y261 F	++	++	++
Y261 E	++	++	++
Y261 F	++	++	++

Taken together, CLIP-170 behaved differently than CLIP-115 when tyrosines positioned in the microtubule-binding CAP-Gly domains were substituted by glutamic acid. Though, mutating tyrosines of both CAP-Gly domains could decrease the binding efficiency of CLIP-170 proteins, but did not necessarily evoke a complete loss of microtubule binding, as observed for CLIP-115. These data indicate a different impact of those tyrosines on the affinity of CLIP-115 and CLIP-170 to microtubules.

3.3.5.4. Search for CLIP-115 phosphorylation sites by mass spectrometry

The results from CLIP-115 mutation experiments indicated tyrosine 270 to be a potential phosphorylation site being involved in microtubule binding. However, not only the tyrosine substitution by glutamic acid mimicking phosphorylation but also the introduction of alanine reduced CLIP-115 binding to microtubule plus-ends. As a consequence, a structural change of the CAP-Gly domain caused by the mutation instead of a different phosphorylation pattern could be the reason for the observed CLIP-115 mislocalisation. Nevertheless, treatments of MEF lysates with a phosphatase as well as treatments of the MEFs with sodium vanadate revealed a differential phosphorylation state of CLIP-115 in wild type and *TTL*-/- MEFs. To identify the affected CLIP-115 regions, the protein was enriched by

immunoprecipitation from total cell lysates obtained from wild type and *TTL*-/- MEFs and analysed by mass spectrometry (MS).

For the first MS analysis, wild type and *TTL*-/- MEF cell lysates were obtained from 20 confluent 10 cm dishes. As the obtained CLIP-115 amount was still very little, total cell lysates from 75 confluent 10 cm dishes were employed in a second experiment. Samples of the different immunoprecipitation steps were separated by SDS-PAGE followed by Western blotting to examine the efficiency of the immunoprecipitation (Fig. 33a). The different molecular weights of CLIP-115 from wild type and *TTL*-/- MEFs was visible in the total cell lysates (lanes 1) and the precleared lysates (lanes 2), but disappeared after immunoprecipitation (lanes 3 and 4). Nevertheless, CLIP-115 could partly be precipitated from MEF lysates. CLIP-115-enriched samples were separated from co-precipitated proteins by SDS-PAGE followed by staining of the gel with colloidal Coomassie (Fig. 33b). Stained protein bands were cut out of the gel and employed in a tryptic digest. After extraction from the gel, peptides were separated by HPLC and analysed by mass spectrometry using a Q-TOF micro mass spectrometer. The CLIP-115 bands resulting from the second, larger approach were first stored at –20 °C and later analysed using the more sensitive LTQ Orbitrap XL.

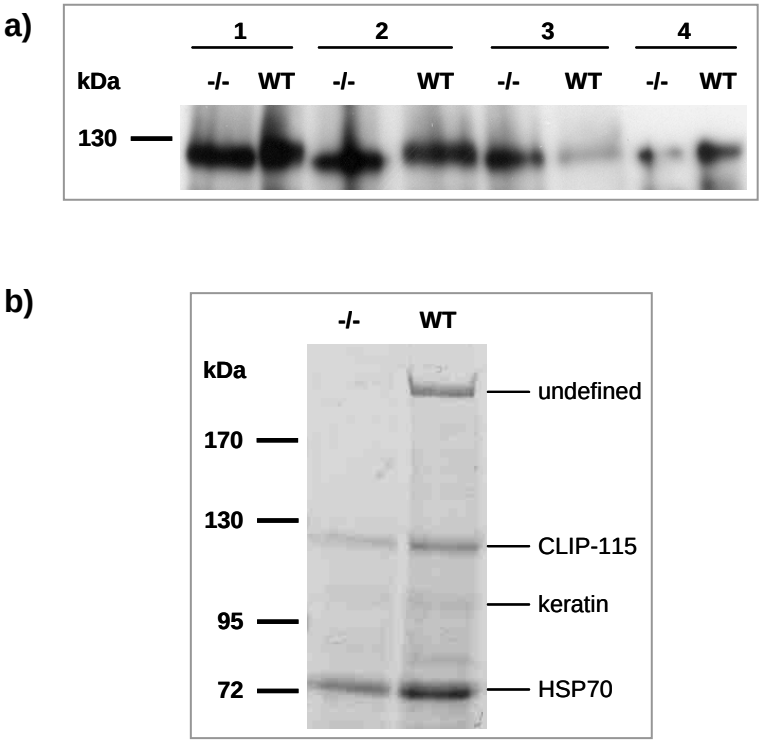

Fig. 33: Immunoprecipitation of CLIP-115 from *TTL*-/- and wild type MEF lysates. a) Western blot analysis of CLIP-115 immunoprecipitation fractions using antibody #2163. Loaded samples were total cell lysates from *TTL*-/- and wild type MEFs (1), lysates after preclearing with protein G-coupled sepharose (2), lysates after immunoprecipitation (3) and the immunoprecipitated proteins (4). Note the CLIP-115 mass shift between *TTL*-/- and wild type in samples 1 and 2. **b)** Immunoprecipitated proteins from *TTL*-/- and wild type MEF lysates separated by SDS-PAGE and stained with colloidal Coomassie. Marked bands were cut off the gel and analysed by mass spectrometry. Predicted proteins are given.

Data obtained by MS analysis was processed using a MASCOT server as online database. MS/MS-based sequencing of the most intensive signals of identified CLIP-115 peptides did not reveal any phosphorylation at all and consequently no difference between wild type and *TTL* knockout samples. In total, 14 peptides could be identified and sequenced covering 15.7 % of the complete CLIP-115 sequence (159 amino acids from a total of 1012). Co-immunoprecipitated proteins from both experiments were analysed by Q-TOF micro and turned out to be contaminations instead of genuine CLIP-115 interaction partners. The protein band of about 250 kDa remained undefined, whereas that of around 100 kDa was identified to be most probably keratin and that of around 75 kDa to be heat shock protein 70 (HSP70/GRP78; Fig. 33b).

As the first MS experiments did not show any indication of a differential CLIP-115 phosphorylation, the immunoprecipitation was subsequently optimized to maintain the mass shift of CLIP-115 in wild type and *TTL*-/- MEFs. Therefore, the protocol was shortened and phosphatase inhibitors were added. Samples of the different immunoprecipitation steps were separated by SDS-PAGE followed by Western blotting to examine the efficiency of the immunoprecipitation (Fig. 34). Again, CLIP-115 could successfully be precipitated from total cell lysates (lanes 4). Due to the shorter incubation times a higher amount of the protein remained in the lysates after the immunoprecipitation (lanes 3). The difference in CLIP-115 phosphorylation between wild type and *TTL*-/- could partly be conserved as shown by the CLIP-115 double band in wild type samples (lanes 3 and 4, wild type).

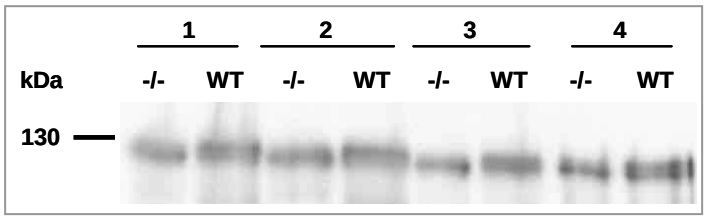

Fig. 34: Optimized immunoprecipitation of CLIP-115 from *TTL*-/- and wild type MEF lysates. Western blot analysis of CLIP-115 immunoprecipitation fractions pooled from three independent experiments using antibody #2163. Loaded samples were the total cell lysates from *TTL*-/- and wild type MEFs (1), lysates after preclearing with protein G-coupled sepharose (2), lysates after immunoprecipitation (3) and the immunoprecipitated proteins (4). In all wild type samples CLIP-115 appeared as a double band indicating the presence of multiple phosphorylation states.

Protein samples obtained from three independent CLIP-115 immunoprecipitations using lysates from three 14 cm dishes were pooled and separated by SDS-PAGE. The gel was again stained with colloidal Coomassie and the CLIP-115 bands analysed by mass spectrometry. In this new set-up, the mass spectrometer was calibrated for the CLIP-115 peptide containing tyrosine 270 to optimize sensitivity. For this purpose, synthetic peptides of the CLIP-115 region around tyrosine 270 were used to mirror phosphorylated and non-phosphorylated fragments of endogenous CLIP-115 after tryptic digestion and served as calibration standards for MS (see chapter 2.5.10., Tab. 5, and chapter 2.5.11.). After calibration, CLIP-115 protein bands from wild type and *TTL*-/- MEFs were analysed. However, with the known retention times and peptide masses, in three independent experiments only the non-phosphorylated peptide could clearly be identified in samples from both wild type and *TTL*-/- MEFs, whereas the phosphorylated peptide could not be determined.

As the shift of the CLIP-115 molecular weight obviously is caused by phosphorylation (as described in chapters 3.3.3. and 3.3.4.), all peptides produced by tryptic digest were compared with potential phosphorylation sites predicted by the NetPhos 2.0 server to search the obtained MS data for the existence of other phosphorylation sites. In total, 32 peptides containing one or multiple predicted phosphorylation sites were identified. Subsequently, their molecular masses with or without phosphate residues were calculated. Therefore, the mass of one or several phosphate residues (HPO_3 = 79.9663 Da) divided by the charge was added to the peptide mass divided by the charge (m/z). By that, 249 mass/charge ratios for two-, three- and fourfold

charged peptides carrying up to four phosphate residues were calculated. MS data obtained from the general peptide scans combined with MS/MS in two independent experiments and processed using the MASCOT server were screened for the presence of the calculated peptide mass/charge ratios using MassLynx 4.1 and Xcalibur software. In total, 13 non-phosphorylated peptides were detected by this analysis. Phosphorylated equivalents could be identified in two cases. Both peptides contained predicted phosphorylation sites at serine residues. Table 14 summarizes the results of the MS data analysis.

Table 14: Summary of identified CLIP-115 peptides by mass spectrometry. Bold mass/charge ratios were clearly detected at the expected retention time and with the correct charge. Amino acids predicted to be phosphorylation sites in the respective peptide are bold, whereas the numbers give the first residue of the respective CLIP-115 peptide.

Mass/charge of peptide [m/z], z = 2	Mass/charge of phosphorylated peptide [m/z], z = 2	Amino acids predicted as phosphorylation sites
459.2506 $^{WT/TTL-/-}$	**499.2337** $^{TTL-/-}$	$_{720}$EQI**S**LAEK
467.7400 $^{WT/TTL-/-}$	507.7232 $^{TTL-/-}$ *	$_{450}$VEEE**S**ITK
480.2615 $^{WT/TTL-/-}$	-	$_{817}$AQV**S**ALENK
481.7613 $^{WT/TTL-/-}$	-	$_{190}$E**S**VLNS**S**VK
492.2377 $^{TTL-/-}$	-	$_{539}$TYQ**T**EVDK
502.7742 $^{WT/TTL-/-}$	542.7574 ^{WT} **	$_{289}$IGFP**S**T**S**PAK
518.7691 $^{WT/TTL-/-}$	-	$_{554}$**Y**AQEVADLK
525.7750 $^{WT/TTL-/-}$	-	$_{338}$**S**GLLTETSSR
558.7984 $^{WT/TTL-/-}$	-	$_{843}$LEAELEAV**S**R
588.3114 $^{WT/TTL-/-}$	628.2945 ^{WT} ***	$_{458}$GDLEL**T**TVAEK
664.8747 ^{WT}	704.8578 $^{TTL-/-}$ ****	$_{471}$VLQLEEEL**S**LR
769.8501 $^{WT/TTL-/-}$	**809.8333** $^{TTL-/-}$	$_{199}$TGNE**S**GSNL**S**D**S**G**S**VK
771.9243 ^{WT}	-	$_{938}$Y**S**LIDPA**S**PPELLK

$^{WT/TTL-/-}$ Peptide identified in wild type and *TTL*-/- samples

^{WT} Peptide identified only in wild type sample

$^{TTL-/-}$ Peptide identified only in *TTL*-/- sample

* Signal masked from similar mass/charge

** Peptide with wrong charge

*** Signal with wrong retention time

**** Signal very insecure

In this screen, two CLIP-115 peptides (bold in Tab. 14) derived from *TTL*-/- MEFs exhibited a molecular weight corresponding to an additional phosphate residue and an earlier retention time as their non-phosphorylated equivalents. In contrast, data from wild type MEF samples did only contain clear signals from non-phosphorylated peptides, which could be justified with the higher purity of the *TTL*-/- MEF samples.
According to an increased incorporation of C_{13} molecules besides the more frequent C_{12}, a peptide gives multiple peaks in MS. The characteristic peak patterns with an increasing mass/charge ratio of 1/z per incorporated C_{13} molecule are shown for the two identified CLIP-115 peptides in Figure 35. Additionally, the corresponding chromatograms with the respective retention times of the non-phosphorylated peptide and the phosphorylated equivalent are included. As all identified peptides were double charged, the shift of the mass/charge ratio for each additional C_{13} molecule is 0.5.

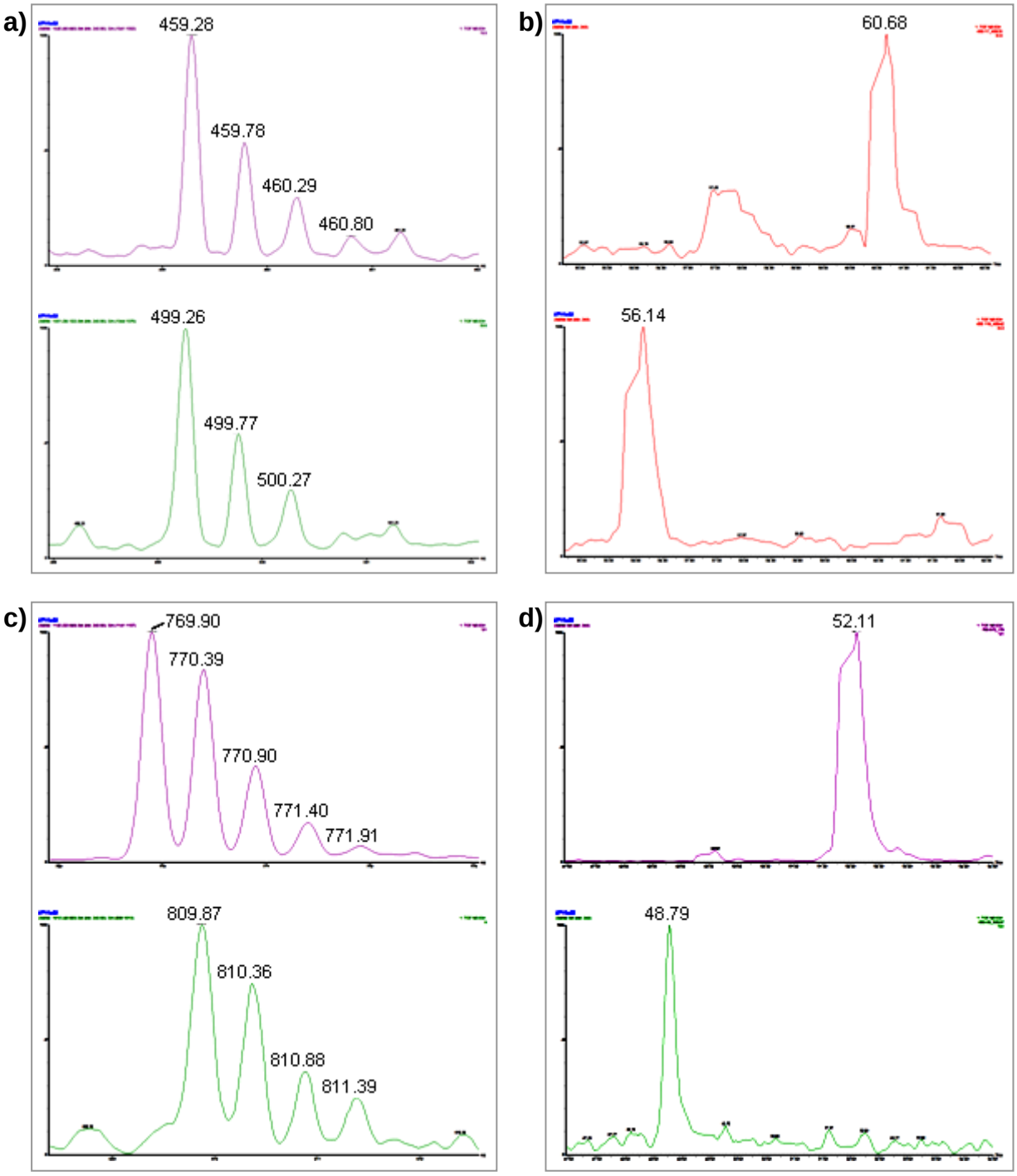

Fig. 35: Analysis of MS data obtained from *TTL-/-* MEF CLIP-115 samples revealed two non-phosphorylated peptides with phosphorylated equivalents. a) Mass spectra showing the signal intensity at the corresponding mass/charge ratio of the CLIP-115 peptide from amino acid 720 to 727. The upper spectrum shows the non-phosphorylated (calculated m/z = 459.2506) and the lower spectrum the phosphorylated form (calculated m/z = 499.2337). **b)** Chromatograms of the overall peptide flow intensity with the respective retention time in minutes corresponding to the peptides in a). **c)** Mass spectra showing the signal intensity at the corresponding mass/charge ratio of the CLIP-115

peptide from amino acid 199 to 214. The upper spectrum shows the non-phosphorylated (calculated m/z = 769.8501) and the lower spectrum the phosphorylated form (calculated m/z = 809.8333). **d)** Chromatograms of the overall peptide flow intensity with the respective retention time in minutes corresponding to the peptides in c). Due to their higher polarity phosphorylated peptides eluted earlier from the column.

In summary, MS analysis of enriched CLIP-115 samples from wild type and *TTL*-/- MEFs did not confirm the data of our mutagenesis experiments. Instead, MS data supported a non-phosphorylated state of tyrosine 270 as shown by direct search for the corresponding CLIP-115 peptides. Together with the absence of changes in the molecular weight of CLIP-115 mutants, these results indicate a differential phosphorylation of CLIP-115 in *TTL*-/- MEFs at a different position than tyrosine 270. Nevertheless, the tyrosine 270 occupies a key position for binding of CLIP-115 to microtubules, at least by determining the conformation of the second CAP-Gly domain. Moreover, CLIP-115 shows a differential phosphorylation pattern as well as a different phenotype when bound to microtubule plus-ends in wild type and *TTL*-/- MEFs. Hence, phosphorylation seems to be a major mechanism to regulate the binding behaviour of CLIP-115. Further analysis of the obtained MS data already revealed two peptide candidates that seem to carry a serine phosphorylation. Although they were both identified in *TTL*-/- samples, their existence in wild type samples cannot be excluded as those contained more contaminating proteins decreasing the quality of the MS data.

Additionally, rabbit antibodies against CLIP-115 peptides containing either phosphorylated or non-phosphorylated tyrosine 270 were generated (BioGenes GmbH). Antibodies were tested on synthetic CLIP-115 peptides in ELISA and on cell lysates in Western blotting. In both experiments, the antibodies turned out not to be highly specific. The amount of bound antibody was low in ELISA and the antibody against phosphorylated tyrosine 270 also recognized overexpressed mutant CLIP-115 containing tyrosine-substitutions in Western blot analysis (not shown). Nevertheless, the antibody against phosphorylated tyrosine 270 detected endogenous CLIP-115 in wild type and *TTL*-/- MEF lysates including the observed shift in molecular weight. Again, these results support the differential phosphorylation of CLIP-115 in wild type and TTL-deficient MEFs, albeit by a different origin than the predicted tyrosine 270.

4. Discussion

Microtubule dynamics and functions are regulated by the interaction with numerous microtubule-associated proteins. Binding of interaction partners depends on their affinity for microtubules, which can be influenced by regulation mechanisms as phosphorylation, autoinhibition, interaction with other proteins or the structure of the microtubule itself. The incorporated αβ-tubulin heterodimers are targets for several posttranslational modifications. Therefore, the binding sites for interacting proteins change their structural and electrostatic properties. Both can either promote or impair the interaction with specific binding partners. For example, posttranslational acetylation as well as detyrosination of α-tubulin is reported to affect the interaction between microtubules and kinesins. Acetylation promotes kinesin-1 loading onto microtubules (Reed et al., 2006), whereas detyrosination inhibits the interaction with microtubule-depolymerizing kinesin-13 motors (Peris et al., 2009).

In several cases, the impact of a posttranslational tubulin-modification was examined by mutating the respective modification sites within the tubulin subunits (see chapter 1.4.; Sharma et al., 2007; Westermann & Weber, 2003; Xia et al., 2000). The exact functions and mechanisms of posttranslational modifications of microtubules are still under investigation. One of the main problems in recent years was the fact that many of the involved enzymes were still unknown. The only enzyme being identified already many years ago is the tubulin-tyrosine ligase (TTL; Arce et al., 1975), which is involved in the tubulin tyrosination cycle (see chapter 1.4.4.). After incorporation of the αβ-tubulin heterodimers into microtubules, the C-terminal tyrosine residue of the α-tubulin subunits is removed by a yet unknown carboxypeptidase. Subsequent to depolymerization, TTL re-adds a tyrosine to the C-terminus of soluble detyrosinated α-tubulin. Detyrosination appears especially on stable microtubules, but does not directly increase stability by itself (Webster et al., 1990). Furthermore, TTL activity is decreased in tumour progression leading to a high level of detyrosination of microtubules (Lafanechère et al., 1998). The physiological meaning of the tyrosination cycle, though, remained unclear.

The identification of the TTL gene (Erck et al., 2003) and the subsequent generation of *TTL* knockout mice (Erck et al., 2005) allow the direct investigation of the tyrosination cycle of α-tubulin and its relevance for cellular processes in more detail. The importance of the tyrosination cycle became obvious since TTL-deficient mice died within 24 hours after birth due to malformations in the brain. However, the molecular basis still remained unknown. In *TTL* knockout neurons, the microtubule plus-end tracking protein CLIP-170 is mislocalised indicating an influence of tubulin detyrosination on the binding of microtubule-associated proteins (MAPs).

Several groups reported an interaction between the microtubule network and the actin cytoskeleton. This interaction is believed to promote cell polarization and is proposed to be linked to the tyrosination state of the microtubules. One example is a signal transduction cascade mediated through the actin-regulating small GTPase Rho that triggers microtubule detyrosination (Cook et al., 1998). Furthermore, the linkage of microtubules to actin by a complex of CLIP-170 and another actin-associated protein, IQGAP1, was discovered (Fukata et al., 2002; Gundersen, 2002). As CLIP-170 is mislocalised in neurons (Erck et al., 2005) and in Tyr-negative cells (Peris et al., 2006), a disruption of the cross-talk with the actin network can be assumed. Accordingly, Tyr-negative *TTL* knockout MEFs showed a disturbed development of lamellipodia indicating a defect in polarization (Peris et al., 2006).

Due to ongoing protein biosynthesis *TTL* knockout cells still contain residual amounts of tyrosinated (Tyr-) tubulin (Erck et al., 2005; Peris et al., 2006). To gain more insight into the relevance of the tubulin tyrosination state for cell polarity and migration as well as for interactions with plus-end tracking proteins in non-neuronal cells, it was necessary to generate a homogeneous cell population free of Tyr-tubulin for further experiments.

4.1. Depletion of tyrosinated tubulin in *TTL* knockout cells and investigation of cell polarity

Two strategies were followed to obtain Tyr-negative cells. First, *TTL* knockout cells were chemically treated either to inhibit protein synthesis or to arrest the cell cycle. Cells were then used in wound-healing experiments to investigate their ability to

polarize and migrate. Secondly, microinjection of blocking antibodies was performed to generate cells without any available tyrosine residue at the α-tubulin C-termini.

4.1.1. Chemical treatments

For testing chemical treatments to deplete the remaining Tyr-tubulin in TTL-deficient cells, two immortalized *TTL* knockout cell lines (see Tab. 8 in chapter 2.7.1.) were employed due to their higher stability in cell culture compared to primary cells.

The application of the DNA cross-linker mitomycin C alone did not result in the reduction of Tyr-tubulin in TTL-deficient cells. Therefore, cycloheximide was additionally used to inhibit mRNA synthesis. In contrast to mitomycin C-treatment, the application of cycloheximide strongly reduced the level of Tyr-tubulin (see Tab. 9). Unfortunately, due to the complete loss of protein biosynthesis and, by that, the ability to divide, cells died and could not be used for further experiments.

A more gentle approach to suppress ongoing protein biosynthesis is the arrest of the cell cycle. For that, cells were exposed to thymidine, nocodazole or taxol. However, none of the treatments succeeded in a complete inhibition of the tubulin synthesis, since *TTL* knockout cells still contained residual Tyr-tubulin amounts. Again, only in combination with cycloheximide, the application of these chemicals led to a reduction of the Tyr-tubulin level in *TTL* knockout cells, but once more cell viability was severely impaired and made further experiments impossible. Finally, the carboxypeptidase-activating drug forskolin was employed in combination with taxol to promote the detyrosination reaction (Wehland & Weber, 1987b). As TTL is missing, an increased carboxypeptidase activity should clearly reduce levels of Tyr-tubulin, but this effect could not be observed here (see Tab. 9). Cells obviously produced sufficient tubulin to compensate the increased carboxypeptidase activity.

Notably, the performed chemical treatments affected *TTL* knockout (II) cells more drastically than the temperature-sensitive *TTL* knockout (I) cells (see Tab. 8 and 9). Two days of serum starvation combined with doxycycline-withdrawal inactivated the cells sufficiently to reduce the Tyr-tubulin amount by at least 50 %, as determined by Western blotting (not shown). Since *TTL* knockout (II) cells were in good condition after starvation, it was decided to use these cells in wound-healing experiments.

Previously, defective cell polarization in the absence of TTL has been reported (Peris et al., 2006). In those studies only the shape of single cells was analysed without

considering the ability of Golgi reorientation or cell migration. The observed mislocalisation of CLIP-170 in the absence of TTL in those studies may have influenced the cross-talk with the actin cytoskeleton and, by that, resulted in the reported defects in cell polarization. Despite the reduced amount of Tyr-tubulin, starved *TTL* knockout (II) cells still polarized in our experimental set-up as demonstrated by Golgi reorientation after wounding a cell monolayer (Fig. 14; Palazzo et al., 2001). Furthermore, cells migrated into the wound until closure. Consequently, a reduction of tyrosinated tubulin did not obviously hinder cell polarization and migration, so that a complete depletion of Tyr-tubulin is necessary to gain more convincing results.

4.1.2. Microinjection of antibodies

As chemical treatments did not completely eliminate Tyr-tubulin levels, antibodies specific for the tyrosinated α-tubulin C-terminus were microinjected in *TTL* knockout cells to block the remaining C-terminal tyrosines. For microinjection experiments, the monoclonal antibodies 20C6 from mouse and YL1/2 from rat were successfully purified and microinjected into *TTL* knockout (II) cells in different amounts. Already an antibody concentration of 0.5 mg/ml resulted in clearly visible microtubule bundles originating from antibody-mediated microtubule cross-linking (Wehland et al., 1983). To avoid microtubule cross-linking, antibody F_{ab} fragments were employed.

Besides the immortalized *TTL* knockout cells, also primary wild type and TTL-deficient mouse embryonic fibroblasts (MEFs) were used for injections. As expected, F_{ab} fragments did not cross-link microtubules but obviously affected the localisation of the plus-end tracking protein CLIP-170. Approximately 25 % of microinjected wild type and TTL-deficient MEFs lacked CLIP-170 at the microtubule plus-ends. Notably, the majority of injected MEFs had a normal distribution of CLIP-170. These results indicate that CLIP-170 mislocalisation in microinjected cells is not necessarily a consequence of a F_{ab} fragment-mediated masking of the C-terminal tyrosine residues of α-tubulin. Thus, high amounts of injected F_{ab} fragments might disturb the microtubule plus-end-associated protein complex.

Interestingly, all non-injected *TTL* knockout MEFs that were stained for CLIP-170 in the microinjection experiments, did show a normal CLIP-170 localisation at microtubule plus-ends similar to wild type MEFs. This result is in contrast to the

published mislocalisation of CLIP-170 in Tyr-negative *TTL* knockout MEFs (Peris et al., 2006). As microinjection experiments did not give clear results, but raised discrepancies to recently published data, we decided to focus the further studies on a detailed characterization of primary TTL-deficient MEFs.

4.2. Characterization of tubulin pools in TTL-deficient mouse embryonic fibroblasts

For the characterization of non-neuronal *TTL* knockout cells, 13 days old embryos were isolated from heterozygous mice followed by the establishment of primary MEFs in cell culture. Mitotic TTL-deficient cells were reported to still contain a residual pool of tyrosinated tubulin due to ongoing protein biosynthesis (Erck et al., 2005), which could also be observed in our *TTL* knockout MEFs. To decrease cell activity and thereby protein synthesis, MEFs were starved in serum-free medium for two days. Subsequent immunofluorescence analysis revealed high levels of Tyr-tubulin in cells containing the TTL gene (wild type and *TTL* heterozygous MEFs), whereas TTL-deficient MEFs possessed only weak Tyr-tubulin-like structures (Fig. 15). Moreover, wild type and *TTL* heterozygous MEFs contained very low levels of detyrosinated (Glu-) and Δ2-Glu-tubulin, an α-tubulin variant that is missing both the C-terminal tyrosine and the penultimate glutamic acid residue. As expected, those tubulin pools were present at high levels in *TTL* knockout MEFs. In Western blot analysis, the results were even more obvious: Tyr-tubulin could only be identified in cell lysates from TTL-containing MEFs, whereas Glu- and Δ2-Glu-tubulin were exclusively present in lysates obtained from TTL-deficient MEFs (Fig. 16). According to the lack of TTL activity, Glu-tubulin and, as a consequence, also Δ2-Glu-tubulin accumulates in *TTL* knockout MEFs.

However, immunofluorescent staining using highly purified and concentrated YL1/2 antibody against the C-terminus of Tyr-tubulin identified a population of *TTL* knockout MEFs that still contained Tyr-tubulin (Tyr-positive), as has been reported previously (Peris et al., 2006). Interestingly, the content of Tyr-positive MEFs was observed to be negatively correlated to increasing passages in our cell culture set-up. Therefore, TTL-deficient MEFs containing and lacking Tyr-tubulin were considered separately in the following analysis of microtubule plus-end tracking proteins.

4.3. Characterization of microtubule plus-end tracking proteins in mouse embryonic fibroblasts

Microtubule-associated proteins play a major role in regulating microtubule dynamics and functions. An important group of those proteins is formed by the plus-end tracking proteins (+TIPs), which specifically bind growing microtubule plus-ends and largely influence their dynamic behaviour. As mentioned above, a mislocalisation of the +TIP CLIP-170 in *TTL* knockout neurons as well as a depleted microtubule binding of CAP-Gly domain-containing +TIPs in MEFs lacking Tyr-tubulin have already been reported (Erck et al., 2005; Peris et al., 2006). In order to gain deeper insight in the effects of TTL deficiency on the interaction between microtubules and +TIPs, wild type and *TTL* knockout MEFs were analysed by immunofluorescence and Western blotting.

4.3.1. Localisation and comet length of +TIPs

Consistent with published results, immunofluorescent stainings for end binding proteins (EBs) revealed a localisation to microtubule plus-ends independently from the genotype and the presence of Tyr-tubulin (Erck et al., 2005; Peris et al., 2006). EB proteins could thus be used as plus-end markers (Fig. 17). As EB proteins possess a higher affinity for GTP-loaded tubulin than for GDP-loaded tubulin, they most probably recognize the growing microtubule plus-ends due to the newly incorporated GTP-loaded tubulin heterodimers (Dragestein et al., 2008; Zanic et al., 2009). For that reason, the tyrosination state of the α-tubulin subunits does not influence EB binding.

Surprisingly, the CAP-Gly domain-containing proteins CLIP-170, CLIP-115 and $p150^{Glued}$ all localised to microtubule plus-ends in the absence of tyrosinated tubulin. Staining of Tyr-tubulin using highly concentrated YL1/2 antibody divided the *TTL* knockout MEF population into Tyr-positive and Tyr-negative cells, as described by Peris et al. (2006). In contrast to their results, CLIP-170 clearly co-localised with EB1 at microtubule plus-ends in all investigated MEFs in this study (Fig. 17). Since the length of CLIP-170 plus-end comets also was similar in all MEFs (Fig. 19), no genotype- or Tyr-tubulin-dependent localisation of CLIP-170 could be observed. A mislocalisation of CLIP-170 was also reported in TTL-deficient neurons, but even

though the neuronal cell body lacked Tyr-tubulin, CLIP-170 was concentrated in that region (Erck et al., 2005). If only the tyrosination state of microtubules controlled CLIP-170 localisation, the cellular CLIP-170 distribution should correlate with the distribution of Tyr-tubulin. In the absence of Tyr-tubulin, CLIP-170 would be evenly distributed in the neuronal cytoplasm. This already indicates a different regulatory mechanism for CLIP-170 binding to microtubules than tubulin detyrosination itself.

However, the C-terminal tyrosine residue of α-tubulin strongly increases CLIP-170 affinity for microtubule binding (Mishima et al., 2007). CLIP-170 binding is only reduced and not completely abolished at microtubules lacking the complete acidic tails of α- and β-tubulin. Especially the second CAP-Gly domain of CLIP-170, together with the adjacent serine-rich regions, also binds to the so-called H12 helices of α- and β-tubulin, which precede the acidic C-terminal tails (Fig. 36; Gupta et al., 2010). Furthermore, CLIP-170 recruitment to plus-ends depends on the presence of EB1 (Komarova et al., 2005; Bieling et al., 2008). This indicates that the observed CLIP-170 localisation at microtubule plus-ends of Tyr-negative MEFs is mediated through a direct interaction with EB1 and the tubulin H12 helices. Taken together, the results presented here are not in agreement with an essential role of the C-terminal tyrosine of α-tubulin in CLIP-170 plus-end tracking and support the existence of additional binding sites for CAP-Gly domain-containing proteins on tubulin.

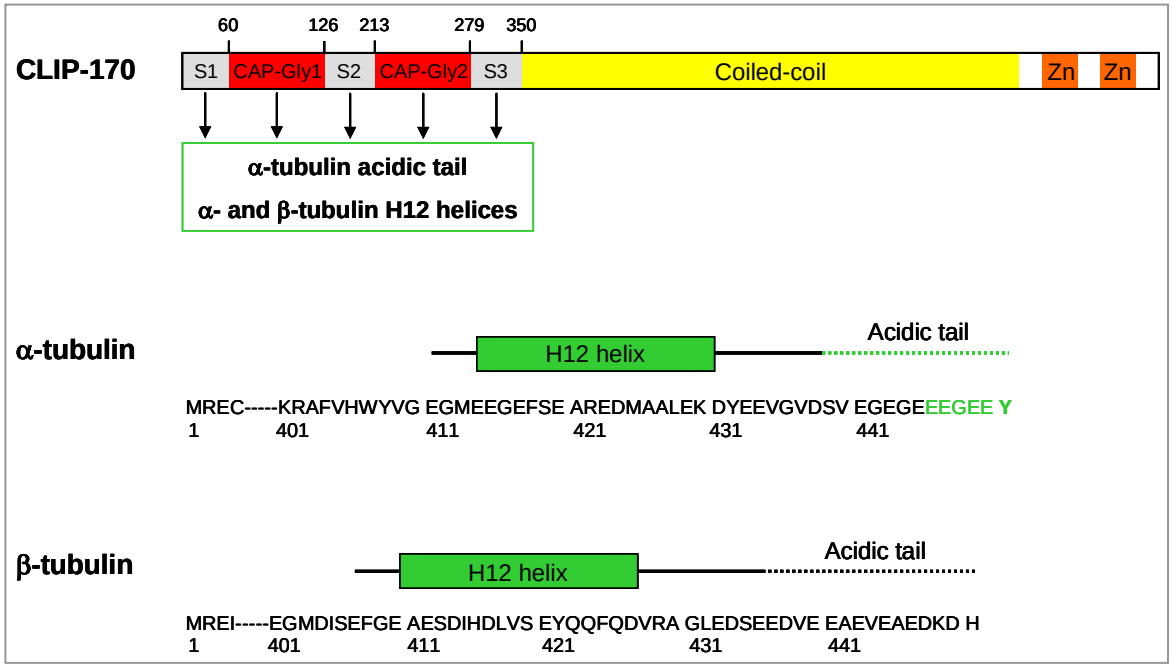

Fig. 36: Schematic structures of CLIP-170 and the respective target sites on α- and β-tubulin.
The CLIP-170 domain structure is illustrated schematically including both CAP-Gly domains, the adjacent serine-rich regions (S1 – S3), the coiled-coil domain and both zinc knuckles (Zn). Additionally, the C-terminal structures of α- and β-tubulin are shown including the H12 helices and the acidic tails. The amino acid sequences of murine α- and β-tubulin 1 are listed. Interaction targets of CLIP-170 are coloured in green. The CAP-Gly domains and the serine-rich regions of CLIP-170 are able to interact with the acidic tail of α-tubulin as well as with the H12 helices of both α- and β-tubulin. The C-terminal tyrosine of the α-tubulin acidic tail (bold) ensures high affinity of CLIP-170 for α-tubulin, but is not essential for microtubule binding (adapted from Gupta et al., 2010; Mishima et al., 2007).

Additionally, $p150^{Glued}$ co-localised with CLIP-170 demonstrated by equivalent staining patterns in all investigated MEFs. This observation corresponds with the reported recruitment of the dynein/dynactin complex to microtubule plus-ends through the interaction of CLIP-170 with $p150^{Glued}$ (Weisbrich et al., 2007). Furthermore, the $p150^{Glued}$ CAP-Gly domain possesses only a weak affinity for microtubules, but a much higher affinity for the CLIP-170 zinc knuckles and, therefore, binds predominantly to CLIP-170 (Mishima et al., 2007).
The only difference between Tyr-positive and Tyr-negative MEFs concerning the +TIPs could be observed in the CLIP-115 localisation. Although CLIP-115 was present at microtubule plus-ends in all MEFs, the CLIP-115 plus-end comets were significantly elongated in *TTL* knockout MEFs lacking Tyr-tubulin (Fig. 18 and 19). This result has not been reported in literature yet. To confirm the connection of CLIP-115 plus-end length with the presence of Tyr-tubulin, an exogenous *TTL* cDNA was expressed in TTL-deficient MEFs. These rescue experiments could completely restore the CLIP-115 phenotype of Tyr-positive MEFs (Fig. 20). In contrast to CLIP-115, CLIP-170 and EB1 comet lengths were not influenced by the expression of the exogenous TTL (Fig. 21). The determined comet lengths varied from approximately 0.4 – 2.0 µm (Figures 19 and 20), which is consistent with a published plus-end length of 0.5 – 2.0 µm (Akhmanova & Steinmetz, 2008; also compare Bieling et al., 2008, and Peris et al., 2006). Thus, comet lengths at single plus-ends varied in a broad range, which can be explained by different angles and growth speeds. Although a higher speed of microtubule growth results in longer comet tails of plus-end associated proteins (Bieling et al., 2008), the demonstrated overall elongation of CLIP-115 plus-end comets in Tyr-negative MEFs seems to originate from a different

mechanism since both CLIP-170 and EB1 comet lengths were unaffected. Furthermore, the microtubule growth rate measured in *TTL* knockout MEFs appears to be in the same range as in wild type MEFs (Peris et al., 2009). A temporally longer existence of +TIP binding sites due to a delay in structural changes or GTP-hydrolysis at the microtubule plus-ends in cells lacking Tyr-tubulin can also be excluded as this would influence all +TIPs. This indicates that the absence of Tyr-tubulin directly affects CLIP-115 or reactions concerning CLIP-115 binding. Since CLIP-115 functions as a rescue factor (Galjart, 2005), modulated binding to microtubules may, therefore, influence microtubule dynamics.

4.3.2. Biochemical analysis of +TIPs

To gain a deeper insight in effects of TTL deficiency on plus-end tracking proteins, EB1 and the CLIPs were investigated in biochemical experiments. By Western blot analysis, differences in the expression pattern as well as putative posttranslational modifications of the proteins can be uncovered. For further characterization of +TIPs in wild type, heterozygous and *TTL* knockout MEFs, cell lysates were examined in Western blot analyses using specific antibodies against EB1, CLIP-170 and CLIP-115. As expected from previous results, the presence of one *TTL* allele in heterozygous MEFs was enough to maintain the wild type phenotype for all proteins. Consistent with the immunofluorescence analyses, EB1 and CLIP-170 were similar in all genotypes regarding their molecular weight. Also the respective expression levels did not reveal any genotype dependency (Fig. 22). Notably, CLIP-170 appeared as a double band in Western blotting, as it is expressed in two isoforms resulting from alternative splicing (Griparic & Keller, 1998). Although CLIP-115 also exists in two splice variants, a single band was visible on Western blots representing either the presence of only one isoform in the investigated MEFs or isoform-specific antibody specificity. In contrast to EB1 and CLIP-170, CLIP-115 possessed a slightly lower molecular weight in TTL-deficient MEFs compared to wild type and heterozygous MEFs. The different molecular weights of CLIP-115 in the presence and the absence of TTL indicate a genotype-specific posttranslational modification. Since +TIPs often are targets of phosphorylation events, which modulate their microtubule affinity, as shown for CLIP-170 (Yang et al., 2009), CLASP2 (Kumar et al., 2009), MAP1B (Trivedi et al., 2005) and tau (Drewes et al., 1997), a phosphorylation could also be

the origin of the observed CLIP-115 mass shift. Indeed, phosphatase treatment decreased the molecular weight of CLIP-115 in wild type MEF lysates, but had no effect in *TTL* knockout MEF lysates (Fig. 23). Thus, CLIP-115 is additionally phosphorylated in wild type MEFs and exists in a less phosphorylated state in the absence of TTL. The observed difference in the molecular weight, therefore, does not derive from alternative splicing. Since in many cases phosphorylation of microtubule-associated proteins reduces the affinity for microtubules (Rickard & Kreis, 1991), it may be assumed that the pool of less phosphorylated CLIP-115 in TTL-deficient MEFs results in higher affinity to microtubules. This in turn can explain the origin of the observed elongated CLIP-115 microtubule plus-ends in *TTL* knockout MEFs lacking Tyr-tubulin.

As described above, phosphorylation of CLIP-115 results in a higher molecular weight visible in SDS-PAGE. To determine the number of additional phosphate residues that evoke the mass shift, total protein samples obtained from wild type and *TTL* knockout MEF lysates were analysed in two-dimensional SDS-PAGE. Every additional phosphate residue causes a shift of the isoelectric point of a protein and, therefore, the number of phosphorylations on CLIP-115 should be quantified. Unfortunately, variable protein amounts, loading techniques and different methods for isoelectric focussing did not succeed in an appropriate separation of CLIP-115. Although other proteins in the samples were focussed in the first dimension as demonstrated in Coomassie-stained SDS gels, CLIP-115 remained distributed over a broad pH range. Therefore, the inability of CLIP-115 focussing most probably originates from the specific protein properties. For instance, the relatively large size of CLIP-115 could be one reason why this protein could not be focussed. Additionally, single or several unknown modifications resulting in a higher hydrophobicity of CLIP-115 or even the presence of other proteins could explain the inability of isoelectric focussing. Direct after starting isoelectric focussing, some proteins tend to precipitate due to increasing condensation of the protein sample (Klose & Kobalz, 1995), which may explain the inability of CLIP-115 focussing observed in our studies.

4.3.3. Effects of phosphatase and kinase inhibition on CLIP-115

In order to identify the type of amino acid that is targeted by phosphorylation of CLIP-115, wild type and *TTL* knockout MEFs were treated with different phosphatase and kinase inhibitors. Western blot analysis of cell lysates revealed an obvious effect only after application of sodium vanadate, a tyrosine phosphatases inhibitor. After vanadate treatment, the CLIP-115 signal appeared as two bands in *TTL* knockout MEFs. The new appearing band could be observed at the molecular weight of CLIP-115 as seen in wild type MEFs. Thus, the inhibition of tyrosine dephosphorylation seems to restore the wild type phenotype of CLIP-115 in TTL-deficient MEFs at least partly. In contrast, inhibition of serine/threonine phosphatases by okadaic acid and calyculin A did not affect the molecular weight of CLIP-115 in TTL-deficient MEFs. The molecular weight of CLIP-115 remained constant in wild type MEFs through all treatments. Moreover, the molecular weight of CLIP-170 was unaffected after all treatments (Fig. 24). Additionally, wild type and *TTL* knockout MEFs were investigated by immunofluorescence after variable incubation times with phosphatase inhibitors. Again, only sodium vanadate affected the localisation of +TIPs. Interestingly, EB1, CLIP-170 and CLIP-115 were all eliminated from microtubule plus-ends after sodium vanadate treatment. Effects evoked by sodium vanadate were completely reversible since +TIPs reappeared after vanadate washout (Fig. 25 and 26).

Taken together, Western blot and immunofluorescence analyses revealed an influence of vanadate on CLIP-115 phosphorylation and plus-end localisation, respectively. These results indicate the phosphorylation of a tyrosine residue of CLIP-115, which is involved in microtubule plus-end binding and reduces the affinity for microtubules. Accordingly, either the CLIP-115 phosphorylation by a kinase is decreased or the dephosphorylation by a phosphatase is increased in TTL-deficient MEFs. Although sodium vanadate did not affect EB1 and CLIP-170 molecular weights, it abolished their binding to microtubule plus-ends analogous to CLIP-115. The inhibition of tyrosine phosphatases results in a substantial intervention in cell function and most probably affects numerous processes. Therefore, a secondary effect of vanadate must be taken into consideration for the observed removal of CLIP-115, CLIP-170 and EB1 from microtubule plus-ends instead of a phosphorylation on the proteins themselves.

Both the inhibition of kinases by staurosporine as well as the more specific inhibition of tyrosine kinases by genistein did not affect CLIP-115 or CLIP-170 molecular weights (Fig. 24).

4.3.4. Identification of putative phosphorylation sites in CLIP-115

As the inhibition of tyrosine phosphatases influenced CLIP-115 localisation and biochemical properties, we expected a tyrosine phosphorylation to be the most probable origin of the observed difference in CLIP-115, derived from wild type and *TTL* knockout MEFs. Using the online NetPhosK 1.0 and NetPhos 2.0 Servers (Technical University of Denmark), six tyrosines were predicted as potential phosphorylation sites. One of them (tyrosine residue 270) is located in a conserved region of the second CAP-Gly domain (see Tab. 11 and Fig. 27). A corresponding tyrosine residue, although not predicted as a phosphosite, is also present in the first CAP-Gly domain (tyrosine residue 130) and, therefore, was included in the subsequent experiments. The respective tyrosines were substituted either by glutamic acid mimicking phosphorylation or by non-phosphorylatable phenylalanine in full length CLIP-115-EGFP fusion constructs. Mutant CLIP-115-EGFP fusion proteins were then overexpressed for example in *CLIP-115* knockout and *CLIP-170/CLIP-115* double knockout MEFs, which were employed to eliminate the competition with endogenous CLIP-115.

Only mutations of tyrosines 130 and 270 into glutamic acid influenced CLIP-115 binding to microtubules. The respective mutation of tyrosine 270 strongly reduced the localisation of CLIP-115 at microtubules, whereas the mutation of tyrosine 130 only moderately reduced microtubule binding. In contrast, the introduction of phenylalanine had no effects. The combined mutation of both tyrosines into glutamic acid completely removed EGFP-CLIP-115 fusion proteins from microtubules. Since the second CAP-Gly domain possesses a higher affinity for microtubules (Hoogenraad et al., 2000), it can almost completely compensate for a mutation in the first CAP-Gly domain. In contrast, the first CAP-Gly domain can scarcely maintain CLIP-115 binding to microtubules when the second CAP-Gly domain is mutated. As a consequence, EGFP-CLIP-115 fusion proteins carrying mutations in both CAP-Gly domains were not able to bind microtubules anymore (Fig. 29 and 30). In conclusion, these results indicate that a phosphorylation of tyrosine 270 would severely decrease

CLIP-115 binding to microtubule plus-ends and could, therefore, act as a regulatory mechanism for CLIP-115 interaction with microtubules. Binding of CLIP-115 to microtubules is based on electrostatic interaction. Thereby, the major interaction takes place between the positively charged, hydrophobic cavity of the CAP-Gly domain and the negatively charged acidic tail of α-tubulin (Weisbrich et al., 2007). Phosphorylation of the CAP-Gly domain in its binding area would introduce a negative charge and by that reduce the affinity for tubulin. On the other hand, the mutation can also induce a conformational change of the domain structure leading to an impaired microtubule-binding capacity. This could be the case when tyrosine is substituted with glutamic acid, a structurally different amino acid that introduces a negative charge (Fig. 37a). In contrast, phenylalanine resembles the structure and hydrophobicity of tyrosine (Fig. 37a) and, thereby, the protein conformation most probably is maintained.

Additionally, a mutation of tyrosine 270 into alanine was performed as an alternative non-phosphorylation mimic. Similar to glutamic acid, alanine reduced CLIP-115 localisation at microtubules and completely disrupted microtubule binding in combination with a glutamic acid at position 130 (Fig. 30). Also alanine differs structurally from tyrosine (Fig. 37a) and seems to cause conformational changes of the CAP-Gly domain, as shown by a substantial reduction in the microtubule-binding capacity of CLIP-115. The structure of the closely related CAP-Gly domain of $p150^{Glued}$ including amino acids of the conserved hydrophobic cavity and the investigated tyrosine is illustrated in Figure 37b. The hydrophobic cavity mainly consists of four conserved amino acids (highlighted in red in Fig. 37b), whereas the corresponding tyrosine (blue) stabilizes the structure from the backside. Consequently, the substitution of this tyrosine with glutamic acid or alanine could destabilize the hydrophobic cavity by introducing a negative charge in a hydrophobic environment or removing the aromatic ring. Both changes most probably affect the domain structure and, therefore, can result in disturbed microtubule binding.

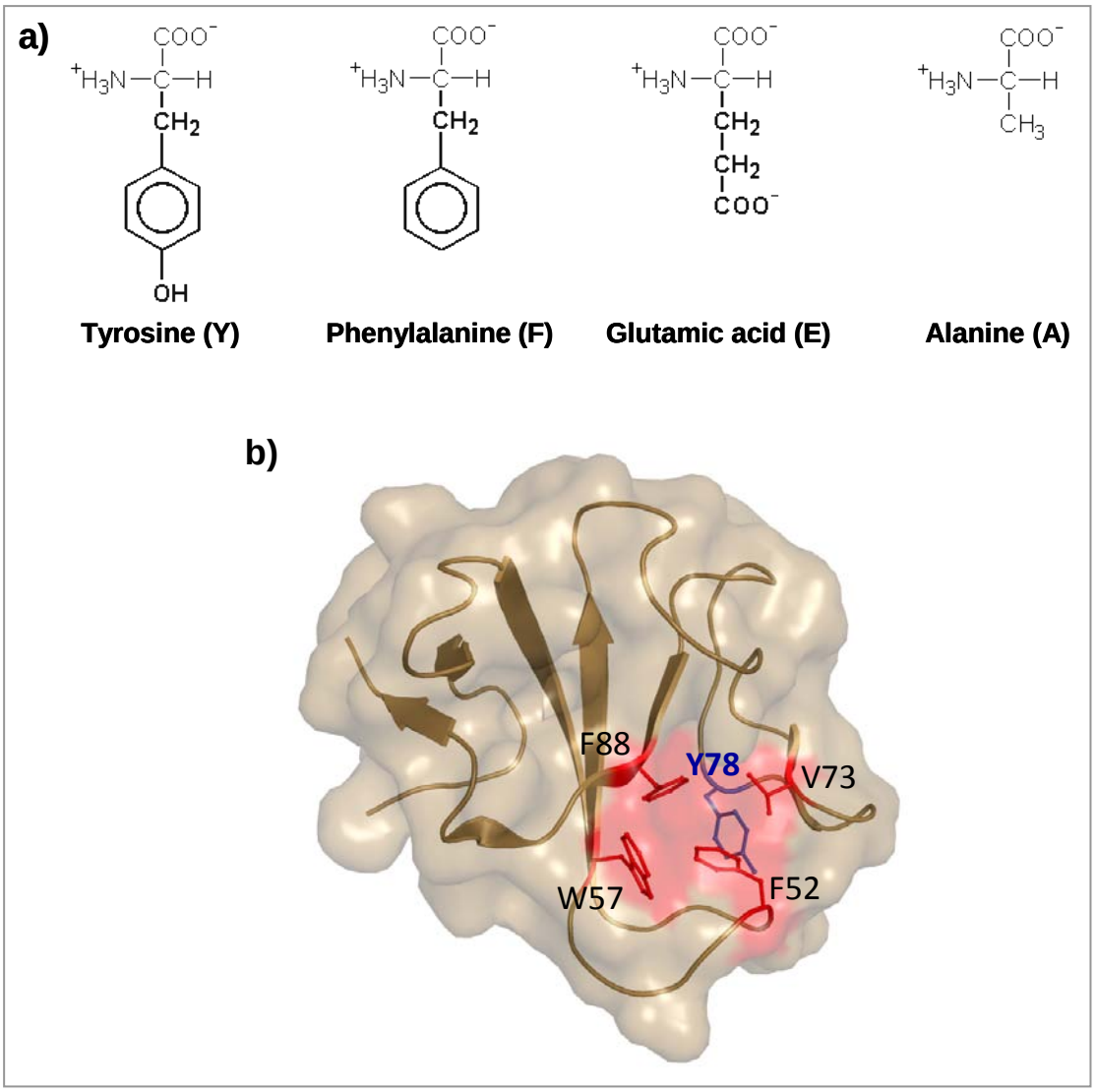

Fig. 37: Relevant amino acids and structure of the p150^{Glued} CAP-Gly domain. a) Structural formulas of tyrosine, phenylalanine, glutamic acid and alanine. **b)** Ribbon plot of the p150^{Glued} CAP-Gly domain with the conserved amino acids phenylalanine 52, tryptophan 57, valine 73 and phenylalanine 88 of the hydrophobic cavity depicted in stick and ball presentation in red. Tyrosine 78 (highlighted in blue) corresponds to the investigated CLIP-115 tyrosine residues 130 and 270 as well as to the CLIP-170 tyrosine residues 108 and 261. The ribbon plot is overlaid with a surface presentation including the hydrophobic cavity highlighted in red (Protein Data Bank code 2PZO; Weisbrich et al., 2007).

For example, site-directed mutagenesis experiments on tau showed that the aromatic ring of tyrosine residue 310, which is located in the microtubule-binding domain of tau, is necessary for correct protein folding and, thereby, for microtubule binding (Nishiura et al., 2009). The presence of an aromatic ring, which is part of both tyrosine and phenylalanine, at amino acid residue 270 of CLIP-115 might therefore

be essential for domain conformation or folding. Thus, the structural data support the hypothesis that phosphorylation of CLIP-115 tyrosine 270 could function as regulative mechanism for CLIP-115.

In studies on CLASP2 fragments, the mutation of phosphorylation sites influenced the molecular weight in SDS-PAGE, whereas mutations of residues that are no phosphorylation targets did not affect the molecular weight (Kumar et al., 2009). In our experiments, all mutant fusion proteins appeared at the same molecular weight. This indicates that the mutated tyrosine residues are probably not affected by phosphorylation. However, the fusion of CLIP-115 to EGFP might occlude the changes in charge evoked by the introduced mutations and, therefore, alters its behaviour during SDS-PAGE. Furthermore, the engagement of full length CLIP-115 might mask weak effects caused by mutagenesis.

As CAP-Gly domains are highly conserved through different proteins and organisms, the respective domains of CLIP-115 and CLIP-170 share great identity. Therefore, tyrosines 130 and 270 of CLIP-115 possess conserved homologues in CLIP-170, tyrosines 108 and 261, respectively. In order to compare the impact on microtubule binding, also these tyrosines were mutated either into phenylalanine or glutamic acid. Interestingly, only a combined mutation of both tyrosine residues into glutamic acids significantly reduced binding to microtubules. In some cells, CLIP-170 localisation to microtubule plus-ends was completely disrupted (Fig. 32 and Tab. 13). Remarkably, the mutations had a clearly less drastic effect in CLIP-170 than in CLIP-115. The second CAP-Gly domain of CLIP-170 contains two additional basic residues, arginines 297 and 298, compared to CLIP-115. Consequently, it possesses a more positively charged binding groove and, by that, a higher binding affinity for microtubules (Mishima et al., 2007). The introduction of a negative charge by the phosphorylation-mimicking mutation of tyrosine 261 into glutamic acid therefore has a weaker effect on the total domain charge and the structure than the corresponding mutation in CLIP-115.

In conclusion, these results demonstrate a vital role of tyrosine residues 130 and, especially, 270 in microtubule binding of CLIP-115. The introduction of a phosphorylation-mimicking mutation significantly reduced microtubule binding, while mimicking non-phosphorylation had opposite effects. Tyrosine-resembling phenylalanine did not alter microtubule binding, whereas alanine reduced CLIP-115

localisation at microtubules. Mutation analysis unfortunately did not clearly reveal whether the respective tyrosine residues within the CLIP-115 and CLIP-170 CAP-Gly domains appear as phosphorylation sites or as structure-stabilizing elements.

4.3.5. Search for CLIP-115 phosphorylation sites by mass spectrometry

As described above, treatments of *TTL* knockout MEFs with sodium vanadate indicated a tyrosine phosphorylation of CLIP-115. Subsequent mutation experiments could identify tyrosine residue 270 to be important for microtubule binding, but the exact role of this tyrosine could not be unravelled. Since CLIP-115 definitely appears differentially phosphorylated in wild type and *TTL* knockout MEFs, mass spectrometry (MS) was used to identify the involved phosphorylation site(s).

In order to enrich CLIP-115 from lysates obtained from wild type and TTL-deficient MEFs, immunoprecipitation was performed. Unfortunately, in first experiments the mass shift of CLIP-115 could not be maintained during the procedure (Fig. 33a). Therefore, the subsequent MS analysis failed in detecting a phosphorylation-based difference between CLIP-115 from wild type and *TTL* knockout MEFs. Furthermore, the identified peptides only covered 15.7 % of the complete CLIP-115 sequence limiting the probability for identifying a phosphorylated residue.

In subsequent experiments, the different molecular masses of CLIP-115 from wild type and *TTL* knockout MEFs could partly be maintained (Fig. 34). Synthetic peptides corresponding to the phosphorylated or non-phosphorylated CLIP-115 tryptic digest product containing tyrosine 270 were used as calibration standards in mass spectrometry. As the respective retention times and peptide masses were known, the CLIP-115 samples were specifically analysed by mass spectrometry regarding the tyrosine residue 270-containing peptide. The peptide with a non-phosphorylated tyrosine 270 was clearly identified in both wild type and *TTL* knockout samples. In contrast, in three independent experiments a peptide containing a phosphorylation at tyrosine 270 could not be detected. In conclusion, either the phosphorylation state of CLIP-115 could not be maintained during the experimental procedure or the tyrosine residue 270 is not phosphorylated *in vivo* indicative for a different origin of the observed mass shift of CLIP-115 in wild type and *TTL*-/- MEFs.

Previous experiments clearly demonstrated a phosphorylation of CLIP-115. However, the expected tyrosine phosphorylation could not be confirmed in our experimental

set-up. Since antibodies raised against phosphorylated tyrosine 270 of CLIP-115 also detected a different molecular weight of CLIP-115 in wild type and *TTL* knockout MEFs, a phosphorylation at a different amino acid residue is supported. Therefore, the received MS data was searched for the presence of other phosphorylated peptides. All possible CLIP-115 peptides produced by tryptic digest that contain a predicted phosphorylation site for serines, threonines and tyrosines were compared. Peptide masses were then calculated for different charges and the presence or absence of phosphate residues. Screening the CLIP-115 MS data revealed only two peptides derived from *TTL* knockout samples that were most probably phosphorylated (Tab. 14, Fig. 35). According to previous results demonstrating CLIP-115 to be phosphorylated to a higher degree in wild type, the detection of phosphorylated peptides in *TTL* knockout samples might be surprising. Here, the higher purity of the *TTL* knockout samples improved peptide detection in general.

One of the identified phosphopeptides contains serine residue 723, which is located in the coiled-coil domain of CLIP-115 and for that is most probably not involved in microtubule binding. However, phosphorylation of this residue might influence CLIP-115 dimerization, which is mediated by the coiled-coil domain.

Interestingly, the other identified peptide is located in the second serine-rich region and therefore covers a section of the microtubule-binding area of CLIP-115. This peptide includes serine residues 203, 208, 210 and 212 as predicted phosphorylation sites. Notably, CLIP-115 serines 203, 208 and 212 are conserved and correspond to CLIP-170 serines 194, 199 and 203. A screen of phosphopeptides derived from CLIP-170 already identified those serine residues as potentially phosphorylated amino acids (personal communication with A. Akhmanova, Department of Cell Biology, Erasmus Medical Center, Rotterdam).

In summary, the CLIP-115 peptide from amino acid residue 199 to 214 is a promissing candidate harbouring a phosphorylation site. Since it covers a region within the microtubule-binding area of CLIP-115, phosphorylation of one or multiple serines could act as a regulatory mechanism for CLIP-115 binding to microtubules.

To identify potential interaction partners of CLIP-115, proteins that were co-immunoprecipitated with CLIP-115 were also analysed by mass spectrometry and identified to be keratin and heat shock protein 70 (glucose-related protein 78). Most

probably, these proteins do not interact with CLIP-115, as they are common contaminations of protein preparations and frequently occur in MS analyses.

4.4. Conclusions and outlook

In order to gain more insight in the role of tubulin detyrosination, MEFs lacking the tubulin-tyrosine ligase were characterized. Wound-healing experiments using *TTL* knockout cells could not reveal an impact of reduced Tyr-tubulin levels on cell polarization and migration, as assumed in previous studies (Erck et al., 2005; Peris et al., 2006). Since we did not succeed in generating a population of Tyr-negative cells, future experiments should concentrate on the analysis of single Tyr-negative *TTL* knockout cells in order to unravel a potential impairment of cellular processes like polarization and migration in TTL-deficient MEFs. Furthermore, Golgi reorientation as well as the migration velocity should be determined in standardized wound-healing assays using live cell imaging and cell tracking. To enable single cell recovery after cell tracking, cells could be grown on coverslips containing a grid or coordinate system. By that, Tyr-negative cells could be detected in subsequent Tyr-tubulin staining. Finally, commercial Transwell migration assays could be performed to investigate the chemotactic behaviour of wild type and TTL-deficient MEFs. Serum-starved cells migrate in the direction of increasing serum concentration and can be fixed after a defined migration time for subsequent immunofluorescence analysis. Moreover, primary *TTL* knockout neurons could be used in further investigations of TTL deficiency since these cells show a more drastic *TTL* knockout phenotype than fibroblasts and are free of Tyr-tubulin (Erck et al., 2005).

Here we clearly demonstrated the ability of CAP-Gly domain-containing proteins to bind microtubule plus-ends independently from the presence of tyrosinated tubulin. Thus, the physiological relevance of the α-tubulin tyrosination cycle cannot be pinpointed to the regulation of microtubule interactions with CAP-Gly proteins alone (Peris et al., 2006). Remarkably, CLIP-115 even showed significantly elongated plus-end comets in *TTL* knockout MEFs lacking Tyr-tubulin. Additionally, CLIP-115 possessed a slightly smaller molecular weight in TTL-deficient MEFs compared to wild type MEFs. This mass shift turned out to be a consequence of differential phosphorylation most probably at a tyrosine residue. Although results from vanadate treatments indicate a tyrosine phosphorylation, more detailed experiments with other

phosphatase inhibitors as okadaic acid or calyculin A should be performed. Interestingly, *in vitro* co-sedimentation experiments revealed a slightly higher molecular weight of CLIP-115 peptides that were not bound to microtubules in the presence of the serine phosphatase inhibitor okadaic acid (Hoogenraad et al., 2000). Soluble CLIP-115 obviously was phosphorylated at a serine residue, whereas non-phosphorylated CLIP-115 co-sedimented with microtubules. As we used okadaic acid in a concentration of only 25 nM according to a standard protocol, the concentration probably was too low to evoke a shift of the molecular weight of CLIP-115.

This study already delivers some supporting results for a phosphorylation of CLIP-115 at a serine residue within the second serine-rich region, a section that is involved in microtubule binding. Screening of MS data identified a CLIP-115 peptide most probably carrying a phosphate residue. This peptide consists of amino acids 199 – 214 and contains three serine residues that are predicted as phosphorylation sites. Furthermore, those serines are conserved and phosphorylated in CLIP-170. Site-directed mutagenesis of the respective serine residues in CLIP-115 would facilitate the identification of phosphorylation sites and their potential involvement in microtubule targeting. Additionally, CLIP-115 deletion fragments including those residues could be used in Western blot analyses to reveal possible effects of the introduced mutations on the molecular weight in analogy to CLASP2 mutation studies described above (Kumar et al., 2009). For mapping phosphorylation sites in CLIP-115, phosphoserine and phosphothreonine residues from immunoprecipitated CLIP-115 from wild type and *TTL* knockout MEFs could be chemically converted into aminoethylcysteine and β-methylaminoethylcysteine, respectively. The modified amino acid residues are recognized by proteases that cleave at lysines. Subsequent mass spectrometry could then be used to identify the cleavage sites (Knight et al., 2003).

Detyrosination of α-tubulin definitely affects CLIP-115 localisation at microtubule plus-ends, as the absence of Tyr-tubulin leads to elongated plus-end comets in *TTL* knockout MEFs. Since, in addition, CLIP-115 appears less phosphorylated in the absence of TTL, the effect of detyrosination might be indirect by influencing microtubule interactions with other proteins or enzymes that affect CLIP-115 properties. Therefore, immunoprecipitation experiments of CLIP-115 could be

performed to identify potential interaction partners by subsequent Western blot or mass spectrometry analyses.

Phosphorylation of microtubule-associated proteins often alters the affinity for microtubules and could also be involved in regulating CLIP-115 binding to microtubules, which is supported by the differential phosphorylation of CLIP-115 in wild type and *TTL* knockout MEFs. The less phosphorylated state of CLIP-115 together with elongated plus-end comets in the absence of TTL indicates either an impaired kinase activity or an increased phosphatase activity close to the microtubule plus-ends. Therefore, TTL deficiency obviously alters the cellular phosphorylation pattern.

Kinases as well as phosphatases were already identified to be associated with microtubules either directly or via the interaction with other microtubule-associated proteins as for instance molecular motors. For example, kinesin-1 associates with the c-Jun N-terminal kinase (JNK), the JNK-interacting protein 1 (JIP1) and the mitogen-activated protein kinase-kinases 4 or 7 (MKK4 or MKK7; Daire et al., 2009). Additionally, kinesin-1 preferentially moves along detyrosinated microtubules, although with a slower velocity than on tyrosinated microtubules (Dunn et al., 2008). A modulation of kinesin-1 movement along microtubules provoked by an enhanced detyrosination level could affect local kinase activity at microtubule plus-ends and by that influence the phosphorylation of MAPs like CLIP-115. A potentially altered velocity of kinesin-1 by a lack of Tyr-tubulin could be measured by live cell imaging using wild type and TTL-deficient MEFs that express GFP-labelled kinesin-1 heavy chains.

Very recently, CLIP-170 has been reported to be phosphorylated by cdc2 kinase (Yang et al., 2009), which in turn is activated in the presence of JNK (Goss et al., 2003). Thus, a cdc2-mediated phosphorylation of CLIP-115 could be assumed and tested in experiments using specific cdc2- or JNK-inhibitors. Furthermore, immunoprecipitation either of CLIP-115 or cdc2 should help to unravel an interaction of those proteins. Since the phosphorylation target is already known in CLIP-170 (threonine residue 287; Yang et al., 2009), the corresponding amino acid in CLIP-115 (serine residue 295) could be mutated into non-phosphorylatable alanine to investigate its impact on CLIP-115 localisation.

Next to altered kinase activities in wild type versus TTL-deficient MEFs (as described above), also a misregulation of phosphatase activities should be considered. For example, the protein tyrosine phosphatase ε (PTPε) can bind microtubules. This association subsequently leads to a decrease of its phosphatase activity (Sines et al., 2007). When, for instance, enhanced microtubule detyrosination, as present in *TTL* knockout cells, impairs PTPε association with microtubules, a locally increased phosphatase activity would occur. Although a direct connection between PTPε and +TIPs is not described yet, such a mechanism could explain the less phosphorylated state of CLIP-115 observed in TTL-deficient MEFs. Immunofluorescent staining of PTPε in wild type and Tyr-negative *TTL* knockout MEFs could already reveal a difference in microtubule binding. Co-sedimentation experiments or microtubule polymerization assays could be used to quantify the amount of microtubule-bound PTPε in order to test this hypothesis.

5. Summary

The cytoskeleton is built up from microtubules, the microfilament network and the intermediate filaments. Together, they play an important role in numerous cellular processes. For example, microtubules are involved in the establishment of cell shape and cell polarity, build the mitotic spindle and function as intracellular railways for molecular motors. The involvement in such a large variety of cellular functions is, on the one hand, based on the polar structure and the highly dynamic behaviour of the microtubule itself. On the other hand, interaction partners and several post-translational modifications influence microtubule properties.

This study focuses on the tyrosination cycle, an α-tubulin-specific posttranslational modification. In order to uncover the physiological role of the tyrosination cycle, mouse embryonic fibroblasts (MEFs) lacking tubulin-tyrosine ligase (TTL) were characterized regarding different tubulin pools. Additionally, the influence of detyrosination/tyrosination of α-tubulin on microtubule plus-end tracking proteins (+TIPs) was analysed.

In the past, a mislocalisation of the +TIP CLIP-170 in *TTL* knockout neurons (Erck et al., 2005) as well as the inability of CAP-Gly domain-containing +TIPs to bind microtubule plus-ends in Tyr-negative MEFs have been reported (Peris et al., 2006). In contrast, here we clearly demonstrate that CAP-Gly domain-containing proteins localise at microtubule plus-ends independently from the presence or absence of tyrosinated tubulin. Interestingly, CLIP-115-decorated microtubule plus-end comets are elongated in Tyr-negative TTL-deficient MEFs. Furthermore, as compared to wild type MEFs, CLIP-115 appears to be in a less phosphorylated state in *TTL* knockout MEFs. The decreased phosphorylation status of CLIP-115 could either result from impaired kinase activity or increased phosphatase activity in the absence of TTL. Experiments using phosphatase inhibitors indicated the involvement of a tyrosine residue in the differential phosphorylation state of CLIP-115. Site-directed mutagenesis revealed an important role for tyrosine 270 in microtubule binding. However, mass spectrometry analyses did not confirm tyrosine 270 phosphorylation. While this residue is heavily involved in the establishment of the α-tubulin-binding hydrophobic cavity in the second CAP-Gly domain, it obviously plays a major role in

the maintenance of the three-dimensional structure instead of being a regulatory residue for microtubule binding.

Furthermore, mass spectrometry analyses identified two CLIP-115 peptides that most probably contain a serine phosphorylation. One of these peptides covers a part of the second serine-rich region of CLIP-115, which is involved in microtubule plus-end tracking. This peptide contains three conserved serine residues that are also present in CLIP-170. Mass spectrometry revealed these CLIP-170 residues to be phosphorylated (personal communication with A. Akhmanova). Moreover, in *in vitro* studies, a negative effect of serine phosphorylation on CLIP-115 binding to microtubules has already been demonstrated (Hoogenraad et al., 2000). Therefore, one or multiple serine residues within the identified CLIP-115 peptide could be target of a phosphorylation that influences or regulates CLIP-115 binding to microtubules. Future experiments should concentrate on the involvement of these serine residues in microtubule binding. Additionally, the identification of kinases or phosphatases that affect CLIP-115 in *TTL* knockout cells will ultimately reveal a new +TIP/microtubule binding mechanism.

6. Appendix

6.1. References

Akhmanova, A., Hoogenraad, C. C., Drabek, K., Stepanova, T., Dortland, B., Verkerk, T., Vermeulen, W., Burgering, B. M., De Zeeuw, C. I., Grosveld, F. and Galjart, N. (2001). CLASPs are CLIP-115 and -170 associating proteins involved in the regional regulation of microtubule dynamics in motile fibroblasts. *Cell* 104 (6), 923-935.

Akhmanova, A. and Steinmetz, M. O. (2008). Tracking the ends: a dynamic protein network controls the fate of microtubule tips. *Nat Rev Mol Cell Biol.* 9 (4), 309-322.

Alberts, B., Johnson, A., Lewis, J., Raff, M., Roberts, K. and Walter, P. (2008). Molecular biology of the cell. Fifth edition. *Garland Science*. Chapter 16, 965-1052.

Arce, C. A., Rodriguez, J. A., Barra, H. S. and Caputo, R. (1975). Incorporation of L-tyrosine, L-phenylalanine and L-3,4-dihydroxyphenylalanine as single units into rat brain tubulin. *Eur J Biochem.* 59, 145-149.

Arnal, I., Heichette, C., Diamantopoulos, G. S. and Chretien, D. (2004). CLIP-170/tubulin-curved oligomers coassemble at microtubule ends and promote rescues. *Curr Biol.* 14, 2086-2095.

Baas, P. W. and Qiang, L. (2005). Neuronal microtubules: when the MAP is the roadblock. *Trends Cell Biol.* 15 (4), 183-187.

Ban, R., Matsuzaki, H., Akashi, T., Sakashita, G., Taniguchi, H., Park, S. Y., Tanaka, H., Furukawa, K. and Urano, T. (2009). Mitotic regulation of the stability of microtubule plus-end tracking protein EB3 by ubiquitin ligase SIAH-1 and Aurora mitotic kinases. *J Biol Chem.* 284 (41), 28367-28381.

Bieling, P., Laan, L., Schek, H., Munteanu, E. L., Sandblad, L., Dogterom, M., Brunner, D. and Surrey, T. (2007). Reconstitution of a microtubule plus end tracking system in vitro. *Nature* 450 (7172), 1100-1105.

Bieling, P., Kandels-Lewis, S., Telley, I. A., van Dijk, J., Janke, C. and Surrey, T. (2008). CLIP-170 tracks growing microtubule ends by dynamically recognizing composite EB1/tubulin-binding sites. *J Cell Biol.* 183 (7), 1223-1233.

Bijur, G. N., De Sarno, P. and Jope, R. S. (2000). Glycogen synthase kinase-3b facilitates staurosporine- and heat shock-induced apoptosis. *J Biol Chem.* 275 (11), 7583-7590.

Blangy, A., Arnaud, L. and Nigg, E. A. (1997). Phosphorylation by $p34^{cdc2}$ protein kinase regulates binding of the kinesin-related motor HsEg5 to the dynactin subunit $p150^{Glued}$. *J Biol Chem.* 272, 19418-19424.

Brouhard, G. J., Stear, J. H., Noetzel, T. L., Al-Bassam, J., Kinoshita, K., Harrison, S. C., Howard, J. and Hyman, A. A. (2008). XMAP215 is a processive microtubule polymerase. *Cell* 132, 79-88.

Caron, J. M., Vega, L. R., Fleming, J., Bishop, R. and Solomon, F. (2001). Single site α-tubulin mutation affects astral microtubules and nuclear positioning during anaphase in *Saccharomyces cerevisiae*: possible role for palmitoylation of α-tubulin. *Mol Biol Cell.* 12 (9), 2672-2687.

Choi, J. H., Bertram, P. G., Drenan, R., Carvalho, J., Zhou, H. H. and Zheng, X. F. (2002). The FKBP12-rapamycin-associated protein (FRAP) is a CLIP-170 kinase. *EMBO Rep.* 3 (10), 988-994.

Cook, T. A., Nagasaki, T. and Gundersen, G. G. (1998). Rho guanosine triphosphatase mediates the selective stabilization of microtubules induced by lysophosphatidic acid. *J Cell Biol.* 141 (1), 175-185.

Coquelle, F. M., Caspi, M., Cordelières, F. P., Dompierre, J. P., Dujardin, D. L., Koifman, C., Martin, P., Hoogenraad, C. C., Akhmanova, A., Galjart, N., De Mey, J. R. and Reiner, O. (2002). LIS1, CLIP-170's key to the dynein/dynactin pathway. *Mol Cell Biol.* 22 (9), 3089-3102.

Daire, V., Guistiniani, J., Leroy-Gori, I., Quesnoit, M., Drevensek, S., Dimitrov, A., Perez, F. and Poüs, C. (2009). Kinesin-1 regulates microtubule dynamics via a c-Jun N-terminal kinase-dependent mechanism. *J Biol Chem.* 284 (46), 31992-32001.

Dammermann, A., Desai, A. and Oegema, K. (2003). The minus end in sight. *Curr Biol.* 13, R614-R624.

Deacon, S. W., Serpinskaya, R. S., Vaughan, P. S., Lopez Fanarraga, M., Vernos, I., Vaughan, K. T. and Gelfand, V. I. (2003). Dynactin is required for bidirectional organelle transport. *J Cell Biol.* 160, 297-301.

Dimitrov, A., Quesnoit, M., Moutel, S., Cantaloube, I., Poüs, C. and Perez, F. (2008). Detection of GTP-tubulin conformation in vivo reveals a role for GTP remnants in microtubule rescues. *Science* 322, 1353-1356.

DiTella, M. C., Feiguin, F., Carri, N., Kosik, K. S. and Cáceres, A. (1996). MAP-1B/TAU functional redundancy during laminin-enhanced axonal growth. *J Cell Sci.* 109, 467-477.

Dragestein, K. A., van Cappellen, W. A., van Haren, J., Tsibidis, G. D., Akhmanova, A., Knoch, T. A., Grosveld, F. and Galjart, N. (2008). Dynamic behaviour of GFP-CLIP-170 reveals fast protein turnover on microtubule plus ends. *J Cell Biol.* 180 (4), 729-737.

Drewes, G., Ebneth, A., Preuss, U., Mandelkow, E. M. and Mandelkow, E. (1997). MARK, a novel family of protein kinases that phosphorylate microtubule-associated proteins and trigger microtubule disruption. *Cell*. 89 (2), 297-308.

Dunn, S., Morrison, E. E., Liverpool, T. B., Molina-París, C., Cross, R. A., Alonso, M. C. and Peckham, M. (2008). Differential trafficking of Kif5c on tyrosinated and detyrosinated microtubules in live cells. *J Cell Sci.* 121, 1085-1095.

Dutcher, S. K. (2003). Long-lost relatives reappear: Identification of new members of the tubulin superfamily. *Curr Opin Microbiol.* 6, 634-640.

Elliot, J., Scarpello, J. H. P. and Morgan, N. G. (2001). Effects of tyrosine kinase inhibitors on cell death induced by sodium fluoride and pertussis toxin in the pancreatic β-cell line, RINm5F. *Brit J Pharmacol.* 132, 119-126.

Erck, C., MacLeod, R. A. and Wehland, J. (2003). Cloning and genomic organization of the TTL gene on mouse chromosome 2 and human chromosome 2q13. *Cytogenet Genome Res.* 101, 47-53.

Erck, C., Peris, L., Andrieux, A., Meissirel, C., Gruber, A. D., Vernet, M., Schweitzer, A., Saoudi, Y., Pointu, H., Bosc, C., Salin, P. A., Job, D. and Wehland, J. (2005). A vital role of tubulin-tyrosine-ligase for neuronal organization. *Proc Natl Acad Sci USA.* 102 (22), 7853-7858.

Etienne-Manneville, S. (2009). From signalling pathways to microtubule dynamics: the key players. *Curr Opin Cell Biol.* 22, 1-8.

Fourest-Lieuvin, A., Peris, L., Gache, V., Garcia-Saez, I., Juillan-Binard, C., Lantez, V. and Job, D. (2006). Microtubule regulation in mitosis: tubulin phosphorylation by the cyclin-dependent kinase Cdk1. *Mol Biol Cell.* 17 (3), 1041-1050.

Francis, F., Koulakoff, A., Boucher, D., Chafey, P., Schaar, B., Vinet, M. C., Friocourt, G., McDonnell, N., Reiner, O., Kahn, A., McConnell, S. K., Berwald Netter, Y., Denoulet, P. and Chelly, J. (1999). Doublecortin is a developmentally regulated, microtubule-associated protein expressed in migrating and differentiating neurons. *Neuron.* 23 (2), 247-256.

Fukata, M., Watanabe, T., Noritake, J., Nakagawa, M., Yamaga, M., Kuroda, S., Matsuura, Y., Iwamatsu, A., Perez, F. and Kaibuchi, K. (2002). Rac1 and Cdc42 capture microtubules through IQGAP1 and CLIP-170. *Cell* 109 (7), 873-885.

Galjart, N. (2005). CLIPS and CLASPS and cellular dynamics. *Nature Rev Mol Cell Biol.* 6, 487-498.

Galperin, M. Y. and Koonin, E. V. (1997). A diverse superfamily of enzymes with ATP-dependent carboxylate-amine/thiol ligase activity. *Protein Sci.* 6 (12), 2639-2643.

Gee, M. A., Heuser, J. E. and Vallee, R. B. (1997). An extended microtubule-binding structure within the dynein motor domain. *Nature* 390, 636-639.

Gleeson, J. G., Lin, P. T., Flanagan, L. A. and Walsh, C. A. (1999). Doublecortin is a microtubule-associated protein and is expressed widely by migrating neurons. *Neuron.* 23 (2), 257-271.

Goss, V. L., Cross, J. V., Ma, K., Qian, Y., Mola, P. W. and Templeton, D. J. (2003). SAPK/JNK regulates cdc2/cyclin B kinase through phosphorylation and inhibition of cdc25c. *Cell Signal.* 15 (7), 709-718.

Griparic, L. and Keller, T. C. (1998). Identification and expression of two novel CLIP-170/Restin isoforms expressed predominantly in muscle. *Biochim Biophys Acta.* 1405 (1-3), 35-46.

Gundersen, G. G., Kim, I. and Chapin, C. J. (1994). Induction of stable microtubules in 3T3 fibroblasts by TGF-β and serum. *J Cell Sci.* 107, 645-659.

Gundersen, G. G. (2002). Microtubule capture: IQGAP and CLIP-170 expand the repertoire. *Curr Biol.* 12 (19), R645-647.

Gupta, A., Tsai, L. H. and Wynshaw-Boris, A. (2002). Life is a journey: a genetic look at neocortical development. *Nat Rev Genet.* 3 (5), 342-355.

Gupta, K. K., Paulson, B. A., Folker, E. S., Charlebois, B., Hunt, A. J. and Goodson, H. V. (2008). The minimal plus-end tracking unit of the cytoplasmic linker protein CLIP-170. *J Biol Chem.* 284 (11), 6735-6742.

Gupta, K. K., Joyce, M. V., Slabbekoorn, A. R., Zhu, Z. C., Paulson, B. A., Boggess, B. and Goodson, H. V. (2010). Probing interactions between CLIP-170, EB1, and microtubules. *J Mol Biol.* 395 (5), 1049-1062.

Gupta, M. L. Jr., Carvalho, P., Roof, D. M. and Pellman, D. (2006). Plus end-specific depolymerase activity of Kip3, a kinesin-8 protein, explains its role in positioning the yeast mitotic spindle. *Nat Cell Biol.* 8 (9), 913-923.

Gurland, G. and Gundersen, G. G. (1995). Stable, detyrosinated microtubules function to localize vimentin intermediate filaments in fibroblasts. *J Cell Biol.* 131 (5), 1275-1290.

Halpain, S. and Dehmelt, L. (2006). The MAP1 family of microtubule-associated proteins. *Genome Biol.* 7 (6), 224.

Hammond, J. W., Cai, D. and Verhey, K. J. (2008). Tubulin modifications and their cellular functions. *Curr Opin Cell Biol.* 20 (1), 71-76.

Hoogenraad, C. C., Akhmanova, A., Grosveld, F., De Zeeuw, C. I. and Galjart, N. (2000). Functional analysis of CLIP-115 and its binding to microtubules. *J Cell Sci.* 113, 2285-2297.

Hoogenraad, C. C., Koekkoek, B., Akhmanova, A., Krugers, H., Dortland, B., Miedema, M., van Alphen, A., Kistler, W. M., Jaegle, M., Koutsourakis, M., Van Camp, N., Verhoye, M., van der Linden, A., Kaverina, I., Grosveld, F., De Zeeuw, C. I. and Galjart, N. (2002). Targeted mutation of Cyln2 in the Williams syndrome critical region links CLIP-115 haploinsufficiency to neurodevelopmental abnormalities in mice. *Nat Genet.* 32 (1), 116-127.

Honnappa, S., John, C. M., Kostrewa, D., Winkler, F. K. and Steinmetz, M. O. (2005). Structural insights into the EB1-APC interaction. *EMBO J.* 24, 261-269.

Honnappa, S., Okhrimenko, O., Jaussi, R., Jawhari, H., Jelesarov, I., Winkler, F. K. and Steinmetz, M. O. (2006). Key interaction modes of dynamic +TIP networks. *Mol Cell* 23, 663-671.

Horio, T. and Hotani, H. (1986). Visualization of the dynamic instability of individual microtubules by dark-field microscopy. *Nature* 321, 605-607.

Howard, J. and Hyman, A. A. (2003). Dynamics and mechanics of the microtubule plus end. *Nature* 422, 753-758.

Hunter, A. W., Caplow, M., Coy, D. L., Hancock, W. O., Diez, S., Wordeman, L. and Howard, J. (2003). The kinesin-related protein MCAK is a microtubule depolymerase that forms an ATP-hydrolyzing complex at microtubule ends. *Mol Cell.* 11 (2), 445-457.

Inoue, Y. H., Savoian, M. S., Suzuki, T., Máthé, E., Yamamoto, M. T. and Glover, D. M. (2004). Mutations in orbit/mast reveal that the central spindle is comprised of two microtubule populations, those that initiate cleavage and those that propagate furrow ingression. *J Cell Biol.* 166 (1), 49-60.

Kardon, J. R. and Vale, R. D. (2009). Regulators of the cytoplasmic dynein motor. *Nat Rev Mol Cell Biol.* 10 (12), 854-865.

Kilmartin, J. V., Wright, B. and Milstein, C. (1982). Rat monoclonal anti-tubulin antibodies derived by using a new nonsecreting rat cell line. *J Cell Biol.* 93, 576-582.

Klose, J. and Kobalz, U. (1995). Two-dimensional electrophoresis of proteins: an updated protocol and implications for a functional analysis of the genome. *Electrophoresis* 16 (6), 1034-1059.

Knight, Z. A., Schilling, B., Row, R. H., Kenski, D. M., Gibson, B. W. and Shokat, K. M. (2003). Phosphospecific proteolysis for mapping sites of protein phosphorylation. *Nat Biotechnol.* 21 (9), 1047-1054.

Komarova, Y., Lansbergen, G., Galjart, N., Grosveld, F., Borisy, G. G. and Akhmanova, A. (2005). EB1 and EB3 control CLIP dissociation from the ends of growing microtubules. *Mol Biol Cell.* 16 (11), 5334-5345.

Komarova, Y., De Groot, C. O., Grigoriev, I., Gouveia, S. M., Munteanu, E. L., Schober, J. M., Honnappa, S., Buey, R. M., Hoogenraad, C. C., Dogterom, M., Borisy, G. G., Steinmetz, M. O. and Akhmanova, A. (2009). Mammalian end binding proteins control persistent microtubule growth. *J Cell Biol.* 184 (5), 691-706.

Kumar, P., Lyle, K. S., Gierke, S., Matov, A., Danuser, G. and Wittmann, T. (2009). GSK3β phosphorylation modulates CLASP–microtubule association and lamella microtubule attachment. *J Cell Biol.* 184 (6), 895-908.

Laemmli, U.K., Beguin, F. and Gujer-Kellenberger, G. (1970). A factor preventing the major head protein of bacteriophage T4 from random aggregation. *J Mol Biol.* 47, 69-85.

Lafanechère, L., Courtay-Cahen, C., Kawakami, T., Jacrot, M., Rüdiger, M., Wehland, J., Job, D. and Margolis, R. L. (1998). Suppression of tubulin tyrosine ligase during tumor growth. *J Cell Sci.* 111, 171-181.

Lansbergen, G., Komarova, Y., Modesti, M., Wyman, C., Hoogenraad, C. C., Goodson, H. V., Lemaitre, R. P., Drechsel, D. N., van Munster, E., Gadella, T. W. Jr., Grosveld, F., Galjart, N., Borisy, G. G. and Akhmanova, A. (2004). Conformational changes in CLIP-170 regulate its binding to microtubules and dynactin localization. *J Cell Biol.* 166 (7), 1003-1014.

Lansbergen, G. and Akhmanova, A. (2006). Microtubule plus end: a hub of cellular activities. *Traffic* 7, 499-507.

Lansbergen, G., Grigoriev, I., Mimori-Kiyosue, Y., Ohtsuka, T., Higa, S., Kitajima, I., Demmers, J., Galjart, N., Houtsmuller, A. B., Grosveld, F. and Akhmanova, A. (2006). CLASPs attach microtubule plus ends to the cell cortex through a complex with LL5β. *Dev Cell.* 11 (1), 21-32.

Lewkowicz, E., Herit, F., Le Clainche, C., Bourdoncle, P., Perez, F. and Niedergang, F. (2008). The microtubule-binding protein CLIP-170 coordinates mDia1 and actin reorganization during CR3-mediated phagocytosis. *J Cell Biol.* 183 (7), 1287-1298.

Liao, G. and Gundersen, G. G. (1998). Kinesin is a candidate for cross-bridging microtubules and intermediate filaments. Selective binding of kinesin to detyrosinated tubulin and vimentin. *J Biol Chem.* 273 (16), 9797-9803.

Lomakin, A. J., Semenova, I., Zaliapin, P., Nadezhdina, E., Slepchenko, B. M., Akhmanova, A. and Rodionov, V. (2009). CLIP-170-dependent capture of membrane organelles by microtubules initiate minus-end directed transport. *Dev Cell* 17 (3), 323-333.

Maiato, H., Sampaio, P., Lemos, C. L., Findlay, J., Carmena, M., Earnshaw, W. C. and Sunkel, C. E. (2002). MAST/Orbit has a role in microtubule-kinetochore attachment and is essential for chromosome alignment and maintenance of spindle bipolarity. *J Cell Biol.* 157 (5), 749-760.

Maiato, H., Fairley, E. A., Rieder, C. L., Swedlow, J. R., Sunkel, C. E. and Earnshaw, W. C. (2003). Human CLASP1 is an outer kinetochore component that regulates spindle microtubule dynamics. *Cell* 113 (7), 891-904.

Matsuyama, A., Shimazu, T., Sumida, Y., Saito, A., Yoshimatsu, Y., Seigneurin Berny, D., Osada, H., Komatsu, Y., Nishino, N., Khochbin, S., Horinouchi, S. and Yoshida, M. (2002). *In vivo* destabilization of dynamic microtubules by HDAC6-mediated deacetylation. *EMBO J.* 21 (24), 6820-6831.

McNally, K. P., Bazirgan, O. A. and McNally, F. J. (2000). Two domains of p80 katanin regulate microtubule severing and spindle pole targeting by p60 katanin. *J Cell Sci*. 113, 1623-1633.

Mialhe, A., Lafanechère, L., Treilleux, I., Peloux, N., Dumontet, C., Brémond, A., Panh, M. H., Payan, R., Wehland, J., Margolis, R. L. and Job, D. (2001). Tubulin detyrosination is a frequent occurrence in breast cancers of poor prognosis. *Cancer Res.* 61 (13), 5024-5027.

Mimori-Kiyosue, Y., Grigoriev, I., Lansbergen, G., Sasaki, H., Matsui, C., Severin, F., Galjart, N., Grosveld, F., Vorobjev, I., Tsukita, S. and Akhmanova, A. (2005). CLASP1 and CLASP2 bind to EB1 and regulate microtubule plus-end dynamics at the cell cortex. *J Cell Biol.* 168 (1), 141-153.

Mishima, M., Maesaki, R., Kasa, M., Watanabe, T., Fukata, M., Kaibuchi, K. and Hakoshima, T. (2007). Structural basis for tubulin recognition by cytoplasmic linker protein 170 and its autoinhibition. *Proc Natl Acad Sci USA.* 104 (25), 10346-10351.

Mitchison, T. and Kirschner, M. (1984). Dynamic instability of microtubule growth. *Nature* 312, 237-242.

Moritz, M. and Agard, D. A. (2001). Gamma-tubulin complexes and microtubule nucleation. *Curr Opin Struct Biol.* 11 (2), 174-181.

Nan, X., Sims, P. A., Chen, P. and Xie, X. S. (2005). Observation of individual microtubule motor steps in living cells with endocytosed quantum dots. *J Phys Chem B.* 109 (51), 24220-24224.

Newton, C. N., Wagenbach, M., Ovechkina, Y., Wordeman, L. and Wilson, L. (2004). MCAK, a Kin I kinesin, increases the catastrophe frequency of steady state HeLa cell microtubules in an ATP-dependent manner in vitro. *FEBS Lett.* 572, 80-84.

Nishiura, C., Takeuchi, K., Minoura, K., Sumida, M., Taniguchi, T., Tomoo, K. and Ishida, T. (2010). Importance of Tyr310 residue in the third repeat of microtubule binding domain for filament formation of tau protein. *J Biochem.* 147 (3), 405-414.

North, B. J., Marshall, B. L., Borra, M. T., Denu, J. M. and Verdin, E. (2003). The human Sir2 ortholog, SIRT2, is an NAD+-dependent tubulin deacetylase. *Mol Cell.* 11 (2), 437-444.

Oakely, C. E. and Oakely, B. R. (1989). Identification of γ-tubulin, a new member of the tubulin superfamily encoded by mibA gene of *Aspergillus nidulans*. *Nature* 338, 662-664.

Palazzo, A. F., Joseph, H. L., Chen, Y. J., Dujardin, D. L., Alberts, A. S., Pfister, K. K., Vallee, R. B. and Gundersen, G. G. (2001). Cdc42, dynein, and dynactin regulate MTOC reorientation independent of Rho-regulated microtubule stabilization. *Curr Biol.* 11 (19), 1536-1541.

Paturle-Lafanechère, L., Eddé, B., Denoulet, P., Van Dorsselaer, A., Mazarguil, H., Le Caer, J. P., Wehland, J. and Job, D. (1991). Characterization of a major brain tubulin variant which cannot be tyrosinated. *Biochemistry.* 30 (43), 10523-10528.

Paturle-Lafanechère, L., Manier, M., Trigault, N., Pirollet, F., Mazarguil, H. and Job, D. (1994). Accumulation of delta 2-tubulin, a major tubulin variant that cannot be tyrosinated, in neuronal tissues and in stable microtubule assemblies. *J Cell Sci.* 107, 1529-1543.

Perez, F., Diamantopoulos, G. S., Stalder, R. and Kreis, T. E. (1999). CLIP-170 highlights growing microtubule ends in vivo. *Cell.* 96 (4), 517-527.

Peris, L., Thery, M., Fauré, J., Saoudi, Y., Lafanechère, L., Chilton, J. K., Gordon Weeks, P., Galjart, N., Bornens, M., Wordeman, L., Wehland, J., Andrieux, A. and Job, D. (2006). Tubulin tyrosination is a major factor affecting the recruitment of CAP-Gly proteins at microtubule plus ends. *J Cell Biol.* 174 (6), 839-849.

Peris, L., Wagenbach, M., Lafanechère, L., Brocard, J., Moore, A. T., Kozielski, F., Job, D., Wordeman, L. and Andrieux, A. (2009). Motor-dependent microtubule disassembly driven by tubulin tyrosination. *J Cell Biol.* 185 (7), 1159-1166.

Pierre, P., Scheel, J., Rickard, J. E. and Kreis, T. E. (1992). CLIP-170 links endocytic vesicles to microtubules. *Cell* 70 (6), 887-900.

Reed, N. A., Cai, D., Blasius, T. L., Jih, G. T., Meyhofer, E., Gaertig, J. and Verhey, K. J. (2006). Microtubule acetylation promotes kinesin-1 binding and transport. *Curr Biol.* 16 (21), 2166-2172.

Rehberg, M. and Gräf, R. (2002). Dictyostelium EB1 is a genuine centrosomal component required for proper spindle formation. *Mol Biol Cell.* 14 (10), 2301-2310.

Rice, L. M., Montabana, E. A. and Agard, D. A. (2008). The lattice as allosteric effector: structural studies of αβ- and γ-tubulin clarify the role of GTP-tubulin in microtubule assembly. *Proc Natl Acad Sci USA*. 105, 5378-5383.

Rickard, J. E. and Kreis, T. E. (1991). Binding of pp170 to microtubules is regulated by phosphorylation. *J Biol Chem.* 266 (26), 17597-17605.

Rüdiger, M., Wehland, J. and Weber, K. (1994). The carboxy-terminal peptide of detyrosinated α tubulin provides a minimal system to study the substrate specificity of tubulin-tyrosine ligase. *Eur J Biochem.* 220 (2), 309-320.

Samsó, M., Radermacher, M., Frank, J. and Koonce, M. P. (1998). Structural characterization of a dynein motor domain. *J Mol Biol.* 276 (5), 927-937.

Sandblad, L., Busch, K. E., Tittmann, P., Gross, H., Brunner, D. and Hoenger, A. (2006). The *Schizosaccharomyces pombe* EB1 homolog Mal3p binds and stabilizes the microtubule lattice seam. *Cell* 127 (7), 1415-1424.

Schober, J. M., Komarova, Y. A., Chaga, O. Y., Akhmanova, A. and Borisy, G. G. (2007). Microtubule-targeting-dependent reorganization of filopodia. *J Cell Sci.* 120, 1235-1244.

Schröder, J. M., Schneider, L., Christensen, S. T. and Pedersen, L. B. (2007). EB1 is required for primary cilia assembly in fibroblasts. *Curr Biol.* 17 (13), 1134-1139.

Severin, F., Habermann, B., Huffaker, T. and Hyman, T. (2001). Stu2 promotes mitotic spindle elongation in anaphase. *J Cell Biol.* 153 (2), 435-442.

Sharma, N., Bryant, J., Wloga, D., Donaldson, R., Davis, R. C., Jerka-Dziadosz, M. and Gaertig, J. (2007). Katanin regulates dynamics of microtubules and biogenesis of motile cilia. *J Cell Biol.* 178 (6), 1065-1079.

Sines, T., Granot-Attas, S., Weisman-Welcher, S. and Elson, A. (2007). Association of tyrosine phosphatase epsilon with microtubules inhibits phosphatase activity and is regulated by the epidermal growth factor receptor. *Mol Cell Biol.* 27 (20), 7102-7112.

Slee, E. A., Zhu, H., Chow, S. C., MacFarlane, M., Nicholson, D. W. and Cohen, G. M. (1996). Benzyloxycarbonyl-Val-Ala-Asp (OMe) fluoromethylketone (Z-VAD.FMK) inhibits apoptosis by blocking the processing of CPP32. *Biochem J.* 315, 21-24.

Slep, K. C. and Vale, R. D. (2007). Structural basis of microtubule plus end tracking by XMAP215, CLIP-170, and EB1. *Mol Cell* 27, 976-991.

Slep, K. C. (2009). Structural and mechanistic insights into microtubule end-binding proteins. *Curr Opin Cell Biol.* 22, 1-8.

Steinmetz, M. O. and Akhmanova, A. (2008). Capturing protein tails by CAP-Gly domains. *Trends Biochem Sci.* 33 (11), 535-545.

Teng, J., Takei, Y., Harada, A., Nakata, T., Chen, J. and Hirokawa, N. (2001). Synergistic effects of MAP2 and MAP1B knockout in neuronal migration, dendritic outgrowth, and microtubule organization. *J Cell Biol*. 155 (1), 65-76.

Thazhath, R., Liu, C. and Gaertig, J. (2002). Polyglycylation domain of β-tubulin maintains axonemal architecture and affects cytokinesis in *Tetrahymena*. *Nat Cell Biol.* 4 (3), 256-259.

Trivedi, N., Marsh, P., Goold, R. G., Wood-Kaczmar, A. and Gordon-Weeks, P. R. (2005). Glycogen synthase kinase-3beta phosphorylation of MAP1B at Ser1260 and Thr1265 is spatially restricted to growing axons. *J Cell Sci*. 118, 993-1005.

Tsvetkov, A. S., Samsonov, A., Akhmanova, A., Galjart, N. and Popov, S. V. (2007). Microtubule-binding proteins CLASP1 and CLASP2 interact with actin filaments. *Cell Motil Cytoskeleton* 64 (7), 519-530.

Vallee, R. B., Williams, J. C., Varma, D. and Barnhart, L. E. (2004). Dynein: an ancient motor protein involved in multiple modes of transport. *J Neurobiol.* 58, 189-200.

Van der Vaart, B., Akhmanova, A. and Straube, A. (2009). Regulation of microtubule dynamic instability. *Biochem Soc Trans.* 37 (5), 1007-1013.

Vaughan, K. T. and Vallee, R. B. (1995). Cytoplasmic dynein binds dynactin through a direct interaction between the intermediate chains and p150^{Glued}. *J Cell Biol.* 131, 1507-1516.

Verhey, K. J., Meyer, D., Deehan, R., Blenis, J., Schnapp, B. J., Rapoport, T. A. and Margolis, B. (2001). Cargo of kinesin identified as JIP scaffolding proteins and associated signaling molecules. *J Cell Biol.* 152 (5), 959-970.

Verhey, K. J. and Gaertig, J. (2007). The tubulin code. *Cell Cycle* 6 (17), 2152-2160.

Vitre, B., Coquelle, F. M., Heichette, C., Garnier, C., Chrétien, D. and Arnal, I. (2008). EB1 regulates microtubule dynamics and tubulin sheet closure in vitro. *Nat Cell Biol.* 10 (4), 415-421.

Wade, R. H. (2009). On and around microtubules: an overview. *Mol Biotechnol.* 43 (2), 177-191.

Waterman-Storer, C. M. and Salmon, E. D. (1997). Actomyosin-based retrograde flow of microtubules in the lamella of migrating epithelial cells influences microtubule dynamic instability and turnover and is associated with microtubule breakage and treadmilling. *J Cell Biol.* 139, 417-434.

Watson, P. and Stephens, D. J. (2006). Microtubule plus-end loading of p150^{Glued} is mediated by EB1 and CLIP-170 but is not required for intracellular membrane traffic in mammalian cells. *J Cell Sci.* 119, 2758-2767.

Webster, D. R., Wehland, J., Weber, K. and Borisy, G. G. (1990). Detyrosination of alpha tubulin does not stabilize microtubules *in vivo*. *J Cell Biol.* 111 (1), 113-122.

Wehland, J., Willingham, M. C. and Sandoval, I. V. (1983). A rat monoclonal antibody reacting specifically with the tyrosylated form of α-tubulin. I. Biochemical characterization, effects on microtubule polymerization in vitro and microtubule polymerization and organization in vivo. *J Cell Biol.* 97, 1467-1475.

Wehland, J. and Weber, K. (1987a). Tubulin-tyrosine ligase has a binding site on β-tubulin: a two domain structure of the enzyme. *J Cell Biol.* 104, 1059-1067.

Wehland, J. and Weber, K. (1987b). Turnover of the carboxy-terminal tyrosine of α-tubulin and means of reaching elevated levels of detyrosination in living cells. *J Cell Sci.* 88, 185-203.

Weisbrich, A., Honnappa, S., Jaussi, R., Okhrimenko, O., Frey, D., Jelesarov, I., Akhmanova, A. and Steinmetz, M. O. (2007). Structure-function relationship of CAP-Gly domains. *Nat Struct Mol Biol.* 14 (10), 959-967.

Wessel, D. and Flügge, U. I. (1984). A method for the quantitative recovery of protein in dilute solution in the presence of detergents and lipids. *Anal Biochem.* 138 (1), 141-143.

Westermann, S. and Weber, K. (2003). Post-translational modifications regulate microtubule function. *Nat Rev Mol Cell Biol.* 4 (12), 938-947.

Wittmann, T. and Waterman-Storer, C. M. (2005). Spatial regulation of CLASP affinity for microtubules by Rac1 and GSK3β in migrating epithelial cells. *J Cell Biol.* 169 (6), 929-939.

Xia, L., Hai, B., Gao, Y., Burnette, D., Thazhath, R., Duan, J., Bré, M. H., Levilliers, N., Gorovsky, M. A. and Gaertig, J. (2000). Polyglycylation of tubulin is essential and affects cell motility and division in *Tetrahymena thermophila*. *J Cell Biol.* 149 (5), 1097-1106.

Yang, X., Li, H., Liu, S., Deng, A. and Liu, X. (2009). Cdc2-mediated phosphorylation of CLIP-170 is essential for its inhibition of centrosome reduplication. *J Biol Chem.* 284 (42), 28775-28782.

Zanic, M., Stear, J. H., Hyman, A. A. and Howard, J. (2009). EB1 recognizes the nucleotide state of tubulin in the microtubule lattice. *PLoS One* 4 (10), e7585.

Zhang, D., Rogers, G. C., Buster, D. W. and Sharp, D. J. (2007). Three microtubule severing enzymes contribute to the Pacman-flux machinery that moves chromosomes. *J Cell Biol*. 177 (2), 231-242.

Zhu, Z., Gupta, K. K., Slabbekoorn, A. R., Paulson, B. A., Folker, E. S. and Goodson, H. V. (2009). Interactions between EB1 and microtubules: Dramatic effect of affinity tags and evidence for cooperative behaviour. *J Biol Chem.* 284 (47), 32651-32661.

Zimniak, T., Stengl, K., Mechtler, K. and Westermann, S. (2009). Phosphoregulation of the budding yeast EB1 homologue Bim1p by Aurora/Ipl1p. *J Cell Biol.* 186 (3), 379-391.

6.2. List of figures

6.3. List of tables

6.4. Abbreviations

A	Ampere
AAA	ATPases associated with various cellular activities
Ac	acetate
ADP	adenosine diphosphate
APC	adenomatous polyposis coli
APS	ammonium persulphate
ATP	adenosine triphosphate
bp	base pairs
BSA	bovine serum albumin
CA	calyculin A
CAP-Gly	cytoskeleton-associated protein glycine-rich
cdc	cell division control protein
Cdk	cyclin-dependent kinase
cDNA	copy DNA
CH	calponin homology
CHAPS	3-[(3-Cholamidopropyl)dimethylammonio]-1-propanesulfonate
CLASP	cytoplasmic linker protein-associated protein
CLIP	cytoplasmic linker protein
conc.	concentration
Da	Dalton
dCTP	deoxy-cytidine triphosphate
DCX	doublecortin
dil.	dilution
DMEM	Dulbecco's Modified Eagle Medium
DMSO	dimethylsulfoxide
DNA	deoxyribonucleic acid
dNTP	deoxyribonucleosid triphosphate
DTT	dithiothreitol
EB	end binding
EBH	end binding homology
ECL	enhanced chemiluminescence
E. coli	*Escherichia coli*
EDTA	ethylene diamine tetraacetic acid
EGTA	Ethylene glycol-bis(2-aminoethylether)-tetraacetic acid
ELISA	Enzyme-linked Immunosorbent Assay
F_{ab}	fragment antigen-binding
F_c	fragment crystallizable region
FCS	fetal calf serum
FPLC	fast performance liquid chromatography
FRAP	fluorescence recovery after photobleaching
GDP	guanosine diphosphate
GFP	green fluorescent protein
Glu-tubulin	detyrosinated tubulin
GRP	glucose-related protein
GSK3β	glycogen synthase kinase-3β

GTP	guanosine triphosphate
H_2O_{deion}	deionized water
HEAT	huntingtin elongation factor-3, protein phosphatase-2A and target of rapamycin
HEPES	N-2-Hydroxyethylpiperazine-N´-2-ethane sulfonic acid
HPLC	high pressure/performance liquid chromatography
HSP	heat shock protein
Ig	immunoglobuline
IP	immunoprecipitation
JIP1	JNK-interacting protein 1
JNK	c-Jun N-terminal kinase
kVh	kilo Volt hours
LB	Luria Bertani broth
M	molar
MAP	microtubule-associated protein
MARK	microtubule-affinity regulating kinase
MARKK	microtubule-affinity regulating kinase kinase
MAST	multiple asters
Mb	mega base pairs
mc	monoclonal
MCAK	mitotic centromere-associated kinesin
mDia1	mammalian Diaphanus 1
MEF	mouse embryonic fibroblast
MKK	mitogen-activated protein kinase-kinases
mRNA	messenger RNA
MS	mass spectrometry
MT	microtubule
MTOC	microtubule-organizing centre
m/z	mass per charge
n. d.	not determined
NEPHGE	non-equilibrium pH gel electrophoresis
n-red.	non-reducing
OA	okadaic acid
OD	optic density
P	phosphate/phosphatase-treated
PAGE	polyacrylamide gel electrophoresis
PBS	phosphate buffered saline
pc	polyclonal
PFA	paraformaldehyde
PCR	polymerase chain reaction
PP	protein phosphatase
PVDF	polyvinylidene fluoride
Q-TOF	Quadrupole Time-of-Flight
red.	reducing
RNA	ribonucleic acid
rpm	rounds per minute
SAP	shrimp alkaline phosphatase
SDS	sodium dodecyl sulphate
TAE	Tris-acetate-EDTA-buffer

TBS	tris buffered saline
TEMED	N,N,N´,N´-tetramethyl ethylenediamine
TFA	trifluoroacetic acid
+TIP	plus-end tracking protein
T_m	melting temperature
TOG	tumour-overexpressed gene
Tris	Tris-(hydroxymethyl) aminomethane
TTL	tubulin-tyrosine ligase
TTLL	TTL-like
γ-TuRC	γ-tubulin ring complex
γ-TuSC	γ-tubulin small complex
Tyr-tubulin	tyrosinated tubulin
U	unit
V	volt/sodium vanadate-treated
v/v	volume per volume
WT	wild type
w/v	weight per volume
xg	times gravity
XMAP215	*Xenopus laevis* microtubule-associated protein of 215 kDa

6.5. Acknowledgement

I would like to thank my supervisor Prof. Dr. Jürgen Wehland for the opportunity to work on this topic and the support, not only concerning this project, during the time of my PhD work. I also thank my “co-supervisor” Marco van Ham for his help with planning of experiments, many intense discussions and the correction of this thesis.
Additionally, I thank my second referee, Prof. Dr. Michael Steinert, and the chairman of my defence, Prof. Dr. Martin Korte.
Of course, I am very grateful to all my colleagues for their support in the lab, all their helpful advices and the nice atmosphere, so thank you to Ramona Baier, Jennifer Block, Tanja Bosse, Brigitte Denker, Patrick Duwe, Christian Erck, Petra Hagendorff, Jan Hänisch, Marlies Konradt, Margit Oelkers, Kathrin Schloen, Hildegard Schwab-Hanisch, Gosia Szczodrak, Viola Thiem, Marcin Ura, Steffi Weiss and all the others. Special thanks also to Theresia Stradal and Klemens Rottner for their helpful support.
Since the mass spectrometry analyses and the 2D-SDS-PAGE have been performed in the Cellular Proteomics group, I thank Lothar Jänsch, Evelin Dornbusch, Kirsten Minkhart, Reiner Munder, Manfred Nimtz and Josef Wissing for their intense help. Moreover, I want to thank Ulrich Wiesand for helping me with structural issues and the nice figure of the CAP-Gly domain of $p150^{Glued}$.

Nun aber auch ein dickes Dankeschön auf Deutsch an mein privates Umfeld. An erster Stelle möchte ich mich natürlich bei meiner Familie, und dabei ganz besonders bei meinen Eltern und meiner Schwester, für die Unterstützung, das stets offene Ohr und das Vertrauen bedanken. Ebenso vielen Dank an Kathrin und Tante Ulla für ständige Unterstützung und vor allem Motivation. Ein ganz dickes Danke auch an Sebastian für die Rückenstärkung und das große Verständnis im letzten Jahr.
Ganz besonders möchte ich mich bei Kai für seinen wissenschaftlichen Rat, das Korrigieren dieser Arbeit und die unzähligen Veranstaltungen zum Frustabbau bedanken. Ebenso ein Dankeschön an Anja, Annina, Matze und alle weiteren Personen aus meinem Freundeskreis für ihr Verständnis, ihre Ausdauer, viele erfolgreiche Ablenkungsmanöver und einfach fürs „immer da sein“. Ohne Euch wären die letzten Jahre in mehrerer Hinsicht ganz schön schwer geworden.